



UiT The Arctic University of Norway

Faculty of Engineering Science and Technology

Mechanical Properties of Some FDM 3D-printed Infill Structures

Predicting Mechanical Properties with Classical Laminate Theory for Infill Structures for
3D-printed Parts

Erlend Entner

Master's thesis in Engineering Design END-3900 May 2024



Mechanical Properties of Some FDM 3D-printed Infill Structures

Predicting Mechanical Properties with Classical Laminate Theory for Infill Structures for
3D-printed Parts

by: **Erlend Entner**

Thesis in Master program Engineering Design
Civil Engineering



Institutt for Datateknologi og beregningsorienterte ingeniørfag
UiT Arctic University of Norway, Narvik
Norway
15.05.2024

Acknowledgement

My first thanks, goes to UiT Norway's Arctic University for five, challenging, fun, and interesting years. UiT has given me a place to develop and learn so much. Thank you, to all staff and personnel that has made it possible.

Thank you, to my two supervisors Guy B. Mauseth and Joachim J. Ågontes for your, patience, guidance and motivation for me to finish this master thesis. The two of you have been immaculate and I thank the two of you, for it. Thanks again, and again.

Special thanks to Øyvind Søråas, Morten M. Olavsbråten, and Marius Wang that works at grov labben at campus Narvik UiT Norway's Arctic University. For me to use equipment and machines to perform tensile test and build parts that I needed to finish this thesis. Without your help, I don't believe that I would accomplish much with this thesis.

Thank you, Erlend Bjørk. For your expertise in 3D-printing and help with manufacture of 3D-printed parts.

Thank you, my mother, for being my bedrock in my life. You have always been there for me and motivated and supported me all the time. Nå er jeg også, endelig ferdig med den oppgaven mamma.

Abstract

Master thesis documents tensile test of fused deposit modeling 3D-printed parts. Infill configurations that's investigated is line- and grid-pattern with 100% infill density for line pattern. Grid pattern have been printed with 20% and 40% infill density. To predict mechanical properties of 3D-printed parts with line pattern, classical laminate theory is chosen as mathematical model. Performing classical laminate theory calculations, the local mechanical properties of a layer must be determined. This is done by performing three tensile test and the resulting tensile modulus is used in classical laminate theory. Calculations is done with classical laminate theory and compared against a tensile test. The results from classical laminate theory and tensile test shows that classical laminate theory is a good method to determine mechanical properties of fused deposit modeling 3D-printed parts.

Analytical method used for grid pattern is cellular solid theory. For comparison between cellular solid and experimental results there was done with two tensile test. One with 20% and the other one with 40% infill density. Predicted tensile modulus with the use of cellular solid was not deemed a decent prediction compared to the resulting tensile modulus from tensile testing. Test equipment was design with testing of material with higher tensile modulus than fused deposit modeling 3D-printed parts has. Stress-strain curve was not as a continuous curve to where calculation of tensile modulus would be correct. Other factors that has an impact on prediction is manufacture of grid pattern with 3D-printers, and which solid tensile modulus should be used in predicting mechanical properties with cellular solid theory. In summary the use of cellular solid theory for fused deposit modeling 3D-printed parts is inconclusive.

Contents

1	Introduction	1
1.1	Background information	1
1.2	Problem description	4
1.2.1	Aims of this thesis	4
1.2.2	Problem limitations	4
1.2.3	Problem derivatives	4
1.3	Literature Review	5
1.3.1	Research strategy	5
1.3.2	Organization of literature	5
1.3.3	Summary of tensile test bibliography:	6
2	Design Requirements	15
2.1	Standards Used	15
2.2	Experimental Setup & Test Equipment	17
2.3	Manufacture of 3D-printed Specimens	18
2.4	Build of fixture for tensile testing	19
3	Analytical Mathematical Modeling	23
3.1	Classical Laminate Theory	23
3.1.1	Macromechanics of Classical Laminate Theory	24
3.1.2	Micromechanics of Classical Laminate Theory	30
3.2	Cellular Solids	31
4	Numerical Analysis	33
4.1	Coding CLT in Matlab	33
5	Results	37
5.1	Experimental Results	37
5.1.1	Line pattern with raster angle 0°	37
5.1.2	Line pattern with raster angle 90°	39
5.1.3	Line pattern with raster angle 45°	40
5.1.4	Line pattern for CLT computation	42
5.1.5	Grid pattern infill percentage 20	42
5.1.6	Grid pattern infill percentage 40	43
5.2	Analytical & Numerical Results	47
5.2.1	Predicted Stiffness from CLT computation	47
5.2.2	Analytical Prediction for Grid Patterns	47
6	Discussion	49
6.1	Comparison of CLT Results and Tensile Test Results	49
6.2	Comparison of Cellular Solids Results and Tensile Test Results	50
6.3	Failure Mechanisms for 3D-printed Parts	52

6.4	Final Remarks	53
6.5	Future Work	54
7	Conclusion	55
	Bibliography	56
A	Matlab Code for CLT	I
B	Printing Parameters in Ultimaker Cura	I
C	Technical Drawings of Fixture	
D	Matlab Code for Evaluation of Tensile Test	I
E	Technical Data Sheet: Tough PLA from Ultimaker	

List of Figures

1.1	FDM printer creating part layer by layer [1].	1
1.2	Two sliced parts with different layer heights view at layer 30.	2
1.3	Top view of sliced part with wall thickness of 1.2 mm with three lines.	2
1.4	Different raster angles from slicer UltiMaker Cura.	3
1.5	Available infill pattern in UltiMaker Cura.	3
1.6	Infill structure with infill density at 25%, 50%, 75% and 100% with grid pattern.	3
1.7	Article from Zou 2016 used in Litmaps to find more papers that has cited Zou 2016.	5
1.8	Build orientation for test specimen [3].	6
1.9	Build orientation for printing of specimen [5].	8
1.10	Stress-strain curve from tensile stress specimen [5].	8
1.11	Build orientation on 3D-printer [9].	11
1.12	Dog-bone dimension specifications [10].	12
1.13	Different build orientation and raster angles for line- and grid-pattern [11].	13
2.1	Dog-bone dimension from ISO 1926:2009 with gauge length of 50 mm. [12].	15
2.2	Dog-bone specimen with dimensions for tensile test with reinforced rigid cellular plastic with gauge length 50 mm [12].	16
2.3	Material test machine used to perform material test.	17
2.4	Build orientation from technical data sheet for though PLA [16].	18
2.5	3D-model concept for fixture of tensile test specimen.	19
2.6	Produced assembly of fixture for cellular solid test specimen.	20
2.7	Metal plates that reinforces the dog-bone specimen, dimensions in mm.	20
3.1	Laminate built up by five plies with unidirectional fibers [19].	24
3.2	Geometry of a laminate with n layers [19].	25
3.3	Illustration of a ply and it's local coordinate mechanical direction relative to the global coordinate system [19].	25
3.4	Grid pattern with dimensions and tensile modulus direction.	31
3.5	Sliced 3D-model with grid pattern 0° and 20% infill density.	32
5.1	Stress-strain curve from four tensile tests line pattern with raster angle of 0° and 100% infill.	37
5.2	Stress-strain curve from tensile test Line pattern raster angle 0° #1.	38
5.3	Damage on dog-bone for line pattern with raster angle 0° and 100% infill #2.	38
5.4	Failure from tensile test line pattern with raster angle 0° and infill density 100%.	38
5.5	Stress-strain curve from the tensile test of a dog-bone specimen made with a line pattern raster angle of 90° and 100% infill #4.	39
5.6	Failure of a dog-bone with a line pattern raster angle of 90° and 100% infill #4.	40
5.7	Stress-strain curve from line pattern with raster angle $\pm 45^\circ$ and 100% infill.	40
5.8	Dog-bone specimen failure with line pattern, raster angle $\pm 45^\circ$ and 100% infill #1.	41
5.9	Dog-bone specimen failure with line pattern, raster angle $\pm 45^\circ$ and 100% infill #4.	41
5.10	Dog-bone specimen failure with line pattern, raster angle $\pm 45^\circ$ and 100% infill #3	42

5.11	Stress-strain curve from tensile test with line patten, raster angle $[0, \pm 30, \pm 60, 0, 90]_R$, and 100% infill.	42
5.12	Dog-bones after tensile test for line pattern with CLT raster angles.	43
5.13	Stress-strain curve from three tensile test with grid pattern, raster angle 0° and 20% infill.	44
5.14	Fracture of dog-bone specimen number 3, grid pattern, raster angle 0° , and 20% infill.	45
5.15	Connection between fibers in a grid cell from grid pattern with 0° raster angle, and 20% infill.	45
5.16	Stress-strain curve from three tensile test with grid pattern with 40% infill.	45
5.17	Failure of dog-bone specimen #1 from grid pattern with 40% infill.	46
5.18	Y-cell of grid pattern with 40% infill.	46
6.1	Dog-bone specimen with red circles indicating where failures occurred.	52
6.2	Tool-path for FDM 3D-printer for line pattern with raster angle 0° and 100% infill.	52

List of Tables

1.1	Tensile test results calculated as orthotropic material [3].	6
1.2	Engineering constants from tensile test results calculated as orthotropic material [3].	6
1.3	Results: Tensile strength and Young’s Modulus from different 3D-printed parts [4].	7
1.4	Tensile strength of 3D-printed parts by orientation angle [5]. Note STD is standard deviation.	8
1.5	Young’s modulus of 3D-printed parts by orientation angle and calculated as isotropic material [5].	9
1.6	Transverse-isotropic mechanical properties of 3D-printed parts [5].	9
1.7	Parameter settings for test specimen [8].	10
1.8	Tensile strength and Young’s modulus results with STDEV (standard deviation) [9].	11
1.9	Experimental results from tensile test of test specimen [11].	13
1.10	Experimental vs homogenized properties for RVE [11].	13
2.1	Technical data sheet for Thought PLA from Ultimaker [16].	18
5.1	Tensile moduli results for line pattern with raster angle 0° and infill percentage 100.	39
5.2	ultimate tensile stress and elongation at break for line pattern with raster angle 0° and 100% infill.	39
5.3	Mechanical properties from tensile test for line pattern with raster angle $\pm 45^\circ$ and 100% infill.	41
5.4	Mechanical properties from tensile test for line pattern with raster angle $[0, \pm 30, \pm 60, 0, 90]_R$ and 100% infill.	43
5.5	Mechanical properties from tensile test for grid pattern with raster angle 0° and 20% infill.	44
5.6	Mechanical properties from tensile test for grid pattern with 40% infill.	46
5.7	Measurement of grid cells from dog-bone specimen.	47
5.8	Predicted tensile modulus for grid pattern, with solid tensile modulus from experimental results and technical data sheet (TDS) from Ultimaker.	48
6.1	Comparison of CLT prediction and experimental tensile results	49
6.2	Comparison of estimated grid dimensions and measured grid dimensions.	50
6.3	Comparison of experimental and two predicted tensile modulus of grid pattern with 20% and 40% infill density.	51

Chapter 1

Introduction

1.1 Background information

3D-printing has been used for a long time in product design with the use of rapid prototyping. Material such as thermoplastics results in a cheap and easy way to 3D-print prototypes. 3D-printing has become more popular as a method to mass produce parts than a tool for rapid prototyping. This technology can create parts that has a complex geometry that more traditional methods of manufacturing can't easily produce. 3D-printing is believed to be a cost effective method to create prototypes, and to be able to easily test products, in product design process.

Gaining knowledge of how these 3D-printed parts behave mechanically and which printer parameters should be chosen is a subject for great investigation. Fused deposit modeling (FDM) or fused filament fabrication (FFF) are manufacturing methods that fall under the category of additive manufacturing (AM). Parts manufactured using either fabrication method are constructed layer by layer on a build platform. 3D-printers using thermoplastics filaments such as polylactic acid (PLA) and acrylonitrile butadiene styrene (ABS). The filament is driven from a filament spool to the nozzle where the material is heated up to near melting temperature such that the plastic becomes soft, and malleable, and is then extruded through the nozzle of the printer and a heated build platform.

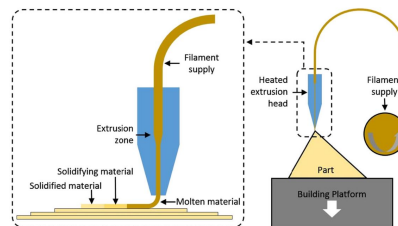


Figure 1.1: FDM printer creating part layer by layer [1].

For an FDM printer to print a part it must be generated in a computer aided design (CAD) software, however, first it must first be processed in a slicer software. A slicer software generates a G-code for the 3D-printer to produce the 3D-printed part. G-code dictates all the printing parameters for a 3D-printer. Slicer software has then an important role in FDM 3D-printing. A Slicer need a 3D-model in a file format that is supported by the slicer software, such as .stl-file for example. Nevertheless, there are different file formats that are supported for different slicer software.

Free to use slicer software that is used in this thesis is the UltiMaker Cura 5.6.0. UltiMaker Cura gives a wide range of printing configurations to create 3D-printed parts. Quality of a print has two configurations that directly determines how fine a 3D-printed part would be after a print and that is the nozzle size and layer height. Nozzle size can be changed physically on the printer where smaller nozzle size arguably gives a higher quality in the finished part. Nozzle size are different for

different printer but generally the sizes are typically 0.25, 0.4, 0.6 and 0.8 mm in diameter. The layer height, on the other hand, determines how tall each layer must be. The smaller layer heights gives better quality of the print but also increases the print time since there are more layers to print. Figure 1.2 shows two printing configurations where layer height is 0.1 and 0.4 mm.

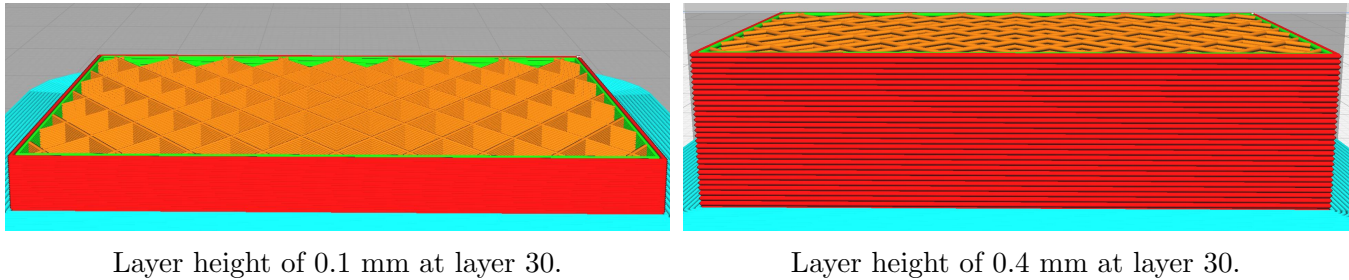


Figure 1.2: Two sliced parts with different layer heights view at layer 30.

Figure 1.2 shows two sliced parts with different layer heights where the part with 0.4 mm layer height is almost done on layer 30 however, the part with layer height of 0.1 mm is not a quarter of the way to completion. When mentioning quality of a print, the focus here is on how thin or fine a line deposited on the part is. Smaller nozzle size and layer height produces a higher quality of 3D-printed parts.

3D-printed parts can be made with walls, floor and roof, though there are parameters for how to control these. Ultimaker Cura gives the user the possibility of changing the thickness of floor and roof and how many layers there will be. Walls can be set with a wall thickness, where the wall line count is determined by the nozzle size. The parameters can also change the amount of lines there are in a wall. Walls, floor and roof exists to create a nicer and smoother finish for 3D-printed part, while also giving some structural integrity.

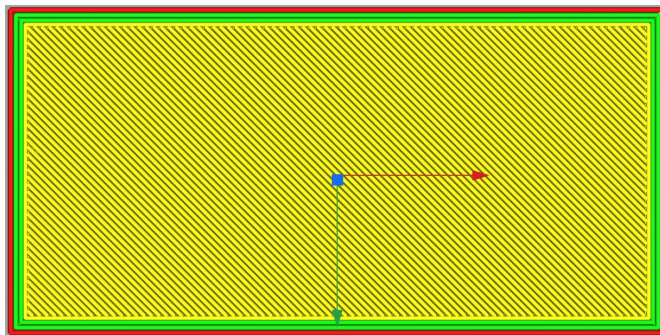


Figure 1.3: Top view of sliced part with wall thickness of 1.2 mm with three lines.

Figure 1.3 shows a sliced part where the wall thickness is 1.2 mm and three lines thick since the nozzle size is fixed at 0.4 mm. The wall in Figure 1.3 are shown as green as the inner line of the wall and red is the outer most line. Yellow part is the floor of the part with line pattern with raster angle -45° . Floor and roof can have line-, concentric- or zig-zag-pattern. Raster angle however, determines in which orientation all patterns are printed in the floor, roof and infill pattern. With infill pattern like line, it is possible to have different layers with different raster angle e.g. Figure 1.4 where the infill pattern have a set of raster angle as $[0, 45, 90, 135]$ respectively.

Layer will repeat the raster angles shown in Figure 1.4 through the part until the roof is built. After the fourth layer is done with raster angle 135° , layer 5 would then have a line with raster angle 0° . The raster angle is rotated clockwise when it starts parallel to the y-axis in the slicer software, which is the green arrow in Figure 1.3. There is a range of different infill patterns to chose from, see Figure 1.5 for an overview of the different patterns.

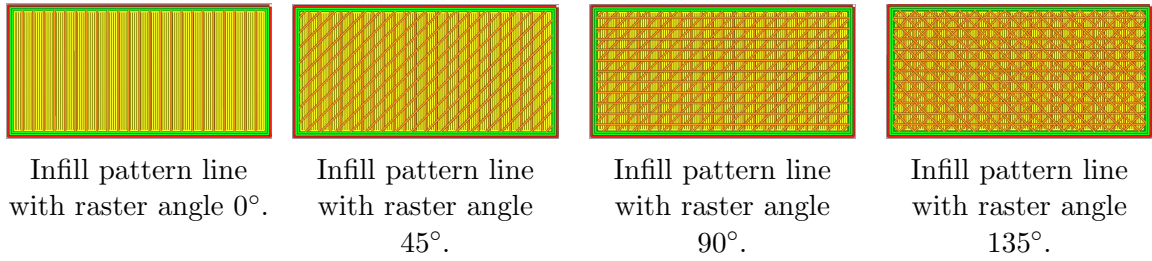


Figure 1.4: Different raster angles from slicer UltiMaker Cura.

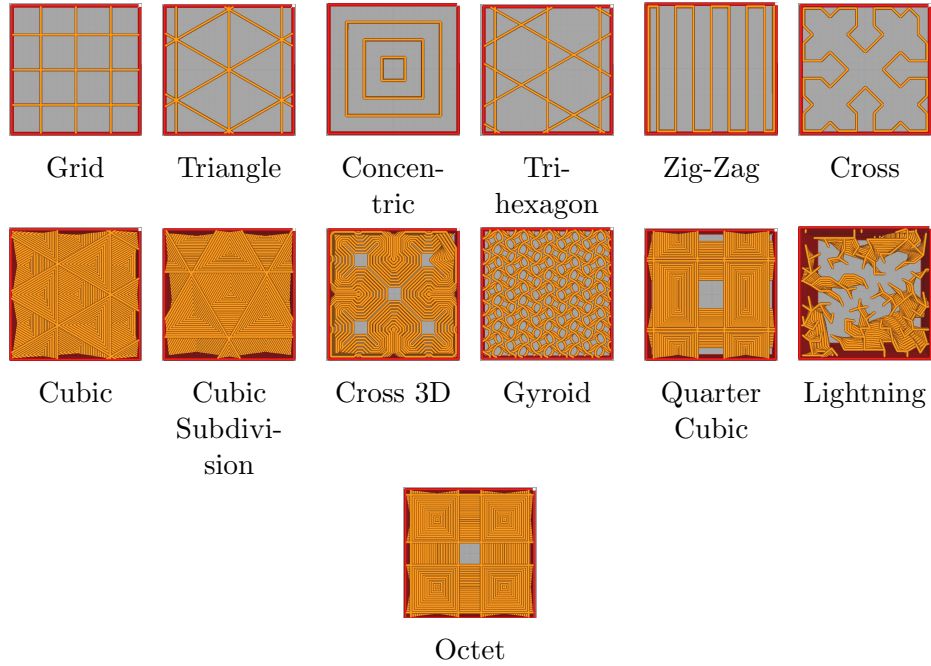


Figure 1.5: Available infill pattern in UltiMaker Cura.

Patterns that doesn't change along the z -axis are Grid, Triangle, Concentric, Trihexagon, Zig-zag and Cross. While Cubic, Cubic Subdivision, Cross 3D, Gyroid, Quarter Cubic, Lightning and Octet, changes as layers are printed. Next parameter that can be changed in infill configuration includes infill density, where infill density ranges from 0% to 100%. Example with different infill density is shown in Figure 1.6 with infill pattern grid.

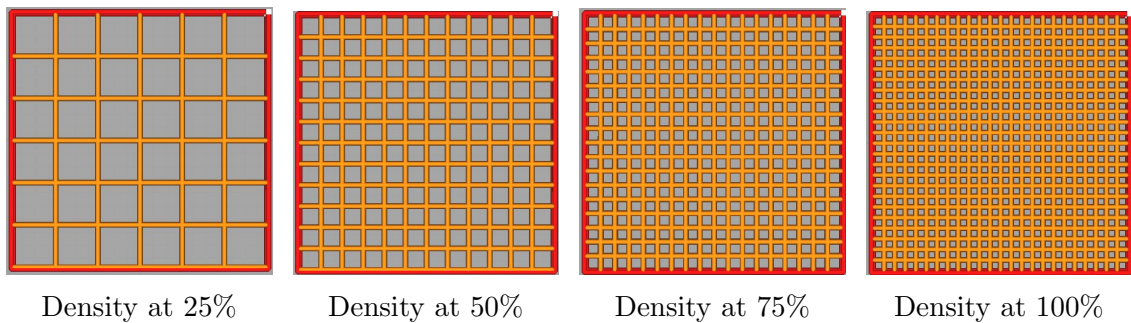


Figure 1.6: Infill structure with infill density at 25%, 50%, 75% and 100% with grid pattern.

1.2 Problem description

This master thesis aims to examine mechanical properties of some 3D-printed parts with different infill configurations. What's of interest are infill patterns, and to some extent infill density. Examining how these parameters impacts the mechanical properties of FDM 3D-printed parts. Main goal is to find a mathematical method to evaluate mechanical properties of infill configuration.

1.2.1 Aims of this thesis

- Create a procedure to perform tensile testing of FDM 3D-printed parts.
- Perform tensile tests of FDM 3D-printed part with different infill configuration to be able to determine mechanical properties.
- Evaluate if Classical Laminate Theory is an applicable mathematical model to determine mechanical properties of FDM 3D-printed parts.
- Evaluate if Cellular Solid Theory is an applicable mathematical model to FDM 3D-printed parts.

1.2.2 Problem limitations

- Infill structure that is investigated are line- and grid-pattern.
- Material used in 3D-printing is Tough PLA from Ultimaker.
- Determination of mechanical properties are limited to a rod in axial tension.
- Mathematical model used is Classical Laminate Theory, and Cellular Solid.
- Printing parameters are the same for all test except infill pattern, and infill density.

1.2.3 Problem derivatives

The investigation will be conducted with experiments of tensile test. Data from testing 3D-printed parts is going to be compared against analytical methods more specifically classical laminate theory (CLT) of predicting deflection and behaviour of test specimen that undergoes axial load. For one the interest is how well CLT can predict mechanical properties such as Young's modulus, Poisson's ratio etc. of 3D-printed parts. Mostly it's predicting tensile modulus using CLT and comparing against actual results from tensile testing.

FDM 3D-printed parts has voids (empty space or air) inside the structure these voids are created by the extrusion nozzle or infill patterns that is chosen in slicer software Ultimake Cura. Since there are voids in FDM 3D-printed parts, parts can then be considered a cellular solids by definition in *Cellular solids: structure and properties* by Gibson and Ashby [2]. In cellular solids there are mainly two groups of material there is foams and honeycombs. Foams have a structure in three dimensions to fill a space while honeycomb material have an array of periodic or non-periodic structure that fills the plane [2]. For this master thesis cellular solid structure that is examined is grid pattern.

1.3 Literature Review

1.3.1 Research strategy

To search for papers over a range of different journals keywords related to mechanical properties of 3D-printed parts have been used. Keywords that has been used are: *fused deposition modeling, mechanical properties, process parameters, Part characteristics, Mechanical characterization, Polylactic acid (PLA), Fill pattern, Fill percentage, Tensile properties, Layer height, Raster angle, Raster width, flexural beam properties, orientation effects, Homogenization, Orthotropic property, RVE homogenisation, Anisotropic property, Constitutive equations.*

To search all journal databases three search engines is used and those are *GoogleScholar, Elicit* and *IEEEXplore*. After an article is found and is deemed related or of interested regarding to the master thesis the article is put into *Litmaps* to find other articles that is citing the first article and articles that is cited in the article. This method is an easy and quick strategy to find articles that are related to this thesis with the keywords that is listed earlier.

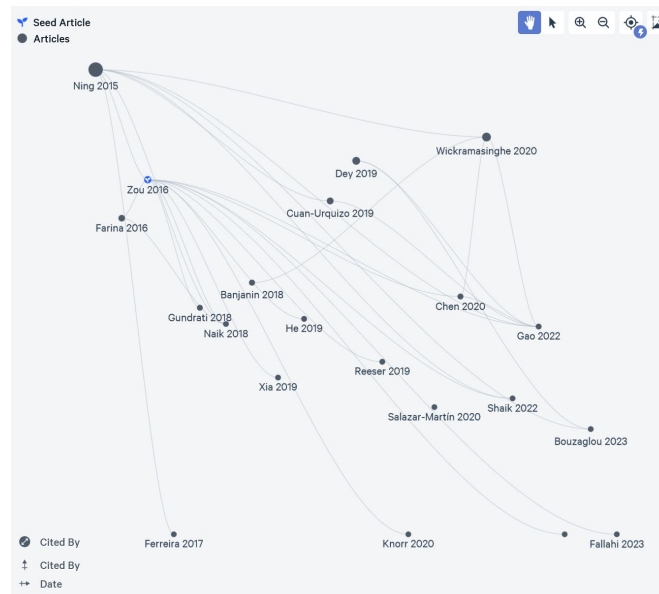


Figure 1.7: Article from Zou 2016 used in Litmaps to find more papers that has cited Zou 2016.

Result of literature review is to have an overview of methods used for determining mechanical properties. With all possible infill configurations there are different methods that can be used for different infill configurations. By observing what method researchers has used to determine mechanical properties. It's observed which method that is used for different infill configuration. After a method is identified, finding books or papers that covers the method is the next step in literature review.

1.3.2 Organization of literature

The interesting thing is an analytical way of predicting mechanical properties of 3D-printed structures. To start with these type of evaluation the simplest type of mechanical problem should be investigated first. Classical mechanical problems are a rod under pure tensile load, cantilever beam with a point load on free end, a simply supported beam with a point load in the middle of the supports, rod under pure torsion load to mention some classical mechanical problems. Therefore, it is intuitive to group articles that are testing what type of mechanical problem they are experimenting with. There is also literature that is more general than others such as, books related to a topic. For example a book on *Theory of elasticity* by S. Timoshenko. Books that cover a whole topic is gather in their own group called *Books General*.

1.3.3 Summary of tensile test bibliography:

Bellini et al. from 2003 *Mechanical characterization of parts fabricated using FDM* [3]

This article is one of the earliest papers gathered during literature review, and shows how long researches have looked into the mechanical behaviour from FDM 3D-printed parts. The paper evaluates 3D-printed ABS parts with a focus on build orientation on the printer bed where the orientation is flat, on-edge, upright, flat +45°, on-edge +45°, and upright +45°, as Figure 1.8 illustrates.

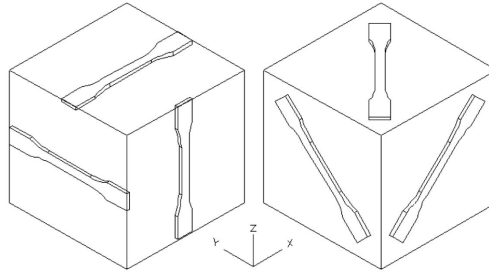


Figure 1.8: Build orientation for test specimen [3].

With an infill pattern of lines with raster angles of [0, 90, +45, -45] degrees where infill percentage is at 100%. Article documents tensile- and flexural-strength of the parts. Where the tensile test gave the mechanical properties in Table 1.1 and Table 1.2.

Build Orientation	Tensile Strength [MPa]	Elastic Modulus [MPa]
xy	11.7	1072.9
yz	15.987	1652.523
xz	7.608	1391.448
xy + 45°	10.808	970.944
yz + 45°	13.465	1519.115
xz + 45°	14.702	1527.6

Table 1.1: Tensile test results calculated as orthotropic material [3].

E_x [MPa]	E_y [MPa]	E_z [MPa]	G_{xy} [MPa]	G_{xz} [MPa]	G_{yz} [MPa]	ν_{xy}	ν_{xz}	ν_{yz}
1072.9	1653	1391.7	369.6	540.5	553	0.3209	0.2707	0.4391

Table 1.2: Engineering constants from tensile test results calculated as orthotropic material [3].

The paper give an insight on how to gain favourable mechanical properties based upon orientation of printing on the 3D-printer bed.

Paper concludes since parts created in 3D-printing are created as layered manufacturing the structure or material behaves orthotropic [3]. Since orientation impacts an optimal tool-path for the extruding nozzle it can be determined that the tool-path is an important aspect for mechanical properties. Based upon results that build orientation has significance to the strength of material and elastic modulus.

Fernandez-Vicente et al. from 2016 *Effect of infill parameters on tensile mechanical behavior in desktop 3D-printing* [4]

Paper conducts an investigation into how different infill-patterns and percentage changes mechanical characteristics in tensile testing with ABS as printing material. Infill patterns that are being investigated are line, rectilinear, honeycomb with infill percentages 20%, 50%, and 100% and compared against raw ABS. Method of printing was flat orientation of all test specimen. One note is that the line pattern has raster angle [+45, -45] degrees. Papers conclusion is that infill density has a significant more impact on mechanical properties than infill patterns. Results for different tensile strength and modulus is given in Table 1.3.

Infill pattern	Infill density	Tensile strength (MPa)	Tensile strain (%)	Elastic modulus (MPa)	Weight (g)
Line	20	16	4,76	499	11,06
Line	50	20,06	4,86	640	13,98
Line	100	35,68	5,3	784	17,54
Rectilinear	20	15,62	5,3	408	10,64
Rectilinear	50	19,58	4,62	659	13,98
Rectilinear	100	36,4	5,36	834	19
Honeycomb	20	16,52	4,44	568	11,22
Honeycomb	50	21,78	4,38	745	14,76
Honeycomb	100	36,1	5,42	802	18,88
Raw ABS	-	36,56	5,44	1826	

Table 1.3: Results: Tensile strength and Young's Modulus from different 3D-printed parts [4].

Paper also gives a tensile strength formula based upon infill percentage of 3D-printed parts [4].

$$\sigma_p = 15.2364 + 0.002083x^2$$

Where σ_p is the predicted tensile strength with respect to infill percentage x e.g. for infill percentage being 20% then $x = 20$ and thus the predicted tensile strength is $\sigma_p = 16.0696$ MPa.

Paper has researched which pattern and infill density gives the best tensile strength and determined Young's modulus. Conclusion from the paper is that best pattern is rectilinear with an infill percentage of 100%. The pattern that showed the best results at a lower infill density was the honeycomb pattern [4].

Zou et al. from 2016 *Isotropic and anisotropic elasticity and yielding of 3D-printed material* [5]

Paper documents 3D-printed parts using FDM with printing material ABS plastic. Paper doesn't state infill configurations however, the assumption from the reader is that the infill percentage is at 100% and the pattern is line. The evaluation of Young's modulus and tensile strength is varied by changing the orientation angle of the test specimen. Paper states that the 3D-printed parts are of anisotropic behaviour and gives then a transverse-isotropic model of 3D-printed parts. The transverse-isotropic model is then compared to an isotropic material model. Paper evaluates the 3D-printed parts as isotropic first and then as anisotropic where the paper states that the 3D-printed parts behave as transverse-isotropic.

The specimen are printed upright to on-edge with various angles from upright to on-edge orientation. For further clearance see Figure 1.9.

From experiments done with tensile test the papers give tensile strength of 3D-printed parts by different build orientation that is given in Table 1.4.

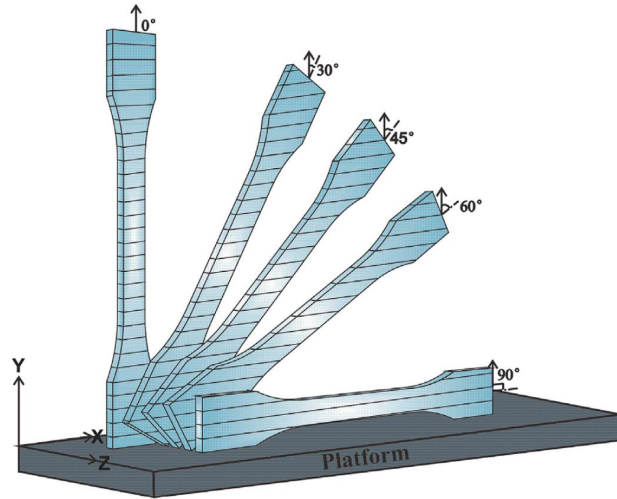


Figure 1.9: Build orientation for printing of specimen [5].

Angle	Tensile Strength [MPa]	STD
0°	25.74	0.38
30°	26.5	1.01
45°	27	0.53
60°	27.34	0.52
90°	27.63	0.28

Table 1.4: Tensile strength of 3D-printed parts by orientation angle [5]. Note STD is standard deviation.

From the results given the strongest specimen was those that was printed on-edge. Figure 1.10 shows the stress-strain for all of the test specimen.

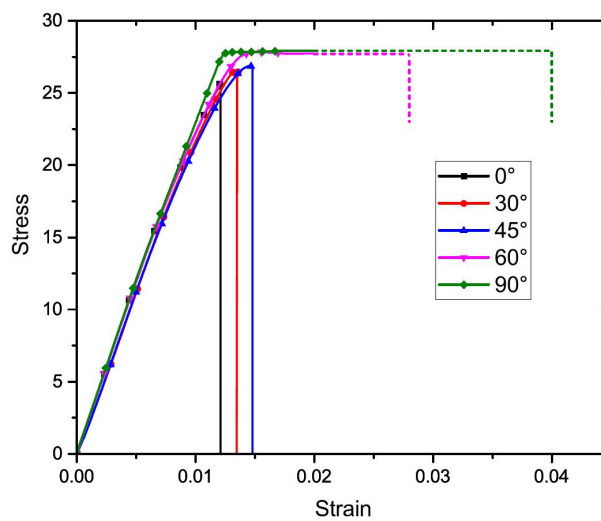


Figure 1.10: Stress-strain curve from tensile stress specimen [5].

Mentioned before they evaluate the parts as isotropic and determine an apparent Young's modulus that is given in Table 1.5.

Result as anisotropic to transverse-isotropic material is given in Table 1.6. E is the Young's

Angle	Young's Modulus [MPa]	STD	Poisson's Ratio	STD
0°	2399.67	117.06	0.37	0.03
30°	2339.42	80.76	0.38	0.04
45°	2420.44	97.27	0.31	0.07
60°	2412.03	40.63	0.37	0.03
90°	2425.94	14.03	0.42	0.09

Table 1.5: Young's modulus of 3D-printed parts by orientation angle and calculated as isotropic material [5].

modulus in the transverse plane and E' works in the principal axis of direction. The same goes for ν in the transverse plane, ν' in principle axis [5].

Set	E (MPa)	E' (MPa)	ν	ν'	G' (MPa)	E/E'	ν/ν'	G/G'
1	2451.81	2477.02	0.21	0.36	838.92	0.99	0.57	1.21
2	2478.98	2331.28	0.27	0.29	799.01	1.06	0.95	1.22
3	2366.09	2292.99	0.25	0.36	853.48	1.03	0.69	1.11
Mean	2432.29	2367.10	0.24	0.34	830.47	1.03	0.72	1.18
STD	48.11	79.29	0.03	0.03	23.03	0.03	0.16	0.05

Table 1.6: Transverse-isotropic mechanical properties of 3D-printed parts [5].

The paper also gives an ultimate tensile strength formulae that can be used to predict tensile strength of 3D-printed part. 3D-printed part must have infill percentage of 100% and line pattern to be accurate in the use of the formula. Tensile strength changes with respect to θ that is the angle of build orientation see Figure 1.9. [5].

$$\sigma(\theta) = \sigma(0^\circ) + \left(\frac{\sigma(90^\circ) - \sigma(0^\circ)}{90} \right) \theta$$

Where $\sigma(0^\circ) = 25.83$ MPa, $\sigma(90^\circ) = 27.86$ MPa [5].

Paper concludes how using constitutive models of isotropic and anisotropic elasticity is used to determine elastic constants from build orientation [5].

Alaimo et al. from 2017 *Influence of meso-structure and chemical composition on FDM 3D-printed parts* [6]

The paper conducts a study into mechanical properties of FDM 3D-printed parts. And is using analytical methods, such as Classical Laminate Theory, to predict failure of test specimen. The 3D-printed parts is constructed by two types of ABS plastic. The test specimen is printed as lines with different raster angles. Method of determining failure criteria for FDM 3D-printed parts with the use of Classical Laminate Theory. The researchers have first test three different groups of line pattern. Where the raster angle is different for each group. With these tensile test they are able to determined longitudinal-, transverse-, and shear-modulus, for parts that is manufactured with ABS in FDM printing. For failure criterion they investigated Tsai-Hill yielding criterion, and

found that the criterion is a well capable of predicting in-plane stiffness and strength. Conclusion from Alaimo et al. was that Classical Laminate Theory was a model that predicted stiffness and strength well.

Rodriguez-Panes et al. from 2018 *The influence of manufacturing parameters on the mechanical behaviour of PLA and ABS pieces manufactured by FDM: A comparative analysis* [7]

Paper compares two types of thermoplastics in FDM 3D-printing PLA and ABS. Where they control how different printing parameters effect the two different printing material with respect to tensile strength. Parameters that were varied in the experiment was layer height, infill density and layer orientation (flat, on-edge, up-right). For tensile strength the most important printing parameter is infill percentage which makes sense since with 100% infill density there is more PLA or ABS in 3D-printed parts. Generally PLA has a greater strength than ABS since pure (raw test specimen of PLA or ABS) PLA is “stronger” than pure ABS [7]. Infill configurations are 0.1 mm layer height, walls are constructed using line pattern, infill percentage being 20% and 50%, and infill patterns of lines with raster angles 45° and 135° [7].

Papers conclusion is that ABS is a difficult printing material for FDM production. Since bonding between layers are weak or difficult to achieve good bonding between layers. Printing orientation such that layers are printed perpendicular to the stress causes premature failure of the test specimen. For the strength of the 3D-printed parts the more dense a test specimen is the stronger it is (i.e. higher infill density higher strength) also smaller layer height is stronger than larger ones for example 0.1 mm layer height has stronger tensile properties than 0.2 mm layer height.

Rajpurohit et al. from 2018 *Effect of process parameters on tensile strength of FDM printed PLA part* [8]

Article completes a study on mechanical behaviour of PLA 3D-printed parts for tensile strength by focusing on three process parameters raster angle, layer height and raster width (raster width is the width of one line deposited by the 3D-printer). The finding of this study was that raster angle at 0° gave the highest tensile strength. Height of each layer has an impact on tensile strength where a relative low layer height is best and a greater line width is also improves tensile strength. All of the finding correlate with intuition since each parameter effects the amount of material that is put into 3D-printed parts. Printing parameters that affects the use of material in a 3D-printed part is layer height and raster width for this study.

Printer settings for all specimen has an infill percentage of 100% with the parameters that are being investigated is given in Table 1.7.

Parameters	Unit	Levels
Raster Angle	°	0, 30, 45, 60, 90
Layer height	μm	100, 150, 200, 250, 300
Raster width	μm	400, 500, 600, 700

Table 1.7: Parameter settings for test specimen [8].

Parameter that has the highest effect on tensile strength is the raster angle where a raster angle of 0° is the best option. The highest tensile strength was measured at 47.5 MPa with layer height of 100 μm and a raster width of 600 μm [8].

Zhao et al. from 2019 *Novel mechanical models of tensile strength and elastic property of FDM AM PLA materials: Experimental and theoretical analyses* [9]

Paper conducts a study on PLA 3D-printed parts with a focus on analytical computations and comparing up against results from the experiments performed and documented in this paper. 3D-printing parameters what changed is the layer thickness with 0.1, 0.2, and 0.3 mm and build orientation from upright to on-edge, refer to Figure 1.11.

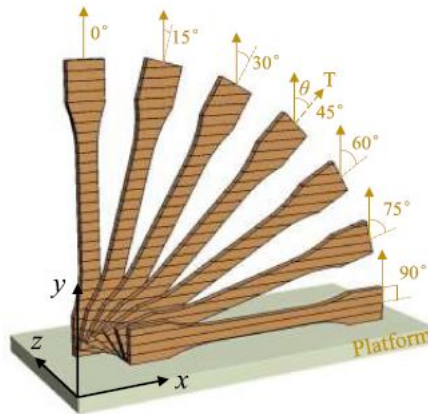


Figure 1.11: Build orientation on 3D-printer [9].

The result was that the part with minimal height of layer thickness and had a printing orientation on-edge was best with respect to tensile strength, with a tensile strength of 49.66 MPa. Full results is shown in Table 1.8.

Angle θ	Tensile Strength [MPa]	STDEV	CV (%)	Young's Modulus [MPa]	STDEV	CV (%)
Layer thickness = 0.1 mm						
0	23,4	1,58	6,75	2444	122	4,99
15	25,69	1,23	4,79	2507	87	3,47
30	29,24	1,56	5,34	2549	41	1,61
45	30,17	1,47	4,87	2659	90	3,38
60	34,59	0,97	2,8	2726	111	4,07
75	43,65	1,91	4,37	2788	77	2,76
90	49,66	1,12	2,25	2864	25	0,87
Layer thickness = 0.2 mm						
0	21,35	0,75	3,51	2108	76	3,6
15	24,14	0,38	1,57	2187	100	4,57
30	25,24	1,37	5,43	2224	77	3,46
45	28,12	1,86	6,61	2273	32	1,41
60	35,85	1,04	2,9	2548	15	0,59
75	43,44	0,63	1,45	2705	49	1,81
90	48,28	0,96	1,98	2816	87	3,09
Layer thickness = 0.3 mm						
0	19,16	0,54	2,82	1825	24	1,32
15	23,02	0,28	1,23	1856	58	3,13
30	23,97	1,15	4,79	1968	106	5,39
45	26,36	0,25	0,95	2037	42	2,06
60	31,57	1,59	5,03	2320	48	2,07
75	36,16	0,15	0,41	2516	39	1,55
90	44,57	1,25	2,8	2683	19	0,71

Table 1.8: Tensile strength and Young's modulus results with STDEV (standard deviation) [9].

For all layer thickness in Table 1.8 the build orientation such that the fibers are perpendicular to the axial force, decreases tensile strength and stiffness. When 3D-printing, it is important that the layers are parallel to the stress and forces to achieve greater strength and stiffness. From Table 1.8 printing layers parallel to the forces acting on the test specimen and low layer thickness is the best solution for stiffness and strength.

Valean et al. from 2020 *Effect of manufacturing parameters on tensile properties of FDM printed specimens* [10]

Paper conducts a tensile test on dog-bone specimen with an infill density of 100% with infill pattern lines with raster angles of $\pm 45^\circ$. Paper changes thickness, width, and different flat orientation on printer bed changes mechanical characteristics. There are three orientation on the printer bed for 3D-printing the dog-bones, first specimen are along the x -axis, second 45° of the x -axis, and the third along the y -axis. Thickness of the specimen ranges from 1.25 mm to 8 mm, and width from 6 mm to 13 mm, see Figure 1.12.

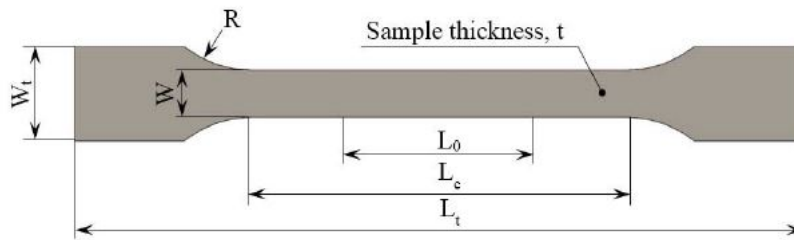


Figure 1.12: Dog-bone dimension specifications [10].

Paper considers more on major dimension other than infill configurations of 3D-printed parts. Build orientation on FDM 3D-printed parts is significant to mechanical properties. Printing parts that has a building orientation that is not parallel to x - or y -axis on the printer bed have a negative impact on mechanical properties.

Nasirov et al. from 2020 *Prediction of mechanical properties of fused filament fabricated structures via asymptotic homogenization* [11]

Paper consider three infill patterns line, grid, and, gyroid for FDM 3D-printed parts where the paper will predict mechanical properties by asymptotic homogenization. Mechanical properties are verified using micro-structural- and experimental- analysis. Printing settings are nozzle diameter 0.4 mm and layer height of 0.2 mm and uses PLA as printing material. For the researches to determine tensile strength and Young's modulus different setups for infill patterns and orientation on printing bed was documented. The test specimen are orientated on the printing bed vertical or horizontal and for infill patterns such as line and grid has a set of raster angles. Line pattern has unidirectional raster angle and $[0, 90]$ degrees layup while grid has 0° and 45° angles, see Figure 1.13.

For 3D-printed parts that has build orientation vertical is denoted as V for line-, and L for grid-pattern, while T, 0, 90, $[0, 90]$ and $[90, 0]$ gives that the parts is printed horizontal. Table 1.9 gives Young's modulus and the tensile strength from FDM 3D-printed parts with different raster angles and orientation on the printer bed. All 3D-printed parts in the experimental results given in Table 1.9 has an infill density of 100%.

Experiment results shows that the strongest configuration is line unidirectional with raster angle 0° . Homogenized Young's modulus for all infill configurations is given in Table 1.10.

Calculated Young's modulus using homogenization theory and the use of finite element method (FEM) has given varied results compared against experimental results. Papers reason the cause

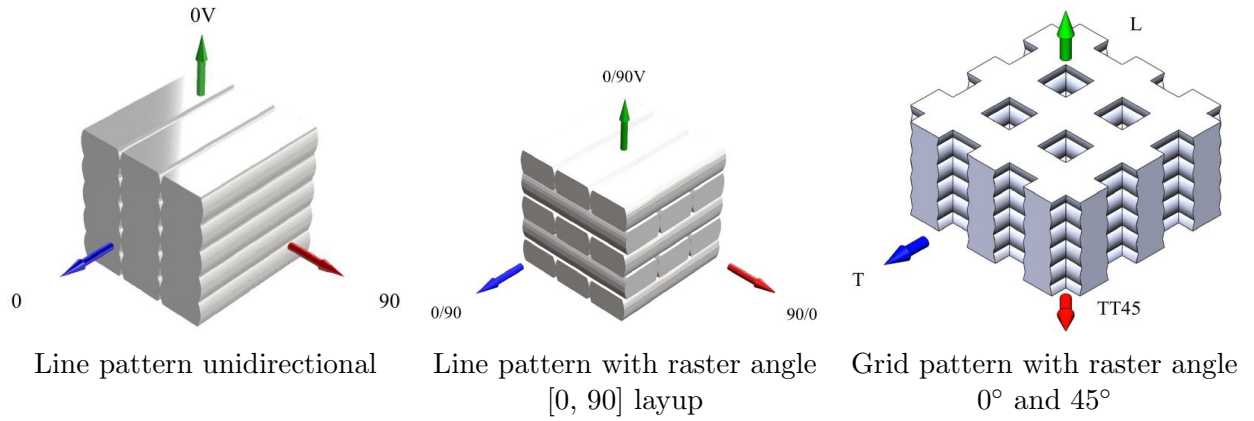


Figure 1.13: Different build orientation and raster angles for line- and grid-pattern [11].

Orientation	Young's Modulus (Gpa)		Tensile Strength (MPa)		
	Mean	Deviation	Mean	Deviation	
Neat PLA	3,5	-	70	-	
Line Unidirectional	0	3,067	0,033	50,59	0,098
	90	2,353	0,076	21,03	0,06
	V	2,064	0,151	18,82	0,318
Line 0, 90	0/90	2,835	0,056	37,73	0,084
	90/0	2,791	0,138	36,11	0,084
	0/90/V	2,653	0,245	26,08	0,57
Grid	L	2,7	0,179	27,138	4,166
	T	2,075	0,081	17,188	4,95
	TT45	1,777	0,183	15,969	3,888

Table 1.9: Experimental results from tensile test of test specimen [11].

Infill	Orientation	Experimental Young's modulus (GPa)	Homogenized Young Modulus (GPa)			
			Ideal RVE	Error (%)	Actual RVE	Error (%)
DU Line	0	3.067	3.349	9.222	3.102	1.159
	90	2.353	2.21	-6.066	2.197	-6.629
	0V	2.064	3.287	59.241	2.453	18.819
0/90 Line	0/90	2.835	2.976	4.978	2.625	-7.396
	90/0	2.791	2.976	6.628	2.625	-5.956
	0/90V	2.653	3.182	19.942	1.764	-33.531
Grid Infill	L	2.7	2.519	-6.705	-	-
	T	2.075	1.883	-9.252	-	-
	TT45	1.777	1.097	-38.260	-	-

Table 1.10: Experimental vs homogenized properties for RVE [11].

of voids and other imperfections that occurs in the FDM 3D-printed parts under printing. Construction of representative volume element (RVE) models that is exact as the real part is difficult to make. Although the actual RVE results are generally closer to the experimental results. Results from Table 1.10 most of the Young's modules from the ideal RVE model is greater than the experimental results which is *bad* in engineering practices as a higher Young's modulus might give that the structure stiffness is greater than it actually is.

Paper documented a method of calculating mechanical properties of FDM 3D-printed parts and compared experimental results with FEM homogenization method. Results shown gave an insight to how complex infill configurations can be to predict mechanical behaviour.

Chapter 2

Design Requirements

2.1 Standards Used

FDM 3D-printed parts is defined as cellular material because of voids in the parts created from nozzle extrusion or infill patterns. The standard for testing tensile properties of cellular plastic material is ISO 1926:2009. This standard states that the dimensions of dog-bone is to be in Figure 2.1.

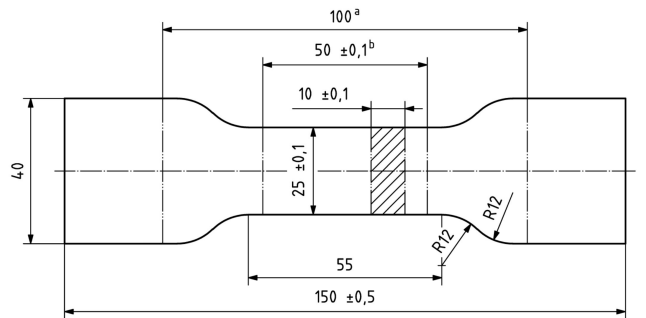


Figure 2.1: Dog-bone dimension from ISO 1926:2009 with gauge length of 50 mm. [12].

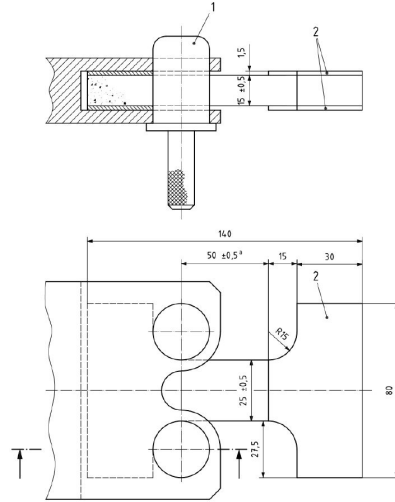
3D-printed parts are brittle depending on the material used in 3D-printing. If the clamps that holds and pulls the test specimen can cause compressive stress beyond the yield stress of the material of the test specimen. When mounting test specimen into the test machine, it is important that the specimen is not damaged before any test is completed. Since this would have an impact on mechanical properties. ISO 1926 cover this aspect as well with different a method to avoid fracture from the clamps on the test machine. With reinforcing the dog-bones with metal plates (preferably aluminium plates) where the clamps holds a fixture for the dog-bone and use four cylinders to pull dog-bone with reinforced metal plates, see Figure 2.2.

After the manufacturing of the dog-bones, measurement of the test specimen must be done in accordance to NS-EN ISO 1923:1981 to ensure that the specimen are within specification. NS-EN ISO 1923:1981 states guidelines on how to measure cellular solids. Method of measure the specimen is done by the use micrometer with five points to measure for width and thickness. Each point shall be measured three times minimum [13].

Determination of tensile mechanical properties ISO 1926 and NS-EN ISO 527-1:2012 *Plastic: Determination of tensile properties* are used. Elongation e is expressed as a percentage of original gauge length (50 mm) of dog-bone and is given by [12].

$$e = \frac{100\Delta L}{L}. \quad (2.1.1)$$

Here L is the gauge length of the dog-bone and ΔL is increase of gauge length under testing both is given in mm. Determination of tensile strength, σ_{max} expressed in MPa is calculated by



1 Cylinder that pulls on metal plates and test specimen
2 Metal plates glued to test specimen

Figure 2.2: Dog-bone specimen with dimensions for tensile test with reinforced rigid cellular plastic with gauge length 50 mm [12].

[12].

$$\sigma_{max} = \frac{F_{max}}{bh} \quad (2.1.2)$$

F_{max} is the maximum force under tensile testing given in Newtons. Width is b , and the height h both expressed in mm. Methods of calculating strains, tensile modulus, and Poisson's ratio ISO 527-1:2012 *Plastic: Determination of tensile properties part 1: general principals* are used. With tensile testing without an extensometer nominal strain is calculated by [14].

$$\varepsilon_t = \frac{\Delta L}{L}. \quad (2.1.3)$$

Here ε_t is the nominal strain in the direction of the axial force which is dimensionless. ΔL and L is the same as in formula (2.1.1). There are two methods of calculating the tensile modulus, method A [14].

$$E_t = \frac{\sigma_2 - \sigma_1}{\varepsilon_2 - \varepsilon_1}. \quad (2.1.4)$$

E_t is the calculated tensile modulus in MPa. σ_1 is the stress from stress-strain curve for $\varepsilon_t = 0.0005$, and σ_2 is the stress from stress-strain curve for when $\varepsilon_t = 0.0025$. Method B uses computer software to calculate the tensile modulus by linear regression [14].

$$E_t = \frac{d\sigma}{d\varepsilon}. \quad (2.1.5)$$

The slope of $d\sigma/d\varepsilon$ is a least-square regression line that fit to the stress-strain curve for the strain interval $0.0005 \leq \varepsilon \leq 0.0025$. To calculate the regression line the least-square method is mentioned. The formula to calculate this is given as [15].

$$\begin{pmatrix} \sum_{i=1}^n x_i^2 & \sum_{i=1}^n x_i \\ \sum_{i=1}^n x_i & n \end{pmatrix} \begin{bmatrix} a \\ b \end{bmatrix} = \begin{pmatrix} \sum_{i=1}^n x_i y_i \\ \sum_{i=1}^n y_i \end{pmatrix}. \quad (2.1.6)$$

Here x_i , y_i is measured points from tensile test in stress-strain curve. x_i is the strain, y_i is the stress, and n is the number of points used in least-square method. Linear regression line is on the form $y = ax + b$ where a is the tensile modulus E_t in formula (2.1.5).

Poisson's ratio needs measurement of the increase in gauge length and decrease in width or thickness of test specimen. Poisson's ratio is calculated by using the formulae (2.1.7) [14].

$$\nu = -\frac{L\Delta n}{n\Delta L}. \quad (2.1.7)$$

Here ν is the Poisson's ratio and is dimensionless. ΔL and L is the same as in formula (2.1.1) and (2.1.3). n is the original width or thickness in direction of perpendicular to the axial force. Δn is the change in width or thickness.

It is possible to measure by hand for determining the Poisson's ratio, but ISO 527 states that a plot of Δn_0 for x-axis and ΔL_0 for y-axis, and determine the slope $\Delta n_0/\Delta L_0$ by linear least-square regression analysis. The slope should be in the interval $0.003 \leq \varepsilon \leq \varepsilon_y$ or in other words above the interval for when tensile modulus is determined and before yielding.

2.2 Experimental Setup & Test Equipment

Tensile test machine is manufacture from Material Test Systems (MTS). Test machine is designed to perform material test for metallic material or material with high tensile properties.



Figure 2.3: Material test machine used to perform material test.

Load frame for test machine is model number 311.31 which has the load capacity of 1000 kN. Hydraulic actuator which applies the force to perform material test. Has the model number 244.52S. The hydraulic actuator gives a maximum force of 1000 kN and has a static stroke length of 152.4 mm. To hold the specimen there are two hydraulic wedge grips in 647 series model number 647.37. This model of hydraulic wedge grip has a maximum hydraulic pre-load grip pressure of 77 MPa.

For tensile testing the extensometers was not available to use instead the internal length transducer was used for measuring displacement in testing. Calibration for internal displacement length transducer has an % error lower than 0.25%. Calibration of load cell for maximum force of 100 kN with calibration are being from 20 kN to 100 kN. Where the measurement of force has an error of ± 0.585 kN for axial force.

2.3 Manufacture of 3D-printed Specimens

To manufacture dog-bone specimen two types of 3D-printers is used. The models is Ultimaker 2+ and Ultimaker 2 Extended+. The difference between the two printers are that the extended model has a higher z-axis. For material to print test specimen the chosen material is Though PLA from Ultimaker. The filament has a diameter of 2.85 mm. Technical data sheet provided by Ultimaker gives the mechanical properties in Table 2.1. The complete Technical Data Sheet is found in Appendix E.

	Orientation		
	XY (Flat)	YZ (Side)	Z (Up)
Tensile modulus [<i>MPa</i>]	2797 ±151	2797 ±99	2696±180
Tensile stress at yield [<i>MPa</i>]	45.3±2	47.5±0.5	33.4±0.5
Tensile stress at break [<i>MPa</i>]	27.5±7.8	31.3±4.4	32.5±0.8
Elongation at yield [%]	3.2 ±0.0	3.5 ±	2.6 ±0.1
Elongation at break [%]	9.4 ±1.9	8.2 ±1.8	3.1 ±0.7

Table 2.1: Technical data sheet for Thought PLA from Ultimaker [16].

Orientation is shown in Figure 2.4.

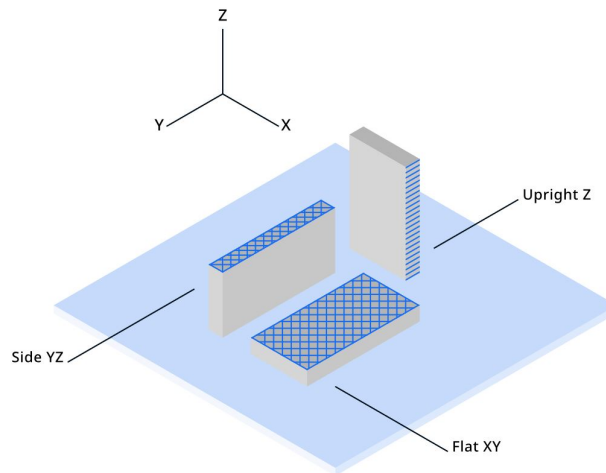


Figure 2.4: Build orientation from technical data sheet for though PLA [16].

Infill configurations is somewhat limited described in the technical data sheet from Ultimaker. Whats mentioned is that the infill percentage is 100% and a layer height of 0.15 mm. The test specimen are printed as rectangular pieces such as they are shown in Figure 2.4 with dimensions $215 \times 20 \times 4$ ($L \times W \times H$) in mm.

All printing parameters for 3D-printing of test specimen is found in Appendix B. For all dog-bone specimen the layer height is set to be 0.1 mm for all layers. With a single line as wall which gives a wall thickness to be 0.4 mm. For all test specimen the floor and roof are not printed. The temperature of nozzle and printing bed is determined by the printer for PLA material. With nozzle temperature at 210 °C and printing bed temperature of 60 °C.

For dog-bone specimen that has line pattern there are two groups of test specimen that has unidirectional raster angles. First one has raster angle 90° in Ultimaker Cura, and in CLT the angle will be 0°. The fibers will be parallel to the axial force in tensile testing. Second has the

raster angle 0° in Ultimaker Cura and for CLT computation the angle is 90° . Such that the fibers are orientated perpendicular to the axial force acting on the dog-bone specimen. To determine the shear moduli for 3D-printed parts where the layers have line patterns. It is necessary to manufacture dog-bone specimen with raster angle $\pm 45^\circ$ in Ultimaker Cura and the raster angles are the same for CLT computation. These specimen by performing a tensile test would be able to determine the shear moduli for line pattern with 100% infill. As these three groups of specimen gives the longitudinal-, transverse-, and shear-moduli. It should then be possible to determine the tensile modulus of a 3D-printed part that uses different raster angles with line pattern and 100% infill using CLT theory. To validate CLT calculations the raster angles in Ultimaker Cura is $[90, 120, 60, 150, 30, 90, 0]$ and for CLT it is $[0, \pm 30, \pm 60, 0, 90]_R$. Subscript R means that the angles are repeating through all layers.

2.4 Build of fixture for tensile testing

Since most of FDM 3D-printed parts has voids even for infill configurations with 100% infill density. It has been chosen to follow ISO 1926 standard for plastic cellular solids for determination of tensile properties. For infill configurations with low infill density the jaws for tensile test machine can easily fracture or damage the test specimen. To not crush the test specimen before any testing it is possible to build an assembly that transfers the axial load without any compression on dog-bones. Illustrated in Figure 2.2.

To construct the assembly that transfers forces from the tensile test machine to the test specimen. There was designed a simple concept for *Grov laben* on UiT campus Narvik to manufacture two fixtures. To be able to perform tensile test without compressive forces acting on dog-bones specimen.

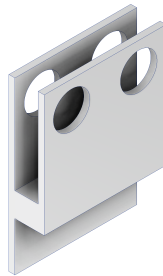


Figure 2.5: 3D-model concept for fixture of tensile test specimen.

The concept shown in Figure 2.5 is made out a solid metal block. Which is time consuming and wasteful with material to produce. It was then put forward from Morten M. Olavsbråten that works in *Grov laben* to use to steel plates and aluminium block with thickness of 5 mm and 19 mm respectively. To fix the steel plates and aluminum block fasteners are used with the help of friction between the surfaces.

Dimensions for fixture are mostly general and does not need high precision to be effective. To be able to mount dog-bone into the fixture it is important that there is at least a gap between the steel plates of 19 mm. Since the thickness of dog-bone is 15 mm plus two metal plates that has a thickness of 1.5 mm. The cylinders that actually pulls on the test specimen needs precision such that they are flush with the radii on dog-bone. The holes in metal plates for the cylinder to be placed in must also be as perpendicular to the axial force from the tensile test machine.

The metal plates that is adherent to the dog-bones has a simple geometry as illustrated in Figure 2.7.

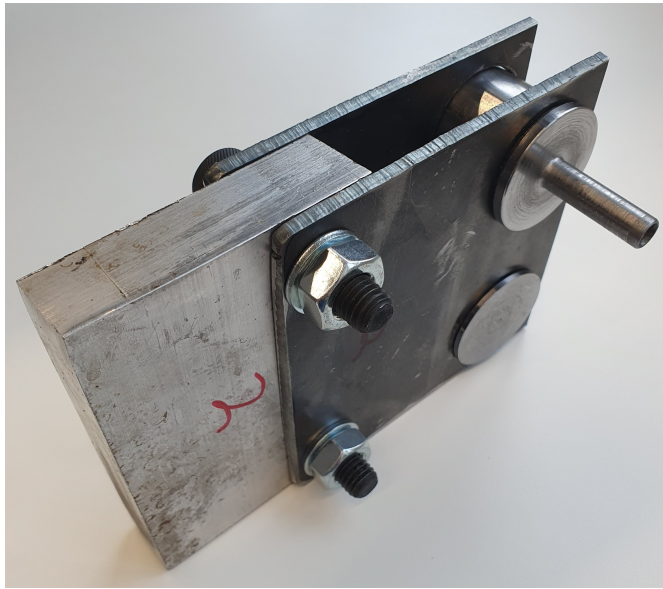


Figure 2.6: Produced assembly of fixture for cellular solid test specimen.

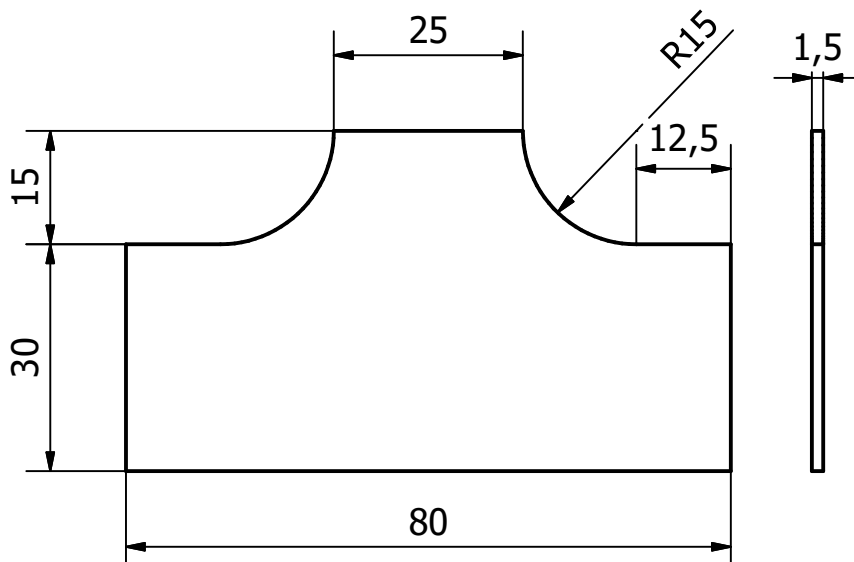


Figure 2.7: Metal plates that reinforces the dog-bone specimen, dimensions in mm.

To be able to run one test with the fixture there needs to be created 20 plates with the dimensions showed in Figure 2.7. This is because there are four plates that is glued to the test specimen and there are five test specimen in each tensile test. To achieve the rectangular dimension is easy by cutting the plates, however the radii is more problematic and time consuming. There are several plates that needs to be manufactured which makes setup to create one plate time consuming. With an discussion with *Grov laben* supervisor Øyvind Søråas, employee Marius Wang, Erlend Entner, and Guy Beeri Mauseth on how to produce the metal plates. Methods of manufacturing were: belt grinder, angle grinder, milling machine, drill-bench, and plasma-cutter. The plates most important feature is the radii such that the axial force is even distributed and good contact with the cylinders under testing. In agreement angle grinder would yield a worse radius than all other manufacturing methods. For milling and drill-bench the setup to create the radii on the plates is time consuming. Since the plates are 1.5 mm in thickness they are easy to bend in a vise or other fixture. Mounting the plates in a vise with the plates being stacked the rectangular form of the plates must be precise such that the plates does not move under milling or drilling. Since the setup is time consuming to produce on plate milling and drilling was deemed not suitable for the manufacturing of the plates. Belt grinding is also time consuming since it

would only be able to manufacture one at a time. There was also a concern of damaging the belts since each operation needs to remove $27.5 \cdot 15 \cdot 1.5mm^3$ material. Last manufacturing method is then plasma-cutter. *Grov laben* has a programmable plasma-cutter where it is possible to code in how it should cut out the metal plates. With this technique the precision is high and setup time is low. Since it only needs to place a metal plate on the plasma-cutters bed and press play. Manufacturing of metal plates is then done with programmable plasma-cutter.

To glue the plates onto test specimen Loctite 431 is chosen since the tensile shear strength is high enough. The tensile breaking force of solid PLA material with the dimension showed in Figure 2.2 has breaking force of 26 KN.

Chapter 3

Analytical Mathematical Modeling

3.1 Classical Laminate Theory

For this thesis, the analytical method of calculations is Classical Laminate Theory. The justification behind this decision is that FDM produces parts on a layer-by-layer basis, where each layer can be manufactured in different directions to obtain desired mechanical properties. CLT offers methods to analytically evaluate each layer to determine tensile and shear modulus, as well as other engineering constants. This thesis will evaluate a laminate that is an FDM 3D-printed part. The method of evaluating a laminate involves determining the micromechanics of a ply, in other words, determining the engineering constants for each ply. For plies with infill patterns such as grid, there are three different sources to determine the mechanical properties of a ply, which are described in Section 3.1.2 and in references [2], [17], [18]. Once the micromechanics of a ply are determined, it is possible to evaluate the macromechanics of the laminate, which will be described in detail in Section 3.1.1.

Firstly, some assumptions (Kirchoff hypothesis) for when CLT is used are cited from [19, p.6-7].

1. Each lamina is considered quasi-homogeneous and orthotropic (in general, the properties can range from isotropic to anisotropic).
2. Each ply or lamina are flat.
3. The laminate consists of perfectly bonded laminae and the bond lines are infinitesimally thin as well as non-shear-deformable.
4. The laminate is thin, i.e., the thickness is small compared to the lateral dimensions, and represents a state of plane stress.
5. Displacements (in thickness and lateral directions) are small compared to the thickness of the laminate.
6. Displacements are continuous throughout the laminate (non-shear-deformable bond lines).
7. In-plane displacements are linear functions of the thickness.
8. Shear strains in planes perpendicular to the middle surface are negligible.
9. Assumptions 7 and 8 imply that a line originally *straight* and *perpendicular* to the laminate middle surface remains so after deformation.
10. Kinematics and constitutive relations are linear.
11. Normal distances from the middle surface remain constant. Thus, the transverse normal strain is negligible compared to the in-plane normal strains.

The points above outline the assumptions under which CLT can be applied to a laminate to evaluate mechanical properties. All laminates are built up by plies or laminae. Each ply is often a composite material consisting of fibers and a matrix (commonly epoxy is used as the matrix to bind fibers in the transverse direction). The fibers can be oriented in unidirectional, woven, randomly distributed short fibers, or particles (such as graphene). For FDM 3D-printing, PLA serves as the fiber, and through pattern selection in Ultimaker Cura, unidirectional fiber are lines, and woven fibers are patterns such as grid.

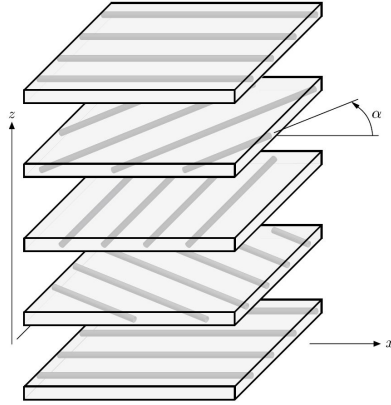


Figure 3.1: Laminate built up by five plies with unidirectional fibers [19].

Figure 3.1 illustrates how a laminate is built up by each ply. The notation of orientation for each ply in a laminate is denoted with brackets [.../.../...]. The input is the α value illustrated in Figure 3.1. It's important to note that for CLT, the x -axis is at 0° , whereas Ultimaker Cura uses the y -axis for 0° . For this master thesis, the test specimen has between 100 to 150 layers that are repeating. Therefore, the repeating angles are used with a subscript of R . For example, a line pattern with raster angles 0, 30, -30, -45, 45, becomes $[0/\pm 30/\mp 45]_R$ for all 100 or 150 layers. The angles of the ply orientation are given from the lowest layer first and continue to the top layer. This thesis will not delve into how CLT is developed or constructed but rather focuses on its application. For further explanation, see [19].

Each ply in a laminate is defined as layer k , with n plies, so layer k is in the region $1 \leq k \leq n$. The thickness of a ply is given as.

$$t_k = z_k - z_{k-1}.$$

Thickness of a whole laminate is calculated by the formula.

$$t = \sum_{k=1}^n t_k.$$

Figure 3.2 shows that layers are counted from lowest ply and up to the top. For when $z = 0$ is in the middle of the laminate in zy -plane. For FDM 3D-printed parts the plies thickness is the same for all layers with the option on selecting layer thickness in Ultimaker Cura.

3.1.1 Macromechanics of Classical Laminate Theory

Macromechanics of CLT views the whole laminate and evaluates them by directional mechanical properties given by fibers and matrix. For evaluation of mechanical properties of a single ply see Section 3.1.2. Each ply has mechanical properties denoted in 1 and 2 direction, see illustration in Figure 3.3.

Figure 3.3 shows a ply with orthotropic mechanical properties, and since there is plane stress for each ply, we have that [20, Video:L-03] [19].

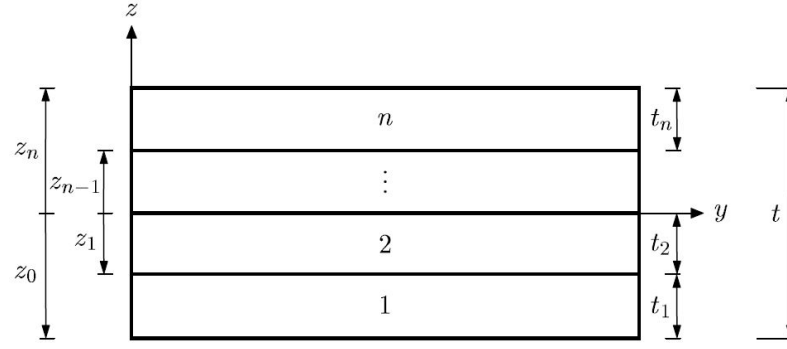


Figure 3.2: Geometry of a laminate with n layers [19].

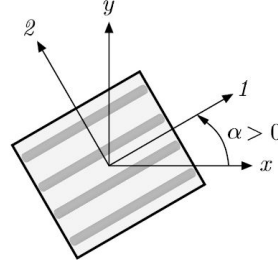


Figure 3.3: Illustration of a ply and its local coordinate mechanical direction relative to the global coordinate system [19].

$$\begin{pmatrix} \sigma_1 \\ \sigma_2 \\ \tau_{12} \end{pmatrix} = \begin{bmatrix} Q_{11} & Q_{12} & 0 \\ Q_{12} & Q_{22} & 0 \\ 0 & 0 & Q_{66} \end{bmatrix} \begin{pmatrix} \varepsilon_1 \\ \varepsilon_2 \\ \gamma_{12} \end{pmatrix}, \quad (3.1.1)$$

Here, the Q matrix for orthotropic material is given by formula (3.1.2) [20].

$$Q = \begin{bmatrix} \frac{E_1}{1-\nu_{12}\nu_{21}} & \frac{\nu_{12}E_1}{1-\nu_{12}\nu_{21}} & 0 \\ \frac{\nu_{12}E_1}{1-\nu_{12}\nu_{21}} & \frac{E_2}{1-\nu_{12}\nu_{21}} & 0 \\ 0 & 0 & G_{12} \end{bmatrix}. \quad (3.1.2)$$

Longitudinal modulus is E_1 , E_2 is the transverse modulus, and the local shear modulus is G_{12} all is given in MPa. The major Poisson's ratio is ν_{12} , and the minor Poisson's ratio ν_{21} . Since the Q matrix describes the stiffness of the material in 12-direction it needs to be transformed to the xy -direction. The new matrix that is calculated is \bar{Q} that gives the expression [20].

$$\sigma_{xy} = \bar{Q}\varepsilon_{xy}, \quad (3.1.3)$$

Where \bar{Q} is defined as [20, Video:L-04].

$$\bar{Q} = T^{-1}QRTR^{-1}. \quad (3.1.4)$$

Where matrix T is an angle transform matrix that transform from xy -direction to 12-direction and is defined in formula (3.1.5). T^{-1} is angle transform matrix from 12-direction to xy -direction defined in formula (3.1.6). Matrix R is factor matrix that changes from true strain to engineering strains and is calculated with formula (3.1.7). Matrix Q is the stiffness matrix for a ply and is calculated by formula (3.1.2).

$$T = \begin{bmatrix} \cos^2 \alpha & \sin^2 \alpha & 2 \sin \alpha \cos \alpha \\ \sin^2 \alpha & \cos^2 \alpha & -2 \sin \alpha \cos \alpha \\ -\sin \alpha \cos \alpha & \sin \alpha \cos \alpha & \cos^2 \alpha - \sin^2 \alpha \end{bmatrix}, \quad (3.1.5)$$

$$T^{-1} = \begin{bmatrix} \cos^2 \alpha & \sin^2 \alpha & -2 \sin \alpha \cos \alpha \\ \sin^2 \alpha & \cos^2 \alpha & 2 \sin \alpha \cos \alpha \\ \sin \alpha \cos \alpha & -\sin \alpha \cos \alpha & \cos^2 \alpha - \sin^2 \alpha \end{bmatrix}, \quad (3.1.6)$$

$$R = \begin{bmatrix} 1 & 0 & 0 \\ 0 & 1 & 0 \\ 0 & 0 & 2 \end{bmatrix}. \quad (3.1.7)$$

As \bar{Q} is found for each layer in a laminate. Next step is to evaluate the laminate by external forces and moments. From [20] the strain in a layer the strain can be expressed as.

$$\begin{pmatrix} \varepsilon_x \\ \varepsilon_y \\ \gamma_{xy} \end{pmatrix}_k = \begin{pmatrix} \varepsilon_x^0 \\ \varepsilon_y^0 \\ \gamma_{xy}^0 \end{pmatrix} + z_k \begin{pmatrix} \kappa_x \\ \kappa_y \\ \kappa_{xy} \end{pmatrix}. \quad (3.1.8)$$

Inserting equation (3.1.8) into equation (3.1.3).

$$\begin{pmatrix} \sigma_x \\ \sigma_y \\ \tau_{xy} \end{pmatrix}_k = \begin{bmatrix} \bar{Q}_{11} & \bar{Q}_{12} & \bar{Q}_{16} \\ \bar{Q}_{12} & \bar{Q}_{22} & \bar{Q}_{26} \\ \bar{Q}_{16} & \bar{Q}_{26} & \bar{Q}_{66} \end{bmatrix}_k \left[\begin{pmatrix} \varepsilon_x^0 \\ \varepsilon_y^0 \\ \gamma_{xy}^0 \end{pmatrix} + z_k \begin{pmatrix} \kappa_x \\ \kappa_y \\ \kappa_{xy} \end{pmatrix} \right]. \quad (3.1.9)$$

The axial forces and moments are given as formulas (3.1.10) and (3.1.11) [20].

$$\begin{pmatrix} N_x \\ N_y \\ N_{xy} \end{pmatrix} = \int_{-t/2}^{t/2} \begin{pmatrix} \sigma_x \\ \sigma_y \\ \tau_{xy} \end{pmatrix} dz, \quad (3.1.10)$$

$$\begin{pmatrix} M_x \\ M_y \\ M_{xy} \end{pmatrix} = \int_{-t/2}^{t/2} \begin{pmatrix} \sigma_x \\ \sigma_y \\ \tau_{xy} \end{pmatrix} z dz. \quad (3.1.11)$$

As the integration is through the whole laminate the integration has to be done layer-by-layer basis, and then equations (3.1.10) and (3.1.11) becomes.

$$\begin{pmatrix} N_x \\ N_y \\ N_{xy} \end{pmatrix} = \sum_{k=1}^n \int_{z_{k-1}}^{z_k} \begin{pmatrix} \sigma_x \\ \sigma_y \\ \tau_{xy} \end{pmatrix} dz = \sum_{k=1}^n \begin{bmatrix} \bar{Q}_{11} & \bar{Q}_{12} & \bar{Q}_{16} \\ \bar{Q}_{12} & \bar{Q}_{22} & \bar{Q}_{26} \\ \bar{Q}_{16} & \bar{Q}_{26} & \bar{Q}_{66} \end{bmatrix}_k \left[\int_{z_{k-1}}^{z_k} \begin{pmatrix} \varepsilon_x^0 \\ \varepsilon_y^0 \\ \gamma_{xy}^0 \end{pmatrix} dz + \int_{z_{k-1}}^{z_k} z \begin{pmatrix} \kappa_x \\ \kappa_y \\ \kappa_{xy} \end{pmatrix} dz \right],$$

$$\begin{pmatrix} M_x \\ M_y \\ M_{xy} \end{pmatrix} = \sum_{k=1}^n \int_{z_{k-1}}^{z_k} \begin{pmatrix} \sigma_x \\ \sigma_y \\ \tau_{xy} \end{pmatrix} z dz = \sum_{k=1}^n \begin{bmatrix} \bar{Q}_{11} & \bar{Q}_{12} & \bar{Q}_{16} \\ \bar{Q}_{12} & \bar{Q}_{22} & \bar{Q}_{26} \\ \bar{Q}_{16} & \bar{Q}_{26} & \bar{Q}_{66} \end{bmatrix}_k \left[\int_{z_{k-1}}^{z_k} \begin{pmatrix} \varepsilon_x^0 \\ \varepsilon_y^0 \\ \gamma_{xy}^0 \end{pmatrix} z dz + \int_{z_{k-1}}^{z_k} \begin{pmatrix} \kappa_x \\ \kappa_y \\ \kappa_{xy} \end{pmatrix} z^2 dz \right].$$

The two equations above is rewritten as formula (3.1.12) [20].

$$\begin{pmatrix} N_x \\ N_y \\ N_{xy} \\ M_x \\ M_y \\ M_{xy} \end{pmatrix} = \begin{bmatrix} A_{11} & A_{12} & A_{16} & B_{11} & B_{12} & B_{16} \\ A_{12} & A_{22} & A_{26} & B_{12} & B_{22} & B_{26} \\ A_{16} & A_{26} & A_{66} & B_{16} & B_{26} & B_{66} \\ B_{11} & B_{12} & B_{16} & D_{11} & D_{12} & D_{16} \\ B_{12} & B_{22} & B_{26} & D_{12} & D_{22} & D_{26} \\ B_{16} & B_{26} & B_{66} & D_{16} & D_{26} & D_{66} \end{bmatrix} \begin{pmatrix} \varepsilon_x^0 \\ \varepsilon_y^0 \\ \gamma_{xy}^0 \\ \kappa_x \\ \kappa_y \\ \kappa_{xy} \end{pmatrix}. \quad (3.1.12)$$

Matrix that is build up by A , B , and D is simply noted as C . Where every entry in A , B , and D is given by [20].

$$A_{ij} = \sum_{k=1}^n (\bar{Q}_{ij})_k (z_k - z_{k-1}), \quad (3.1.13)$$

$$B_{ij} = \frac{1}{2} \sum_{k=1}^n (\bar{Q}_{ij})_k (z_k^2 - z_{k-1}^2), \quad (3.1.14)$$

$$D_{ij} = \frac{1}{3} \sum_{k=1}^n (\bar{Q}_{ij})_k (z_k^3 - z_{k-1}^3). \quad (3.1.15)$$

Laminates with a symmetric layup of layers have the property that the B matrix has all entries is equal to zero in its 3×3 matrix. For example, a laminate with four layers at angles $[0, 45, 45, 0]$ is symmetric. In such laminates, the entries of the B matrix are zero. After performing the calculations outlined above, it becomes possible to determine the effective moduli and other engineering constants. For symmetric laminates, the formulas are provided by [21]. In these formulas, the constant h represents the height of the laminate.

$$\begin{aligned} E_x &= \frac{1}{h} \left(A_{11} + \frac{A_{66} A_{12}^2 - 2 A_{12} A_{16} A_{26} + A_{22} A_{16}^2}{A_{26}^2 - A_{22} A_{66}} \right), \\ E_y &= \frac{1}{h} \left(A_{22} + \frac{A_{66} A_{12}^2 - 2 A_{12} A_{16} A_{26} + A_{11} A_{26}^2}{A_{16}^2 - A_{11} A_{66}} \right), \\ G_{xy} &= \frac{1}{h} \left(A_{66} + \frac{A_{11} A_{26}^2 - 2 A_{12} A_{16} A_{26} + A_{22} A_{16}^2}{A_{12}^2 - A_{11} A_{22}} \right), \\ \nu_{xy} &= \frac{A_{12} A_{66} - A_{16} A_{26}}{A_{22} A_{66} - A_{26}^2}, \\ \nu_{yx} &= \frac{A_{16} A_{26} - A_{12} A_{66}}{A_{16}^2 - A_{11} A_{66}}. \end{aligned}$$

However, there's a simpler approach to calculate various moduli for symmetric laminates. To find the tensile modulus in the x -direction, denoted as E_x , we can utilize the property [21].

$$E_x = \frac{N_x}{h \varepsilon_x}.$$

Since the entries in B matrix is zero, the relation bellow applies.

$$\begin{pmatrix} N_x \\ 0 \\ 0 \end{pmatrix} = \begin{bmatrix} A_{11} & A_{12} & A_{16} \\ A_{12} & A_{22} & A_{26} \\ A_{16} & A_{26} & A_{66} \end{bmatrix} \begin{pmatrix} \varepsilon_x^0 \\ \varepsilon_y^0 \\ \gamma_{xy}^0 \end{pmatrix} \implies N_x \begin{bmatrix} A_{11} & A_{12} & A_{16} \\ A_{12} & A_{22} & A_{26} \\ A_{16} & A_{26} & A_{66} \end{bmatrix}^{-1} \begin{pmatrix} 1 \\ 0 \\ 0 \end{pmatrix} = \begin{pmatrix} \varepsilon_x^0 \\ \varepsilon_y^0 \\ \gamma_{xy}^0 \end{pmatrix}.$$

Let X be a 3x1 matrix that is defined as.

$$\begin{aligned} (X)_{E_x} &= \begin{pmatrix} X_1 \\ X_2 \\ X_3 \end{pmatrix}_{E_x} = \begin{bmatrix} A_{11} & A_{12} & A_{16} \\ A_{12} & A_{22} & A_{26} \\ A_{16} & A_{26} & A_{66} \end{bmatrix}^{-1} \begin{pmatrix} 1 \\ 0 \\ 0 \end{pmatrix}, \\ (X)_{E_y} &= \begin{pmatrix} X_1 \\ X_2 \\ X_3 \end{pmatrix}_{E_y} = \begin{bmatrix} A_{11} & A_{12} & A_{16} \\ A_{12} & A_{22} & A_{26} \\ A_{16} & A_{26} & A_{66} \end{bmatrix}^{-1} \begin{pmatrix} 0 \\ 1 \\ 0 \end{pmatrix}, \\ (X)_{G_{xy}} &= \begin{pmatrix} X_1 \\ X_2 \\ X_3 \end{pmatrix}_{G_{xy}} = \begin{bmatrix} A_{11} & A_{12} & A_{16} \\ A_{12} & A_{22} & A_{26} \\ A_{16} & A_{26} & A_{66} \end{bmatrix}^{-1} \begin{pmatrix} 0 \\ 0 \\ 1 \end{pmatrix}. \end{aligned}$$

Then the relation exist.

$$\begin{aligned} N_x \cdot (X_1)_{E_x} &= \varepsilon_x^0 \implies \frac{N_x}{\varepsilon_x^0} = \frac{1}{(X_1)_{E_x}}, \\ E_x &= \frac{N_x}{h\varepsilon_x^0} = \frac{1}{h(X_1)_{E_x}}. \end{aligned} \tag{3.1.16}$$

By doing the same steps as above to derive formulas for E_y and G_{xy} .

$$E_y = \frac{1}{h(X_2)_{E_y}}, \tag{3.1.17}$$

$$G_{xy} = \frac{1}{h(X_3)_{G_{xy}}}. \tag{3.1.18}$$

Remember that when deriving the formulas for y-direction and the shear moduli that $[0 \ N_y \ 0]^T$ and $[0 \ 0 \ N_{xy}]^T$ matrix is used to determine X matrix respectively. For determining Poisson's ratio in major and minor direction.

$$\nu_{xy} = -\frac{(X_2)_{E_x}}{(X_1)_{E_x}}, \tag{3.1.19}$$

$$\nu_{yx} = -\frac{(X_1)_{E_y}}{(X_2)_{E_y}}. \tag{3.1.20}$$

For unsymmetrical laminate the B matrix is not equal to zero. Equations to determine engineering constants are given by [21].

$$E_x = \frac{1}{h} \frac{\det C}{\begin{vmatrix} A_{22} & A_{26} & B_{12} & B_{22} & B_{26} \\ A_{26} & A_{66} & B_{16} & B_{26} & B_{66} \\ B_{12} & B_{16} & D_{11} & D_{12} & D_{16} \\ B_{22} & B_{26} & D_{12} & D_{22} & D_{26} \\ B_{26} & B_{66} & D_{16} & D_{26} & D_{66} \end{vmatrix}}, \quad (3.1.21)$$

$$E_y = \frac{1}{h} \frac{\det C}{\begin{vmatrix} A_{11} & A_{16} & B_{11} & B_{12} & B_{16} \\ A_{16} & A_{66} & B_{16} & B_{26} & B_{66} \\ B_{11} & B_{16} & D_{11} & D_{12} & D_{16} \\ B_{12} & B_{26} & D_{12} & D_{22} & D_{26} \\ B_{16} & B_{66} & D_{16} & D_{26} & D_{66} \end{vmatrix}}, \quad (3.1.22)$$

$$G_{xy} = \frac{1}{h} \frac{\det C}{\begin{vmatrix} A_{11} & A_{12} & B_{11} & B_{12} & B_{16} \\ A_{12} & A_{22} & B_{12} & B_{22} & B_{26} \\ B_{11} & B_{12} & D_{11} & D_{12} & D_{16} \\ B_{12} & B_{22} & D_{12} & D_{22} & D_{26} \\ B_{16} & B_{26} & D_{16} & D_{26} & D_{66} \end{vmatrix}}, \quad (3.1.23)$$

$$\nu_{xy} = - \frac{\begin{vmatrix} A_{12} & A_{26} & B_{12} & B_{22} & B_{26} \\ A_{16} & A_{66} & B_{16} & B_{26} & B_{66} \\ B_{11} & B_{16} & D_{11} & D_{12} & D_{16} \\ B_{12} & B_{26} & D_{12} & D_{22} & D_{26} \\ B_{16} & B_{66} & D_{16} & D_{26} & D_{66} \end{vmatrix}}{\begin{vmatrix} A_{22} & A_{26} & B_{12} & B_{22} & B_{26} \\ A_{26} & A_{66} & B_{16} & B_{26} & B_{66} \\ B_{12} & B_{16} & D_{11} & D_{12} & D_{16} \\ B_{22} & B_{26} & D_{12} & D_{22} & D_{26} \\ B_{26} & B_{66} & D_{16} & D_{26} & D_{66} \end{vmatrix}}, \quad (3.1.24)$$

$$\nu_{yx} = - \frac{\begin{vmatrix} A_{12} & A_{16} & B_{11} & B_{12} & B_{16} \\ A_{26} & A_{66} & B_{16} & B_{26} & B_{66} \\ B_{12} & B_{16} & D_{11} & D_{12} & D_{16} \\ B_{22} & B_{26} & D_{12} & D_{22} & D_{26} \\ B_{16} & B_{66} & D_{16} & D_{26} & D_{66} \end{vmatrix}}{\begin{vmatrix} A_{11} & A_{16} & B_{12} & B_{22} & B_{26} \\ A_{16} & A_{66} & B_{16} & B_{26} & B_{66} \\ B_{11} & B_{16} & D_{11} & D_{12} & D_{16} \\ B_{12} & B_{26} & D_{12} & D_{22} & D_{26} \\ B_{16} & B_{66} & D_{16} & D_{26} & D_{66} \end{vmatrix}}. \quad (3.1.25)$$

To perform these calculations there is written a Matlab code that is found in Appendix A.

3.1.2 Micromechanics of Classical Laminate Theory

To initiate the macromechanics evaluation of a laminate, it's essential to determine the engineering constants required to compute the entries of the Q matrix. For orthotropic materials, four constants need to be determined: E_1 , E_2 , G_{12} , and ν_{12} . The last, minor Poisson's ratio ν_{21} , can be calculated provided by [19] using the formula.

$$\nu_{21} = \frac{\nu_{12}E_2}{E_1}$$

The paper from G. Alaimo et al. [6] presents a method for determining these engineering constants for line patterns. The method involves conducting three tensile tests with line patterns at raster angles of 0° , 90° , and 45° . The tensile test with a raster angle of 0° yields the tensile modulus E_1 and the major Poisson's ratio ν_{12} . Results from the test specimen with a raster angle of 90° provide the tensile modulus E_2 , from which the minor Poisson's ratio ν_{21} can be calculated using the formula mentioned above. Calculation of the tensile modulus is accomplished using formulas (2.1.4) or (2.1.5). To determine the shear modulus, the test specimen is printed with a raster angle of 45° , and the shear modulus G_{12} can be determined using the provided formula [22].

$$\begin{aligned} \frac{1}{E_x^\alpha} &= \frac{\cos^4(\alpha)}{E_1} + \frac{\sin^4(\alpha)}{E_2} + \frac{1}{4} \left(\frac{1}{G_{12}} - \frac{2\nu_{12}}{E_1} \right) \sin^2(2\alpha) \\ \implies G_{12} &= \left(\frac{2\nu_{12}}{E_1} + \frac{4}{\sin^2(2\alpha)} \left(\frac{1}{E_x^\alpha} - \frac{\cos^4(\alpha)}{E_1} - \frac{\sin^4(\alpha)}{E_2} \right) \right)^{-1}, \end{aligned}$$

Inserting $\alpha = 45^\circ$ and the formula above becomes.

$$G_{12} = \left(\frac{2\nu_{12}}{E_1} + \frac{4}{E_x^{45^\circ}} - \frac{1}{E_1} - \frac{1}{E_2} \right)^{-1}. \quad (3.1.26)$$

Where E_1 , E_2 , and ν_{12} are known from tensile test results for line pattern with raster angle 0° and 90° . Tensile modulus $E_x^{45^\circ}$ is calculated from the tensile test results with raster angle 45° . With the different moduli and Poisson's ratio calculated. The entries in Q matrix can be done for laminate that is constructed with line patterns.

3.2 Cellular Solids

For infill pattern grid the book written by L. J. Gibson and M. F. Ashby [2] has an analytical approach to determine the moduli to then calculate Q matrix or the effective tensile modulus.

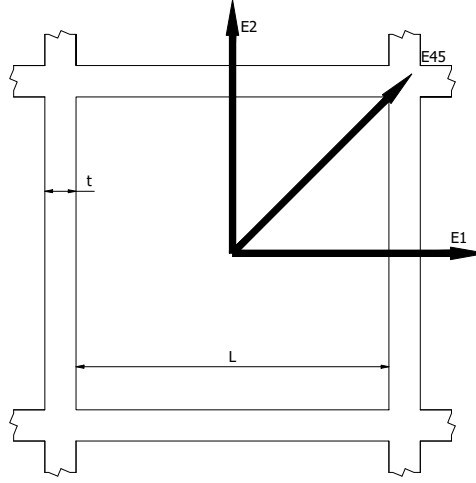


Figure 3.4: Grid pattern with dimensions and tensile modulus direction.

Figure 3.4 shows a grid Y-cell with the dimension length l_{Grid} and thickness t_{Grid} . With tensile modulus E_1 , E_2 , and $E_x^{45^\circ}$. Tensile modulus E_1 and E_2 are calculated by the formula [2].

$$E_1 = E_2 = \frac{t_{Grid}}{l_{Grid}} E_s, \quad (3.2.1)$$

To determine the tensile modulus in 1- and 2-direction the tensile modulus of a solid test specimen of the material is needed. For this thesis the results from tensile test of line with raster angle 0° is used for E_s . While $E_x^{45^\circ}$ is determined by [2].

$$E_x^{45^\circ} = 2 \left(\frac{t_{Grid}}{l_{Grid}} \right)^3 E_s. \quad (3.2.2)$$

Since the manufacture of FDM 3D-printed parts that has grid as infill pattern. Has no different raster angles for different layers the formulas given in (3.2.1) and (3.2.2) is sufficient to have a tensile modulus for grid patterns.

Slicer software Ultimaker Cura does not give the dimensions of grid length or the number of cells in the 3D-printed part. To be able to predict tensile modulus before printing it is necessary to know wall thickness and grid length in a grid cell. Wall thickness is determined by the nozzle size. For example for all 3D-printing in this thesis uses a nozzle size of 0.4 mm, therefore the wall thickness is $t_{grid} \approx 0.4$ mm. For the grid length it is necessary to have the number of grid cells that the slicer has created. This number is not available in the software at the time of writing this thesis. If this a feature in the future calculation of the grid length can be done like this.

$$\begin{aligned} v_f &= \frac{V_{Solid}}{V_{Total}} \implies V_{Solid} = v_f V_{Total} \\ V_{Grid} &= V_{Total} - V_{Solid} = V_{Total}(1 - v_f) \\ V_{Grid} &= nl^2h = V_{Total}(1 - v_f) \\ l_{Grid} &= \sqrt{\frac{V_{Total}(1 - v_f)}{nh}}, \end{aligned}$$

Volume fraction v_f is the infill density, V_{Solid} is the volume of solid material that is deposited onto the part. Total volume of part is V_{Total} , and the empty space in a grid pattern is V_{Grid} . It is assumed that all the cells in slicer is perfect cubic with an area of l_{Grid}^2 and height h which is the same as the height of the part. n is the amount of grid cells in the sliced part which is as of the time of this writing not available. Instead counting the amount of cells across the part should be sufficient.

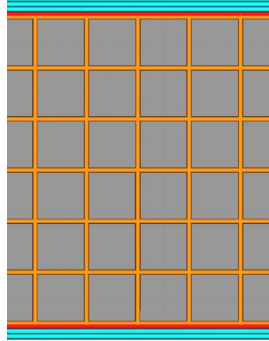


Figure 3.5: Sliced 3D-model with grid pattern 0° and 20% infill density.

For example the Figure 3.5 is of the dog-bone specimen in the smallest section where the width is 25 mm. By counting the number of cells from down to up and horizontal walls the grid length can be estimated with.

$$l_{Grid} = \frac{W - n_{walls}t_{Grid}}{n_{cell}}. \quad (3.2.3)$$

Figure 3.5 has six cells that goes vertical up and in total nine walls. Wall thickness is estimated to be the same as nozzle size at 0.4 mm. The estimated grid length is $l_{grid} \approx 3.567$ mm.

Chapter 4

Numerical Analysis

4.1 Coding CLT in Matlab

To start programming in Matlab the inputs must be defined such as how many plies, layers raster angles, layer thickness, laminate thickness and engineering constants to calculate Q matrix. This is simply done by the code.

```
ply = 15/0.1 ;  
layer_angles = repmat( [0 45 90], [1 (round(ply/3) +1) ]);  
layer_thickness = 0.1;  
laminate_thickness = 15;  
  
longitude_moduli = 1008.621;  
transverse_moduli = 711.108;  
shear_moduli = 268.864;  
poisson_ratio12 = 0.36;  
poisson_ratio21 = transverse_moduli*poisson_ratio12/  
    longitude_moduli;
```

Calculation for number of plies is done by dividing the height of laminate by layer thickness. For this thesis the laminates are 15 mm in height, and all test specimen have a layer thickness of 0.1 mm. To program the different raster angles for each layer the *repmat* function in Matlab is used. This function repeats a input n times. Example `repmat([0 45 90], 3)` gives a 3×9 matrix with repeating 0 45 90 as shown bellow.

$$\text{repmat} \left(\begin{bmatrix} 0 & 45 & 90 \end{bmatrix}, 3 \right) = \begin{pmatrix} 0 & 45 & 90 & 0 & 45 & 90 & 0 & 45 & 90 \\ 0 & 45 & 90 & 0 & 45 & 90 & 0 & 45 & 90 \\ 0 & 45 & 90 & 0 & 45 & 90 & 0 & 45 & 90 \end{pmatrix}$$

To decrease computer time to calculate the *repmat* function. Second part after comma sign in the code restricts the output of *repmat*. Such that the output is giving out one row and 150 columns or 151 columns. With the engineering constants defined the Q matrix is calculated by the formula (3.1.2) and the code.

```
Q = [ longitude_moduli/(1 - poisson_ratio12*poisson_ratio21)  
      transverse_moduli*poisson_ratio12/(1 - poisson_ratio12*  
      poisson_ratio21) 0; transverse_moduli*poisson_ratio12/(1 -  
      poisson_ratio12*poisson_ratio21) transverse_moduli/(1 -  
      poisson_ratio12*poisson_ratio21) 0; 0 0 shear_moduli]
```

Next is to define the laminates plies to correct location and the raster angles to these plies. This is done by creating a 150×4 variable to number each ply, determine the bottom- and top-part of each ply and raster angles to these plies by.

```
lamina_k = zeros(ply,4);
for i = 1:ply
    lamina_k(i,1:4) = [i layer_thickness*(i-1)-ply*layer_thickness
        /2 layer_thickness*i-ply*layer_thickness/2 layer_angles(i)];
end
```

First line creates the 150×4 matrix with zeros, to make computation faster for the for-loop. If the matrix is not created with all its entries set to zero Matlab has to create a new matrix for each loop in the for-loop. Next is the for-loop itself. The plies are number from the lowest ply first and highest ply last. The i is the variable that changes as the loop is progressing. In the for-loop the i determines which row in lamina_k that should be defined, and receive the raster angle from layer_angles matrix. The result from the for-loop is then.

```

1  -7.5000  -7.4000   0
2  -7.4000  -7.3000  45.0000
lamina_k = 3  -7.3000  -7.2000  90.0000
4  -7.2000  -7.1000   0
:      :      :      :
```

The first column is the ply number, second column is the bottom of the ply, third is the top of the ply, and the last column is the raster angle in degrees. Next process is to calculate \bar{Q} for each ply the code for this is.

```
engineeringstrain_trustrain_factorisation = [1 0 0; 0 1 0; 0 0 2];
QBar = zeros(3,3*ply);
for i = 1:ply
    angle_alpha = layer_angles(i)*pi/180;
    c = cos(angle_alpha);
    s = sin(angle_alpha);
    angle_transform = [ c^2 s^2 2*s*c ; s^2 c^2 -2*s*c ; -s*c s*c c
        ^2-s^2 ];
    inv_angle_transform = [c^2 s^2 -2*s*c ; s^2 c^2 2*s*c ; s*c -s*
        c c^2-s^2];
    QBar(1:3,(3*i-2):3*i) = inv_angle_transform * Q *
        engineeringstrain_trustrain_factorisation * angle_transform
        / engineeringstrain_trustrain_factorisation ;
end
```

First line in the code above defined the engineering-strain and true-strain factorisation to calculate \bar{Q} in formula (3.1.4). To decrease computation time the \bar{Q} entries are first set to zero. Since \bar{Q}_k is for a single ply is a 3×3 matrix, the QBar matrix is of size 3×450 for a laminate with 150 layers. The for-loop needs to extract the angles for each ply, this is done by layer_angles(i). Since Matlab calculates cosine and sine in radians the angles in angle_layers needs to be converted from degrees to radians. Next in for-loop is calculation of $[T]$ and $[T]^{-1}$ for each ply, and is done by formulae (3.1.5) and (3.1.6) respectively. Assigning the correct entries to the $QBar(n,m)$ matrix the first part n gives the rows for entries and m determines the columns. Since there are only three rows that is consistent for all entries in QBar n is set to $1 : 3$. $1 : 3$ determines that row one to three is going to be entered. m is set to $(3i-2) : 3i$ that set the columns to be three. For

each positive integer i that represents a ply the columns move three over. For example for $i = 1$ the columns for entries are 1 : 3, or column from columns one to column three. For $i = 2$ the columns for entries are 4 : 6. When $[T]$ and $[T]^{-1}$ is calculated for one ply, \bar{Q}_k can be calculated by formula (3.1.4) and assigned to their respectively 3x3 entry in QBar matrix. Since \bar{Q} is calculated for all plies the C matrix build up by A , B , and D matrices can be calculated by formulae (3.1.13), (3.1.14), and (3.1.15) respectively.

```

A = zeros(3,3);
B = zeros(3,3);
D = zeros(3,3);
for i = 1:3
    for j=1:3
        vectorsummarized_Amatrix = zeros(1,ply);
        for k = 1:ply
            vectorsummarized_Amatrix(1,k) = QBar(i,j+3*k-3) * (
                lamina_k(k,3) - lamina_k(k,2) );
        end
        A(i,j) = sum(vectorsummarized_Amatrix,'all');
    end
end
for i = 1:3
    for j=1:3
        vectorsummarized_Bmatrix = zeros(1,ply);
        for k = 1:ply
            vectorsummarized_Bmatrix(1,k) = QBar(i,j+3*k-3) * (
                lamina_k(k,3)^2 - lamina_k(k,2)^2 );
        end
        B(i,j) = 0.5 * sum(vectorsummarized_Bmatrix,'all');
    end
end
for i = 1:3
    for j=1:3
        vectorsummarized_Dmatrix = zeros(1,ply);
        for k = 1:ply
            vectorsummarized_Dmatrix(1,k) = QBar(i,j+3*k-3) * (
                lamina_k(k,3)^3 - lamina_k(k,2)^3 );
        end
        D(i,j) = 1/3 * sum(vectorsummarized_Dmatrix,'all');
    end
end
C = [ A B ; B D ]

```

The three first lines is to reduce computation time as mentioned earlier. For the for-loops it is little more complex. To calculate A , B , and D matrix there needs to be three for-loops to determine one of the mentioned matrices. The two first for-loops specifies the entries to a matrix while the last for-loop is to summarize \bar{Q}_k through all plies. Variables vectorsummarized is used to store the values of each term in the summation of $\bar{Q}_k(z_k - z_{k-1})$ from formula (3.1.13) for matrix A . Then the function sum in Matlab summarize all entries in the vector vectorsummarized, and stores it in A , B or C determined by i and j . Creating C matrix is done by the last line of code above. After all this is complete now it is possible to determine the mechanical properties of this laminate by using the formulas (3.1.16) to (3.1.25).

```

if all( B(:) == 0) == 1
    calculation_Ex = A \ [1 ; 0 ; 0];

```

```

    tensilemoduli_Ex = 1 / laminate_thickness / calculation_Ex(1,1)
    calculation_Ey = A \ [0 ; 1 ; 0];
    tensilemoduli_Ey = 1 / laminate_thickness / calculation_Ey(2,1)
    calculation_Gxy = A \ [ 0 ; 0 ; 1];
    shearmoduli_Gxy = 1 / laminate_thickness / calculation_Gxy(3,1)
    poisson_ratio_xy = - calculation_Ex(2,1) / calculation_Ex(1,1)
    poisson_ratio_yx = - calculation_Ey(1,1) / calculation_Ey(2,1)
else
    tensilemoduli_Ex = 1 / laminate_thickness * det(C) / det( C
        (2:6,2:6) )
    tensilemoduli_Ey = 1 / laminate_thickness * det(C) / det( [ C
        (1,1) C(1,3:6) ; C(3:6,1) C(3:6,3:6) ])
    shearmoduli_Gxy = 1 / laminate_thickness * det(C) / det( [ C
        (1:2,1:2) C(1:2,4:6) ; C(4:6,1:2) C(4:6,4:6) ])
    poisson_ratio_xy = - det([ C(2:6,1) C(2:6,3:6) ]) / det([ C
        (2:6,2:6) ])
    poisson_ratio_yx = - det([ C(1,2:6) ; C(3:6,2:6) ]) / det([ C
        (1,1) C(1,3:6) ; C(3:6,1) C(3:6,3:6) ])
end

```

Since calculations are different depending on symmetry of the laminate. A code that determines if the laminate is symmetric is needed. This is done by a logic statement in the first line of code above. The function `all` in Matlab determines if all numbers in a vector is nonzero or not. Therefore the code starts with matrix B and asks is all the numbers in matrix B equal to zero. This creates a 9×1 vector with logical 1 and 0 values where the 1 values confirms that the number is in fact zero and if the value is 0 in the vector there is a nonzero number in matrix B . The `all`-function checks the 9×1 vector and if all the numbers in the vector is 1 the output is 1, but if one of the numbers is zero the output is 0. When `all(B(:) == 0) = 1` the matrix B Calculation for the mechanical properties is done by the formulas (3.1.16) to (3.1.20). If the statement in the first line is not true then the laminate is asymmetric and the calculation is done by (3.1.21) to (3.1.25).

Chapter 5

Results

5.1 Experimental Results

5.1.1 Line pattern with raster angle 0°

Results presented in this section are used to determine the longitudinal tensile modulus E_1 for 3D-printed parts with a line pattern and 100% infill. In Ultimaker Cura, the raster angle is set to 90°, but is referred to here and later as a line pattern with a raster angle of 0°. In total, four dog-bone specimens were printed and tested instead of the standard specified amount of five dog-bones. Figure 5.1 shows the stress-strain curves from the four tensile tests.

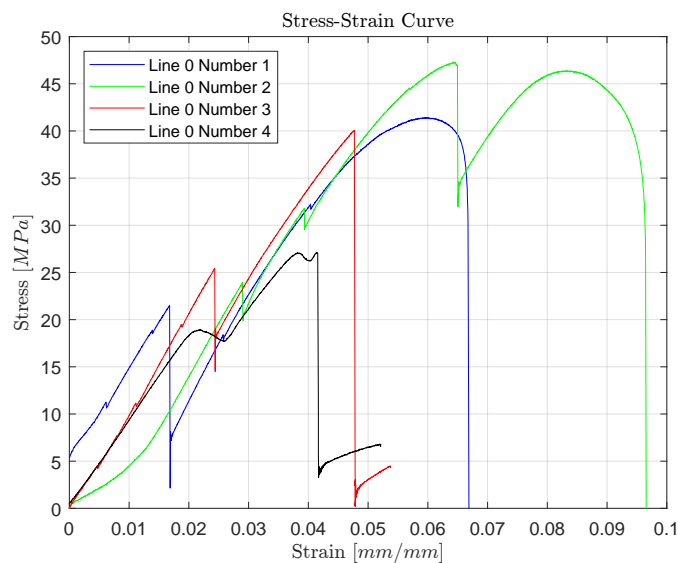


Figure 5.1: Stress-strain curve from four tensile tests line pattern with raster angle of 0° and 100% infill.

Results from the tensile tests are somewhat difficult to evaluate since all tests resulted in fracture outside the gauge length section, refer to Figure 2.2. Additionally, the curves are not as continuous as those seen in stress-strain curves from tensile tests of stronger materials such as steel. Figure 5.2 shows abrupt drops in stress during testing with comments on why these occur.

Figure 5.2 shows six events that occurs under testing, and what these events are. For all tensile testing with metal plates for line pattern with raster angle 0° the adhesive could not withstand the axial force. As mentioned earlier, all fractures occur outside the gauge length section, where the radii end and transition to the rectangular test area, see Figure 5.3. The larger significant drops in stress-strain curve in Figure 5.1 are believed to occur due to fractures in some fibers in a non-critical number of layers at the opposite end. These minor fractures can barely be seen but are visible upon close inspection. Figure 5.3 where the minor fracture is within the red region.

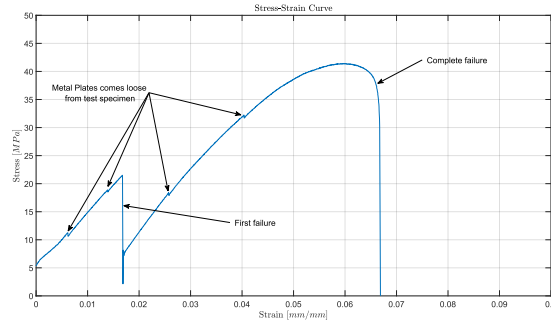


Figure 5.2: Stress-strain curve from tensile test Line pattern raster angle 0° #1.

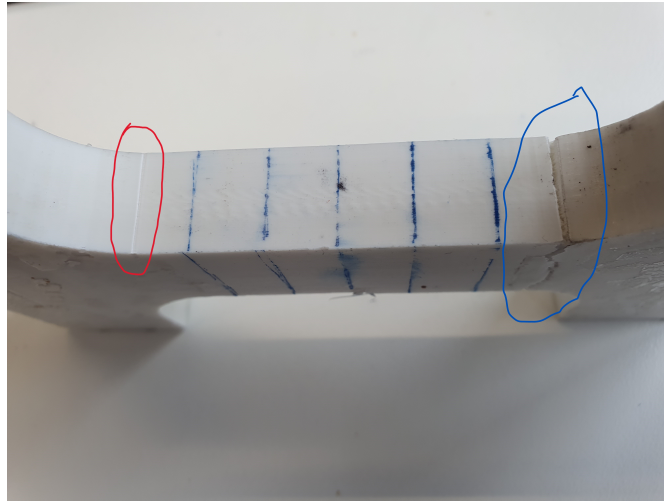


Figure 5.3: Damage on dog-bone for line pattern with raster angle 0° and 100% infill #2.

Figure 5.4a is from tensile tests 1 and 2 which had similar breaks. Fracture is in the area where there is a transition from straight line to the start of the curvature. Figure 5.4b failed due to the “ear” of the dog-bone broke off. For both test the “ear” that breaks is on top-left of the dog-bones. Inspection of the dog-bone does not indicate other damage than the “ear” that has broken off from the rest of the dog-bone.



(a) Number 1 is above and 2 below.

(b) Number 3 is above and 4 below.

Figure 5.4: Failure from tensile test line pattern with raster angle 0° and infill density 100%.

Determination of tensile moduli is done with using formula (2.1.5) and (2.1.6) and the resulting tensile moduli is shown in Table 5.1.

The mean tensile moduli is calculated to be 1008.6 MPa. Which for CLT-computation is the longitudinal moduli E_1 . Maximum elongation and ultimate tensile stress is given in Table 5.2.

	Number 1	Number 2	Number 3	Number 4
Tensile Moduli [MPa]	1198.560	1058.556	920.060	857.306
mean [MPa]	1008.621			
Standard Deviation [MPa]	151.997			
Confidence Interval $\alpha = 0.025$ [MPa]	170.344			

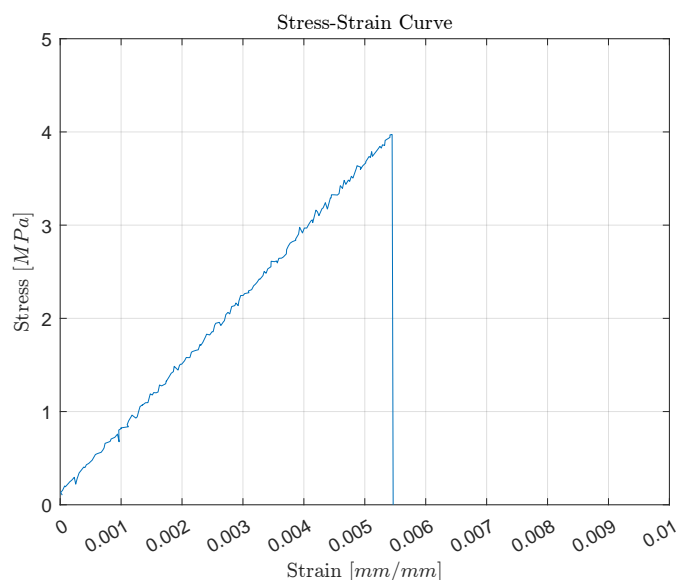
Table 5.1: Tensile moduli results for line pattern with raster angle 0° and infill percentage 100.

	Number 1	Number 2	Number 3	Number 4
Ultimate Tensile stress [MPa]	41.416	47.280	40.079	27.125
mean Ultimate Tensile stress [MPa]	38.975			
Ultimate Tensile stress STD [MPa]	8.496			
Confidence Interval $\alpha = 0.025$ [MPa]	9.522			
Elongation at break [%]	5.987	6.423	4.771	4.146
mean Elongation at break [%]	5.332			
Elongation at break STD [%]	1.055			
Confidence Interval $\alpha = 0.025$ [%]	1.183			

Table 5.2: ultimate tensile stress and elongation at break for line pattern with raster angle 0° and 100% infill.

5.1.2 Line pattern with raster angle 90°

When slicing the dog-bone in Ultimaker Cura, the raster angle is set to 0° . For CLT calculations, the raster angle is converted to 90° , and will be referred to as raster angle 90° from here on out. Due to errors during testing, it was only possible to collect data from one tensile test out of four for the line pattern with a raster angle of 90° and 100% infill. The stress-strain curve from the single tensile test where data is available is shown Figure 5.5.

Figure 5.5: Stress-strain curve from the tensile test of a dog-bone specimen made with a line pattern raster angle of 90° and 100% infill #4.

The transverse tensile modulus E_2 for CLT computation is calculated to be 711.108 MPa. The ultimate tensile stress is 3.972 MPa, with an elongation at break of 0.549%. Since there was only one test with data available, it is not possible to determine the statistical properties of the

dog-bone specimen line pattern with raster angle of 90° and 100% infill.

Data was not collected from all four tests, but all failures occurred similarly to each other. Fracture goes in the bond between the fibers that are perpendicular to the axial forces. Figure 5.6 shows test specimen #4 with fracture inside gauge length section.

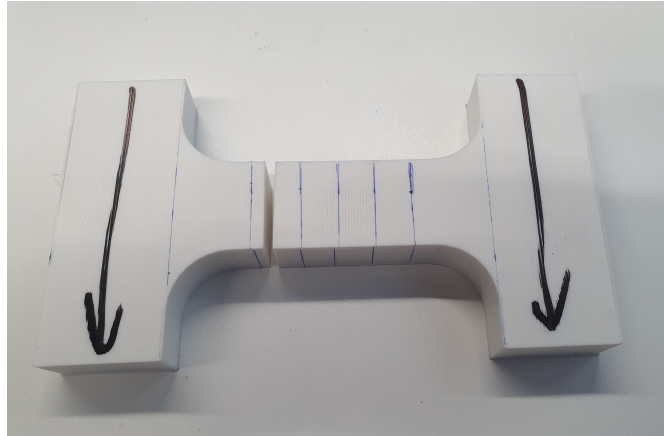


Figure 5.6: Failure of a dog-bone with a line pattern raster angle of 90° and 100% infill #4.

5.1.3 Line pattern with raster angle 45°

For dog-bone specimen with line pattern where the raster angle is $[45, -45]_R$. Four tensile test were completed. Where the stress-strain curve is shown in Figure 5.7.

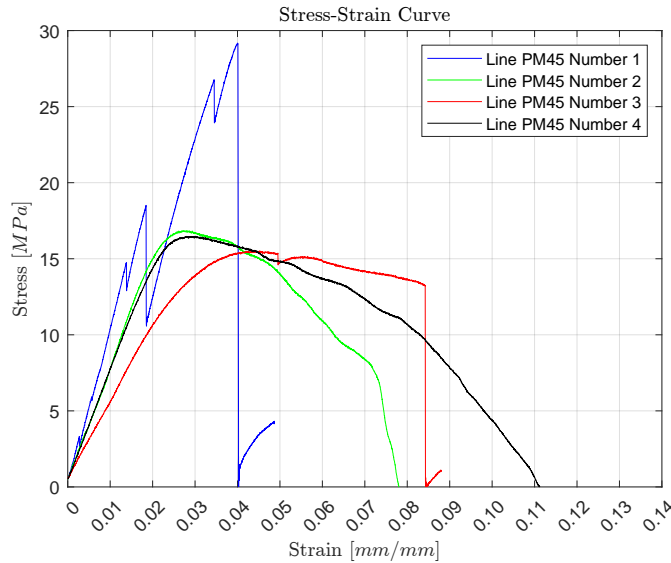


Figure 5.7: Stress-strain curve from line pattern with raster angle $\pm 45^\circ$ and 100% infill.

Three test specimen had glued metal plates where test specimen number 4 had no metal plates. Figure 5.7 shows the similar abrupt drop in stress for number 1 as occurred in line pattern with raster angle 0° . These occur since the plates came loose under tensile testing. The more significant drop in stress is unknown since there is not other damage on dog-bone other than the one fracture. Mechanical properties from tensile testing is given in Table 5.3.

All fractures from the tensile test exhibit a V-shape in the failure mechanisms, with three dog-bones (#1, #2, and #3) experiencing fractures outside the gauge-length section of the specimens. Figure 5.8 depicts the fracture shape of these tests.

From Figure 5.7, specimens number 2, 3, and 4 exhibit ductile failures. There isn't a significant abrupt drop in force, as observed in tests for line patterns with raster angles 0° and 90° .

	Number 1	Number 2	Number 3	Number 4
Tensile Moduli [MPa]	1012.872	721.376	536.029	690.922
mean Tensile Moduli [MPa]	740.300			
STD [MPa]	199.013			
Confidence $\alpha = 0.025$ [MPa]	223.034			
Ultimate Tensile stress [MPa]	29.180	16.836	15.526	16.477
mean Ultimate Tensile stress [MPa]	19.505			
Ultimate Tensile stress STD [MPa]	6.474			
Confidence Interval $\alpha = 0.025$ [MPa]	7.255			
Elongation at break [%]	4.285	2.919	4.627	3.23
mean Elongation at break [%]	3.765			
Elongation at break STD [%]	0.820			
Confidence Interval $\alpha = 0.025$ [%]	0.919			

Table 5.3: Mechanical properties from tensile test for line pattern with raster angle $\pm 45^\circ$ and 100% infill.

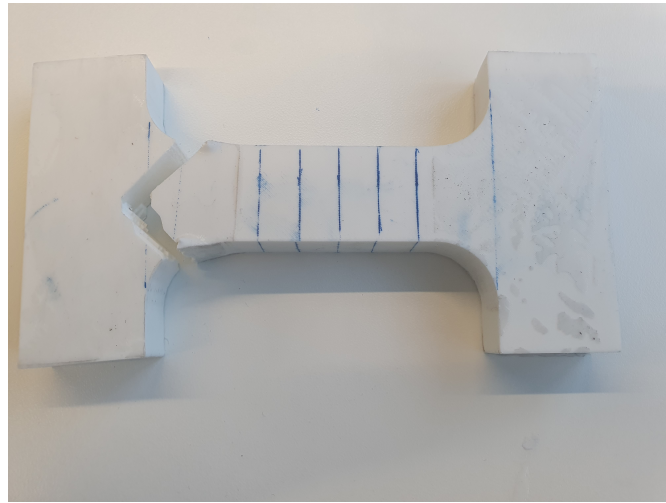


Figure 5.8: Dog-bone specimen failure with line pattern, raster angle $\pm 45^\circ$ and 100% infill #1.

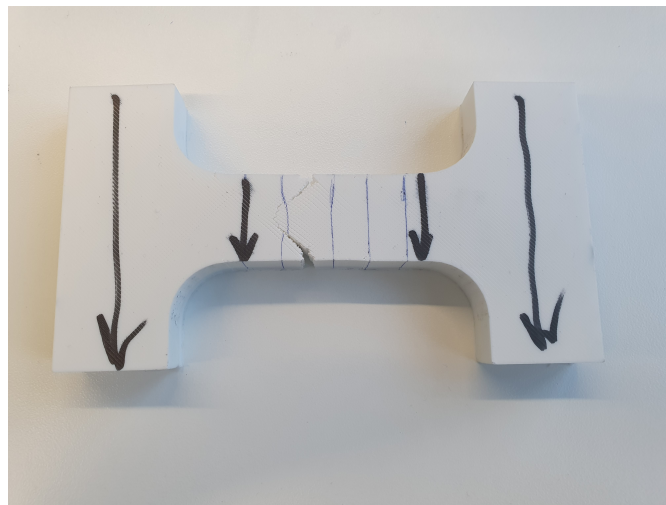


Figure 5.9: Dog-bone specimen failure with line pattern, raster angle $\pm 45^\circ$ and 100% infill #4.

Figure 5.9 illustrates the slowest failure observed among all tensile tests, where fibers in layers failed one by one until there was nothing left. Another notable failure is observed in specimen

number 3, where there are two areas with damage on the test specimen, see Figure 5.10.

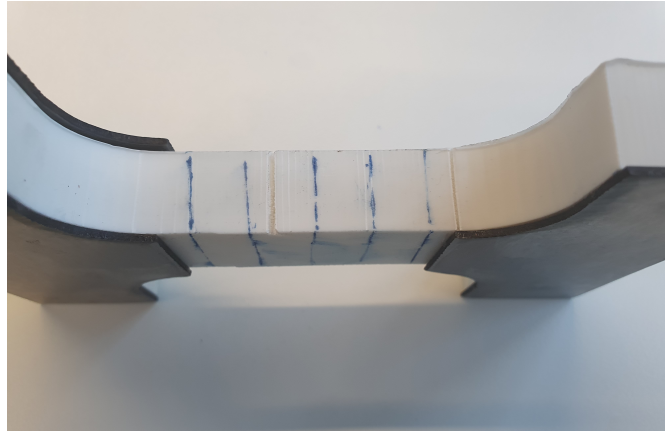


Figure 5.10: Dog-bone specimen failure with line pattern, raster angle $\pm 45^\circ$ and 100% infill #3

5.1.4 Line pattern for CLT computation

For tensile test there was manufactured three dog-bone specimen with raster angle $[0, \pm 30, \pm 60, 0, 90]_R$ and 100% infill. Stress-strain curve is shown in Figure 5.11.

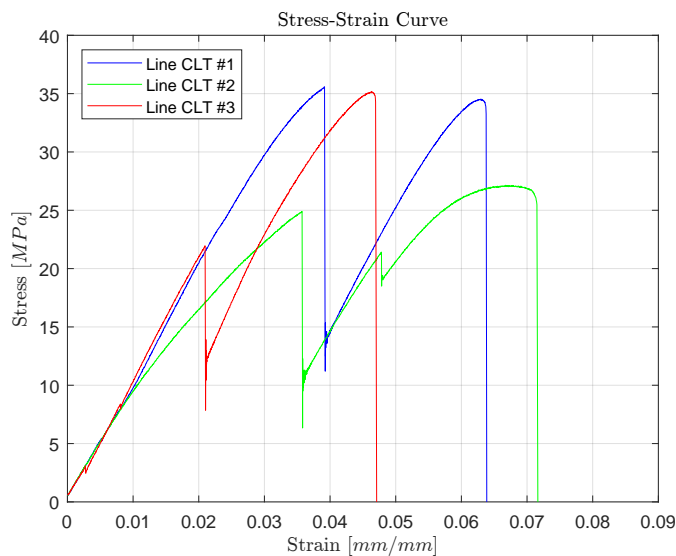


Figure 5.11: Stress-strain curve from tensile test with line patten, raster angle $[0, \pm 30, \pm 60, 0, 90]_R$, and 100% infill.

Where the mechanical properties of tensile testing is given in Table 5.4.

Failures for all test subjects occurred at the transition from rectangular cross-section to the start of curvature. This is the section that has contact with the cylinders from the fixture in Section 2.4.

For tensile testing performed for line pattern with CLT raster angle, all metal plates did not withstand the axial forces for testing.

5.1.5 Grid pattern infill percentage 20

For grid pattern with 20% infill. There was printed three dog-bone specimen for tensile testing. Grid cells had a mean measurement from all dog-bone specimen of grid length to be $l_{Grid} = 3.603$ mm and wall thickness of $t_{Grid} = 0.404$ mm. These measurements will be used to calculate

	Number 1	Number 2	Number 3
Tensile Moduli [MPa]	891.902	888.568	843.227
mean Tensile Moduli [MPa]	874.566		
STD [MPa]	27.191		
Confidence $\alpha = 0.025$ [MPa]	35.187		
Ultimate Tensile stress [MPa]	35.594	27.148	35.172
mean Ultimate Tensile stress [MPa]	32.638		
Ultimate Tensile stress STD [MPa]	4.759		
Confidence Interval $\alpha = 0.025$ [MPa]	6.159		
Elongation at break [%]	7.016	7.415	5.143
mean Elongation at break [%]	6.525		
Elongation at break STD [%]	1.213		
Confidence Interval $\alpha = 0.025$ [%]	1.570		

Table 5.4: Mechanical properties from tensile test for line pattern with raster angle $[0, \pm 30, \pm 60, 0, 90]_R$ and 100% infill.



Figure 5.12: Dog-bones after tensile test for line pattern with CLT raster angles.

theoretical tensile modulus for grid patterns mentioned in Section 3.2, formula (3.2.1). Figure 5.13 shows the results from tensile test as stress-strain curve.

Mechanical properties gathered from tensile test is given in Table 5.5.

All fractures occurred where the radii ends for the gauge-length section of the dog-bone, see Figure 5.14.

When manufacturing the specimen in a 3D-printer the walls for Y-cell for grids is not consistent for the entire wall-length, see Figure 5.15.

5.1.6 Grid pattern infill percentage 40

For tensile testing of grid pattern with 40% infill density. There was printed three dog-bone specimen. The mean measurement of the Y-cell for grids gave a grid length to be $l_{Grid} = 1.521$ mm and for wall thickness $t_{Grid} = 0.460$ mm. The stress-strain curve from tensile testing is given in Figure 5.16.

Mechanical properties from tensile testing is given in Table 5.6.

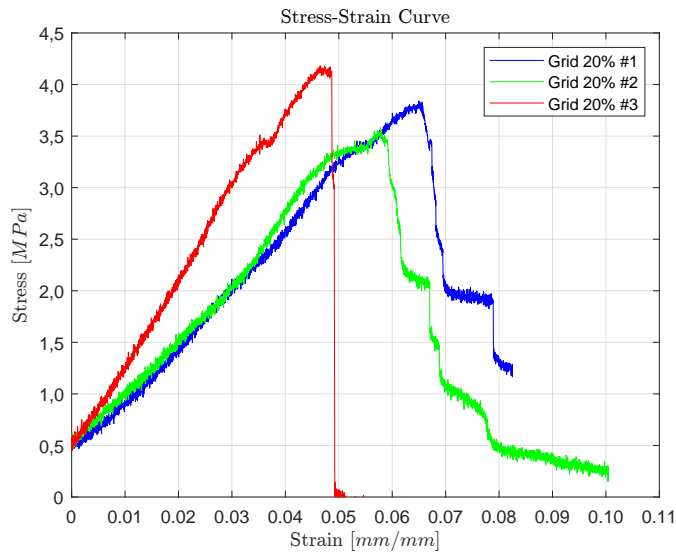


Figure 5.13: Stress-strain curve from three tensile test with grid pattern, raster angle 0° and 20% infill.

	Number 1	Number 2	Number 3
Tensile Moduli [MPa]	69.626	93.684	109.824
mean Tensile Moduli [MPa]		91.045	
STD [MPa]		20.229	
Confidence $\alpha = 0.025$ [MPa]		26.177	
Ultimate Tensile stress [MPa]	4.269	3.983	4.645
mean Ultimate Tensile stress [MPa]		4.299	
Ultimate Tensile stress STD [MPa]		0.332	
Confidence Interval $\alpha = 0.025$ [MPa]		0.430	
Elongation at break [%]	7.088	6.304	5.083
mean Elongation at break [%]		6.158	
Elongation at break STD [%]		1.010	
Confidence Interval $\alpha = 0.025$ [%]		1.308	

Table 5.5: Mechanical properties from tensile test for grid pattern with raster angle 0° and 20% infill.

Failure of all dog-bone tests occurred in the same region. Where the radii ends for the gauge-length section of the specimen, see Figure 5.17.

Figure 5.18 is a photo of grid cells in dog-bone specimen.

Figure 5.18 shows that the vertical lines are uneven distributed. While the horizontal lines are in better production quality. The measurement of vertical lines is more troublesome.



Figure 5.14: Fracture of dog-bone specimen number 3, grid pattern, raster angle 0° , and 20% infill.

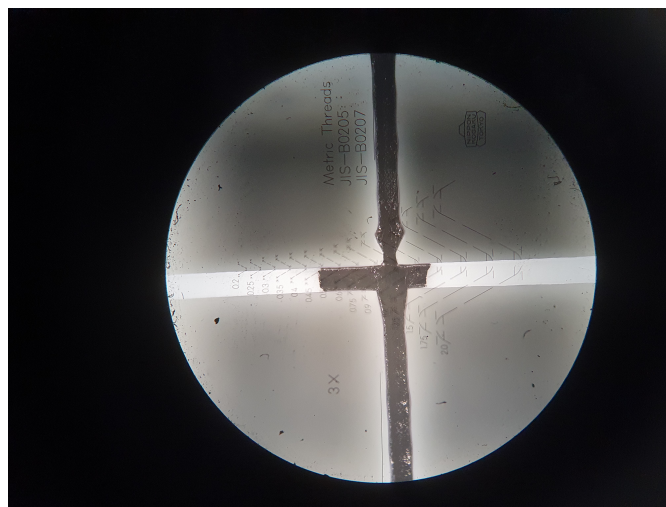


Figure 5.15: Connection between fibers in a grid cell from grid pattern with 0° raster angle, and 20% infill.

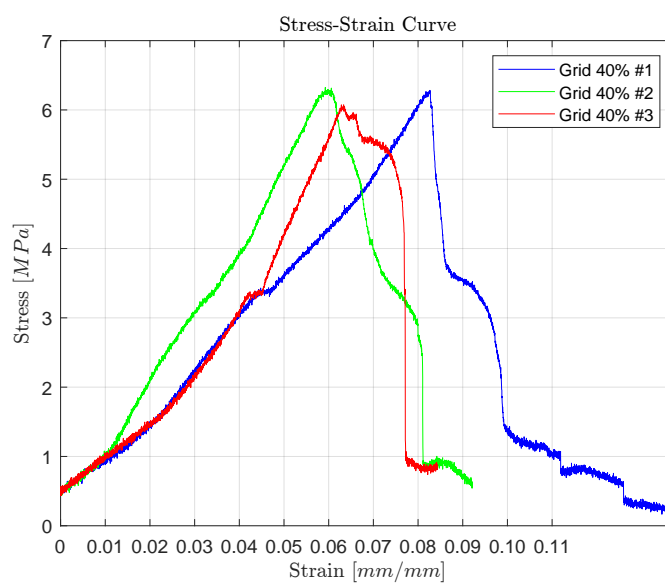


Figure 5.16: Stress-strain curve from three tensile test with grid pattern with 40% infill.

	Number 1	Number 2	Number 3
Tensile Moduli [MPa]	163.340	220.940	145.971
mean Tensile Moduli [MPa]		176.750	
STD [MPa]		39.242	
Confidence $\alpha = 0.025$ [MPa]		50.783	
Ultimate Tensile stress [MPa]	7.180	7.228	6.941
mean Ultimate Tensile stress [MPa]		7.116	
Ultimate Tensile stress STD [MPa]		0.154	
Confidence Interval $\alpha = 0.025$ [MPa]		0.199	
Elongation at break [%]	6.993	4.996	4.955
mean Elongation at break [%]		5.648	
Elongation at break STD [%]		1.165	
Confidence Interval $\alpha = 0.025$ [%]		1.508	

Table 5.6: Mechanical properties from tensile test for grid pattern with 40% infill.

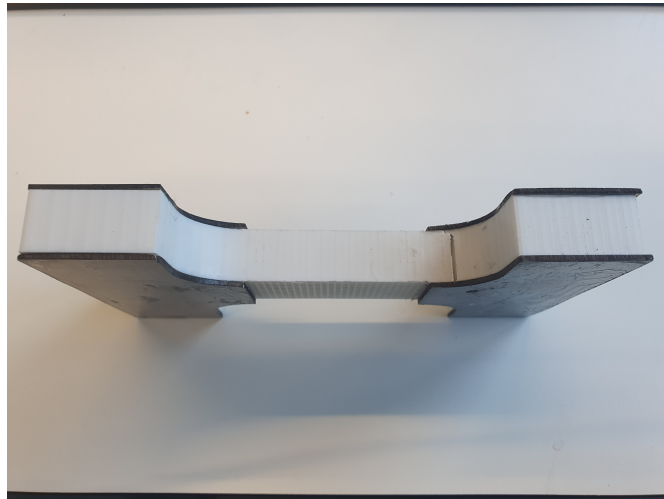


Figure 5.17: Failure of dog-bone specimen #1 from grid pattern with 40% infill.

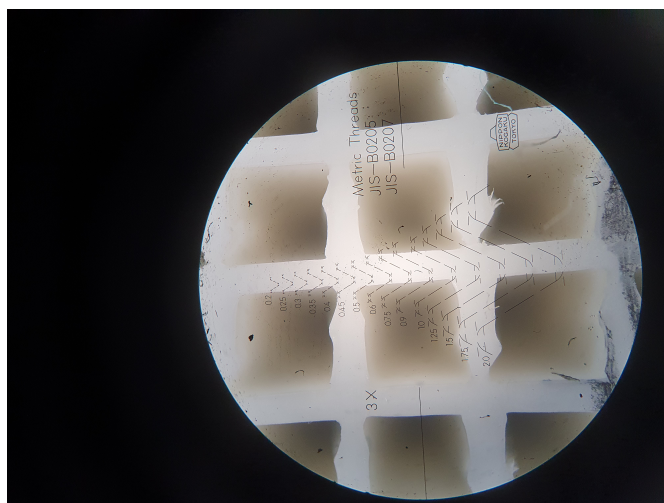


Figure 5.18: Y-cell of grid pattern with 40% infill.

5.2 Analytical & Numerical Results

5.2.1 Predicted Stiffness from CLT computation

To evaluate a laminate with CLT, the mechanical properties in the local coordinate system for a ply need to be known. The tensile modulus determined from tensile testing for line patterns with raster angles of 0° , $\pm 45^\circ$, and 90° are used. The longitudinal tensile modulus E_1 is the resulting mean tensile modulus from tensile tests for the line pattern with a raster angle of 0° and 100% infill. Thus, E_1 is set to 1008.621 MPa. The transverse tensile modulus E_2 is the tensile modulus from the line pattern with a raster angle of 90° , resulting in $E_2 = 711.108$ MPa. The local shear modulus is calculated using the formula (3.1.26). The Poisson's ratio ν_{12} and E_x^{45} is missing. Since the equipment needed to determine the Poisson's ratio was unavailable, the Poisson's ratio ν_{12} is taken from a research paper on PLA material. The paper provides a Poisson's ratio of $\nu_{12} = 0.36$ for PLA [23]. E_x^{45} is the mean tensile modulus from tensile tests of the line pattern with raster angles of $\pm 45^\circ$, which is 740.300 MPa. By setting $E_1 = 1008.621$, $E_2 = 711.108$, $E_x^{45} = 740.300$, and $\nu_{12} = 0.36$ into the formula for local shear modulus, G_{12} , it is then calculated to be 268.864 MPa. Raster angle that CLT computation is compared against, is the tensile test with the line pattern with raster angles $[0, \pm 30, \pm 60, 0, 90]_R$ and 100% infill. These angles are then also used as input to run the CLT computation, the code can then be executed. The predicted tensile modulus in the direction of the applied force is determined to be $E_{CLT} = 837.340$ MPa.

5.2.2 Analytical Prediction for Grid Patterns

In total there was printed six dog-bone specimen with grid pattern. From these six specimens there were measured five Y-cells in the grid pattern in each specimen. Where two measurements was taken for the length of the grid cell, one horizontal- and one vertical-measurement. For the wall thickness there was done four measurements for one grid cell. Measurement are given in Table 5.7.

		Grid 0° 20% Infill #1	Grid 0° 20% Infill #2	Grid 0° 20% Infill #3	Grid 0° 40% Infill #1	Grid 0° 40% Infill #2	Grid 0° 40% Infill #3
Grid cell 1	Grid length [mm]	3.598	3.615	3.596	1.499	1.525	1.480
	Wall thickness [mm]	0.401	0.386	0.415	0.491	0.421	0.489
Grid cell 2	Grid length [mm]	3.632	3.621	3.605	1.485	1.558	1.531
	Wall thickness [mm]	0.392	0.382	0.413	0.486	0.422	0.484
Grid cell 3	Grid length [mm]	3.591	3.606	3.595	1.464	1.585	1.484
	Wall thickness [mm]	0.410	0.385	0.424	0.484	0.403	0.486
Grid cell 4	Grid length [mm]	3.585	3.631	3.580	1.504	1.577	1.500
	Wall thickness [mm]	0.406	0.377	0.422	0.486	0.408	0.479
Grid cell 5	Grid length [mm]	3.574	3.628	3.591	1.524	1.594	1.514
	Wall thickness [mm]	0.438	0.381	0.434	0.472	0.412	0.476

Table 5.7: Measurement of grid cells from dog-bone specimen.

Table 5.7 gives the values of t_{grid} and l_{grid} to calculate theoretical tensile modulus for grid patterns. First lets calculate the estimated grid length with the use of formula (3.2.3). For both estimations for grid pattern with 20% and 40% infill the wall thickness is $t_{Grid} = 0.4$ mm. Grid pattern with 20% infill density has six cells and nine walls. In the section of dog-bone where the width is 25 mm. This gives and estimated grid length of 3.567 mm. Grid pattern with 40% infill density there are 12 cells and 15 walls in the section where the width is 25 mm. Using formula (3.2.3) the estimated grid length is 1.583 mm.

Predicted tensile modulus is calculated by formula (3.2.1). For tensile modulus of solid material is chosen to be from technical data sheet for though PLA from Ultimaker, and the mean tensile modulus from line pattern with raster angle 0° and 100% infill. See results in Table 5.8.

	Predicted Tensile Modulus [MPa]	
	Solid Tensile Modulus from Experimental results	Solid Tensile Modulus from TDS Ultimaker
	$E_s = 1008.621$ MPa	$E_s = 2797$ MPa
Grid raster angle 0° with 20% infill #1	114.837	318.453
Grid raster angle 0° with 20% infill #2	106.471	295.255
Grid raster angle 0° with 20% infill #3	118.348	328.189
Grid raster angle 0° with 40% infill #1	326.144	904.428
Grid raster angle 0° with 40% infill #2	265.911	737.396
Grid raster angle 0° with 40% infill #3	324.339	899.422

Table 5.8: Predicted tensile modulus for grid pattern, with solid tensile modulus from experimental results and technical data sheet (TDS) from Ultimaker.

Chapter 6

Discussion

6.1 Comparison of CLT Results and Tensile Test Results

CLT prediction of tensile modulus was calculated to be $E_{CLT} = 837.340$ MPa, while the mean tensile modulus from experimental result was 874.566 MPa. Which is an absolute error of 37.226 MPa, or an relative error of 4.26% from mean measured tensile modulus. Table 6.1 lists the results from tensile testing and CLT computation.

	CLT Number 1	CLT Number 2	CLT Number 3
Measured Tensile Modulus [MPa]	891.902	888.568	843.227
Mean Measured Tensile Modulus [MPa]		874.566	
CLT Predicted Tensile Modulus [MPa]		837.340	
Absolute Error [MPa]	54.562	51.228	5.887
Relative Error [%]	6.12	5.77	0.70
Mean Absolute Error [MPa]		37.226	
Mean Relative Error [%]		4.26	

Table 6.1: Comparison of CLT prediction and experimental tensile results

To determine the difference in percentage the formula (6.1.1) is used.

$$RE = \frac{|E_{Measured} - E_{CLT}|}{E_{Measured}} \cdot 100\% \quad (6.1.1)$$

Table 6.1 shows that the highest difference is from tensile test number 1 with an relative error of 6.12% from the predicted tensile modulus from CLT.

From this result CLT is a good mathematical model to use for FDM 3D-printed parts to estimate tensile strength and Young's modulus. It is reasonable to assume from the comparison that CLT is applicable to FDM 3D-printed parts. Then it is reasonable to say that all assumptions (Kirchoff hypothesis) stated in Section 3.1 holds for FDM 3D-printed parts.

Another positive factor is that the predicted tensile modulus is less than actual tensile modulus, means that the predicted stiffness is less than the actual stiffness. For designing parts the predicted stiffness and dimension calculations has a small safety factor. Although one test of confirmation is not enough to say that every possible setup is true or similar to the results in this thesis.

To be able use CLT the mechanical properties of a layer must be known e.i. E_1 , E_2 , G_{12} , ν_{12} , and ν_{21} must be determined beforehand. The issue of determining engineering constants is done with performing three different tensile test. However, the solution is case sensitive, meaning that if there are any changes in printing parameters three new test must be conducted to establish a new set of properties. There are several papers that's been summarized in Section 1.3.3 that have

done test to determine which settings that affects mechanical properties and which one to alter for stiffer and stronger 3D-prints. However, an analytical method of determining the micromechanics of a layer with line pattern is still not been studied.

6.2 Comparison of Cellular Solids Results and Tensile Test Results

First, lets start with comparing estimated wall thickness and grid length up against the measured dimensions from dog-bone specimen. Estimation of tensile modulus is done by calculating formulas (3.2.1) and (3.2.2). These two formulas need wall thickness and grid length, so knowing these dimensions before printing is helpful. Calculating the relative error % is done by (6.2.1) and (6.2.2).

$$\text{RE Thickness \%} = \frac{|t_{measured} - t_{assumed}|}{t_{measured}} \cdot 100\%, \quad (6.2.1)$$

$$\text{RE Length \%} = \frac{|l_{measured} - l_{predicted}|}{l_{measured}} \cdot 100\%. \quad (6.2.2)$$

	Grid 20% #1	Grid 20% #2	Grid 20% #3	Grid 40% #1	Grid 40% #2	Grid 40% #3
Mean Wall Thickness Measurement [mm]	0.409	0.382	0.422	0.484	0.413	0.483
Assumed Wall Thickness [mm]	0.4					
Absolute Error Wall Thickness [mm]	0.009	0.018	0.022	0.084	0.013	0.083
Relative Error Wall Thickness [%]	2.20	4.71	5.21	17.36	3.15	17.18
Mean Grid Length Measurement [mm]	3.596	3.620	3.593	1.495	1.568	1.501
Predicted Grid Length [mm]	3.567		1.583			
Absolute Error Length [mm]	0.029	0.053	0.026	0.088	0.015	0.082
Relative Error Length [%]	0.81	1.46	0.72	5.89	0.96	5.46

Table 6.2: Comparison of estimated grid dimensions and measured grid dimensions.

Table 6.2 shows that the assumption for wall thickness is a good estimation. The biggest difference is with grid 40% infill because of the lines are unevenly distributed, as illustrated in Figure 5.18. The measurements of wall thickness and grid length for grid with 40% infill are difficult to measure, the walls are not uniform in thickness.

For calculating effective tensile modulus, higher wall thickness, and smaller grid length, yields a higher effective tensile modulus for grid patterns. Table 6.2 shows that wall thickness estimation is of smaller size than the measured wall thickness, except one. Grid length estimation should ideally be larger in size than the measured grid length. Table 6.2 has that grid pattern with 20% infill has measured grid length that is larger than predicted grid length, while grid 40% has grid length that is less than the prediction. By predicting a wall thickness that is smaller than the measured wall thickness, and predicting a grid length that is larger than the measured grid length, then there is a safety factor in effective tensile modulus.

To reiterate, t_{grid} and l_{grid} that is used to calculate effective tensile modulus is the measured mean values, to reduce noise in comparison of predicted tensile modulus and tested tensile modulus. This gives cellular solid model a more confident comparison to experimental results for

grid patterns. The mean relative error % is done by using formula (6.2.3) with $E_{experimental}$ and $E_{predicted}$ from mean tensile modulus respectively in Table 6.3.

$$RE \% = \frac{|E_{measured} - E_{predicted}|}{E_{measured}} \cdot 100\%. \quad (6.2.3)$$

	Grid 20% #1	Grid 20% #2	Grid 20% #3	Grid 40% #1	Grid 40% #2	Grid 40% #3
Experimental Tensile Modulus [MPa]	69.626	93.684	109.824	163.340	220.940	145.971
Mean Experimental Tensile Modulus [MPa]		91.045			176.750	
Predicted Tensile Modulus with $E_s = 2797$ MPa [MPa]	318.124	295.153	328.509	905.517	736.710	900.034
Mean Predicted Tensile Modulus with $E_s = 2797$ MPa [MPa]		313.929			847.420	
Absolute Difference [MPa]	248.498	201.469	218.685	742.177	515.770	754.063
Relative Error [%]	356.90	215.05	199.12	454.38	233.44	516.58
Mean Relative Error [%]		244.81			379.45	
Predicted Tensile Modulus with $E_s = 1008.620$ MPa [MPa]	114.718	106.435	118.463	326.537	265.664	324.560
Mean Predicted Tensile Modulus with $E_s = 1008.620$ MPa [MPa]		113.205			305.587	
Absolute Difference [MPa]	45.092	12.751	8.639	163.197	44.724	178.589
Relative Error [%]	64.76	13.61	7.87	99.91	20.24	122.35
Mean Relative Error [%]		24.34			72.89	

Table 6.3: Comparison of experimental and two predicted tensile modulus of grid pattern with 20% and 40% infill density.

Prediction with solid tensile modulus of $E_s = 2797$ MPa, from technical data sheet for tough PLA is a wrong prediction. The estimation has an relative error above 200% for both grid patterns. By using a solid tensile modulus that is significantly lower than what is given in technical data sheet, the estimation is better, however, it still has a relatively high estimation than the modulus from tensile testing.

Locally, the curves showed that there are inconsistency or variations in the stress axis, Figure 5.13 and Figure 5.16, which results in readings that returns inconsistent Young's modulus. To resolve this issue, an approximate line which is then laid on-top of the graph and then the rate of increase can be estimated as the Young's modulus. However, this is a deviation from the standard used in testing for this thesis.

To conclude that cellular solids theory is not applicable to FDM 3D-printed parts is a rushed decision. A more interesting perspective is to explore why there is a large deviation between theory and real-world situations. It is clear that the print quality of the grid pattern is sub-optimal. The stress-strain curve can be considered inconclusive since the testing machine has an error of ± 585 Newtons, which is a significant size compared to the force required for testing of grid patterns. Additionally, determining which solid tensile modulus should be used for estimating the effective tensile modulus is crucial. Two different solid tensile moduli were used: one from the technical data sheet from Ultimaker and the second from tensile testing for the line pattern with a raster angle of 0° and 100% infill.

It seems reasonable that the correct solid tensile modulus should come from a tensile test where the parts are printed with the same parameters used for the grid patterns. This thesis includes

four different tensile moduli for line patterns with various raster angles. Using the solid tensile modulus from the line pattern with a raster angle of 90° or $\pm 45^\circ$ would result in a smaller effective tensile modulus. What is missing to accurately determine the effective tensile modulus of the grid pattern is identifying which solid tensile modulus should be used in formulas (3.2.1) and (3.2.2). A literature review shows different papers documenting how various printing parameters affect mechanical properties.

6.3 Failure Mechanisms for 3D-printed Parts

For all tensile testing conducted in this thesis, the standard used was ISO 1926:2009. A fixture was created to ensure no compression was applied to the test specimens during tensile testing. Metal plates were glued to the ends of the specimens to reinforce the areas where force was applied. However, these metal plates detached during the tensile tests for specimens with a line pattern and raster angles of 0° and $[0, \pm 30, \pm 60, 0, 90]_R$. The adhesive used for attaching the metal plates was applied sparingly, which may have contributed to their detachment. Applying more adhesive could potentially resolve this issue. The detachment of the metal plates during testing could have caused collision impacts that might explain the presence of two fractures in some test specimens.

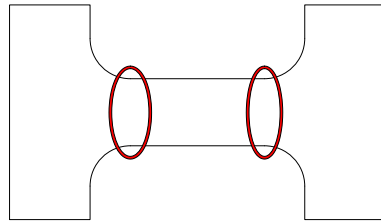


Figure 6.1: Dog-bone specimen with red circles indicating where failures occurred.

Most failures occurred at the transition from the radii to the gauge length section, as illustrated in Figure 6.1. The fractures in most tests did not occur within the gauge length section, as shown in Figure 2.2. Two exceptions were the line pattern specimens with raster angle 0° and 100% infill #3 and #4, which exhibited fractures in the “ear” section that broke off, as depicted in Figure 5.4b. Viewing the printing process in the Ultimaker Cura slicer software revealed that the “ear” section is the last part to be printed in each layer.

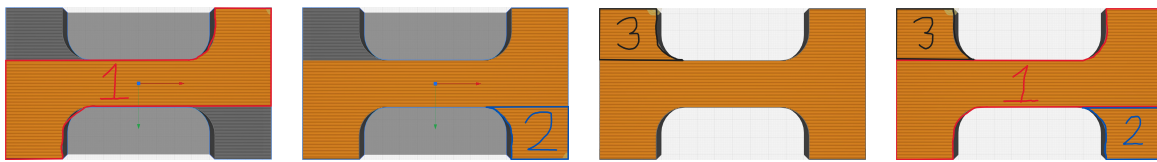


Figure 6.2: Tool-path for FDM 3D-printer for line pattern with raster angle 0° and 100% infill.

Figure 6.2 shows the tool-path for the 3D printer. It starts in the lower left corner, continues up to the right corner, finishes in the lower right corner, and lastly prints the top left “ear”. This tool-path is consistent across all layers of the FDM 3D-printed part. It is speculated that since the top left part is printed last, the bond between the newly deposited fiber and the already printed fiber is weak due to cooling and temperature differences. Enabling the option to randomize the infill start in Ultimaker Cura could mitigate this issue by avoiding the creation of this specific weakness in 3D prints.

For fractures occurring in the radii section, the exact cause is unclear. A literature review revealed that dog-bone specimens with any sort of radius or change in cross-sectional area often fail at these transition points. Interestingly, tensile tests on dog-bone specimens without metal

plates showed failures in the gauge length area, as seen in Figure 5.6 and Figure 5.9. This suggests that the presence of metal plates might influence fractures in the radii of the dog-bone specimens.

Overall, improving the adhesion of the metal plates and addressing the weak bond in the “ear” section through randomizing infill start could enhance the reliability of the tensile testing results. Further investigation into the specific causes of fractures in the radii section is recommended.

6.4 Final Remarks

The manufacture of dog-bone specimens was performed using two printers of the same model, but there was a noticeable variation in print quality depending on the printer. Issues such as shrinking and creep deformed the dog-bones at the points where the metal plates were glued. Observations during printing revealed that the Ultimaker 2+ deposited filament in a way that fibers touched each other, while the Ultimaker Extended 2+ left clear gaps between fibers. Poor print quality can be attributed to factors like inadequate calibration of the printer bed and variations in room temperature where the printers were located. Measurements showed that the dog-bones had a wider width at the bottom, where the parts were in contact with the printer bed, and a narrower width at the top, where the final layers were printed. Since the printers had open cabinets, room temperature fluctuations affected print quality. For parts the size of the dog-bones printed in this thesis, maintaining a consistent temperature, ideally in a closed cabinet, is crucial to ensuring higher print quality.

The standard for determining tensile properties specifies that a test is invalid if the fracture occurs outside the gauge length area, as shown in Figure 2.2. However, this standard was not strictly adhered to in this thesis. If tests with fractures outside the gauge length had been discarded, there would have been no tensile test results to discuss. Thus, exceptions were made to include these tests. This raises the question of whether ISO 1926:2009 *Rigid Cellular Plastics - Determination of tensile properties* is the appropriate standard for FDM 3D-printed parts. The results and comparisons for CLT computations suggest that the results are reasonable. For structures with low infill density that cannot withstand compression forces from the clamps, this standard must be used. Although the Poisson’s ratio was not determined due to the unavailability of an extensometer, failures outside the gauge length are not deemed critical errors in this context.

For future tests, it is recommended to test dog-bone specimens with 100% infill without using metal plates. If metal plates are used, more adhesive should be applied to ensure sufficient adhesion. Metal plates should be used for specimens with infill densities below 60% or 70%. While it is possible to perform tensile tests without the fixture and place the specimen directly in the tensile machine, ensuring that the dog-bone is aligned parallel to the axial force is more challenging without the fixture. The fixture simplifies the process by ensuring proper alignment, which is crucial because misalignment can subject the test object to shear and moment forces in addition to axial forces. Although it takes an average of two hours to set up the fixture correctly, it allows for quick succession testing once in place. However, without the fixture, aligning the non-square sides of the 3D-printed dog-bones becomes difficult, complicating the testing process.

Test machine chosen was not suitable for test of grid pattern with low infill density. Instead a grid pattern with higher infill density should have been used, such as infill density 70% to 90%. This could have mitigate the errors in determining tensile modulus from testing. Measurement of wall thickness and grid length could be more difficult with higher infill density, since grid pattern with 40% infill is already problematic to measure.

6.5 Future Work

There is still much research needed to fully understand the mechanical properties of FDM 3D-printed parts. Various printing parameters significantly influence these properties, even for simple line patterns. To effectively use CLT, it is essential to determine the local mechanical properties before any calculations can be performed. Machine learning can be a valuable tool for the future application of CLT to FDM 3D-printed structures. By adjusting print parameters and performing tensile tests, the results can be fed into an artificial intelligence (AI) system to predict mechanical properties accurately. This requires lots of tests and data to be a valuable resource.

Tool-path considerations are crucial when addressing failure mechanisms in 3D-printed parts. The slicer software's coding of the tool-path should avoid inherent weaknesses in the printed parts. Many geometries used in FDM 3D printing are not convex hulls, which can contribute to failure points, as observed with the line pattern 0° , 100% infill specimens #3 and #4. A convex hull is when a geometry can place two points, and draw a straight line between the two points, and the line does not cross the boundary. For example a circle is a convex hull.

For cellular solids, a simple grid pattern structure was chosen to compare theoretical predictions with actual mechanical properties through tensile testing. The results in this thesis highlighted questions regarding the appropriate solid tensile modulus to use for predicting mechanical properties. The poor print quality for the grid with 40% infill density also affected the mechanical properties. Understanding where predictions fail is of significant interest. Future work should focus on how cellular solid theory applies to FDM 3D-printed parts, as this could provide valuable insights.

Chapter 7

Conclusion

The report documents 21 tensile tests, six of which were conducted with grid pattern and 15 with line pattern. For grid patterns, the mean tensile modulus from testing was 91.045 MPa for 20% infill and 176.750 MPa for 40% infill. These modulus have an relative error of 24.34% and 72.89%, respectively, to the predicted tensile modulus using cellular solid theory. This suggests that the correct use of cellular solid theory to predict mechanical properties of FDM 3D-printed parts was not confirmed in the thesis. Three main factors contributed to the incorrect predictions: the incorrect choice of solid tensile modulus, the imperfect infill structure created during 3D-printing, and wrong test machine for tensile testing, which rendered cellular solid theory inapplicable.

To validate Classical Laminate Theory (CLT), three groups of line patterns were tested to determine local mechanical properties. These groups had raster angles of 0° , 90° , and $\pm 45^\circ$, with mean tensile moduli from testing of $E_1 = 1008.621$ MPa, $E_2 = 711.108$ MPa, and $E_x^{45} = 740.300$ MPa, respectively. Using E_x^{45} to determine the local shear modulus resulted in $G_{12} = 268.864$ MPa. With a major Poisson's ratio of $\nu_{12} = 0.36$, the predicted tensile modulus from CLT was $E_{CLT} = 837.340$ MPa. To evaluate CLT computation, three dog-bones with line patterns and raster angles of $[0, \pm 30, \pm 60, 0, 90]_R$ with 100% infill were printed and tested, yielding a mean tensile modulus of 874.566 MPa. This result had a relative error of 4.26% to the predicted modulus from CLT, suggesting that CLT is a reliable mathematical model for determining the mechanical properties of FDM 3D-printed parts.

The standard ISO 1926:2009 was found to work reasonably well for FDM 3D-printed parts, particularly for dog-bones with low infill density where compression forces could damage or destroy the test object. However, its applicability should be considered based on the specific requirements and characteristics of the printed parts being tested. Dog-bones dimensions given in standard ISO 1926:2009 has not a convex hull geometry. Using a standard or geometry for test specimen that has convex hull properties would eliminate points of failure in tensile testing.

Bibliography

- [1] H. Bikas, P. Stavropoulos, and G. Chryssolouris, “Additive manufacturing methods and modelling approaches: A critical review,” *The International Journal of Advanced Manufacturing Technology*, vol. 83, pp. 389–405, 1-4 Mar. 2016, ISSN: 0268-3768. DOI: 10.1007/s00170-015-7576-2.
- [2] L. J. Gibson and M. F. Ashby, *Cellular Solids: Structure and Properties*, 2nd ed. Cambridge: Cambridge University Press, 1997, ISBN: 0521-49560.
- [3] A. Bellini and S. Güçeri, “Mechanical characterization of parts fabricated using fused deposition modeling,” *Rapid Prototyping Journal*, vol. 9, no. 4, pp. 252–264, Oct. 2003, ISSN: 1355-2546. DOI: 10.1108/13552540310489631. [Online]. Available: <https://www.emerald.com/insight/content/doi/10.1108/13552540310489631/full/html>.
- [4] M. Fernandez-Vicente, W. Calle, S. Ferrandiz, and A. Conejero, “Effect of Infill Parameters on Tensile Mechanical Behavior in Desktop 3D Printing,” *3D Printing and Additive Manufacturing*, vol. 3, no. 3, pp. 183–192, Sep. 2016, ISSN: 2329-7662. DOI: 10.1089/3dp.2015.0036.
- [5] R. Zou, Y. Xia, S. Liu, *et al.*, “Isotropic and anisotropic elasticity and yielding of 3D printed material,” *Composites Part B: Engineering*, vol. 99, pp. 506–513, Aug. 2016, ISSN: 13598368. DOI: 10.1016/j.compositesb.2016.06.009.
- [6] G. Alaimo, S. Marconi, L. Costato, and F. Auricchio, “Influence of meso-structure and chemical composition on fdm 3d-printed parts,” *Composites Part B: Engineering*, vol. 113, pp. 371–380, Mar. 2017, ISSN: 13598368. DOI: 10.1016/j.compositesb.2017.01.019.
- [7] A. Rodríguez-Panes, J. Claver, and A. M. Camacho, “The influence of manufacturing parameters on the mechanical behaviour of PLA and ABS pieces manufactured by FDM: A comparative analysis,” *Materials*, vol. 11, no. 8, Aug. 2018, ISSN: 19961944. DOI: 10.3390/ma11081333.
- [8] S. R. Rajpurohit and H. K. Dave, “Effect of process parameters on tensile strength of FDM printed PLA part,” *Rapid Prototyping Journal*, vol. 24, no. 8, pp. 1317–1324, Nov. 2018, ISSN: 13552546. DOI: 10.1108/RPJ-06-2017-0134.
- [9] Y. Zhao, Y. Chen, and Y. Zhou, “Novel mechanical models of tensile strength and elastic property of FDM AM PLA materials: Experimental and theoretical analyses,” *Materials and Design*, vol. 181, Nov. 2019, ISSN: 18734197. DOI: 10.1016/j.matdes.2019.108089.
- [10] C. Vălean, L. Marşavina, M. Mărghitaş, E. Linul, N. Razavi, and F. Berto, “Effect of manufacturing parameters on tensile properties of FDM printed specimens,” in *Procedia Structural Integrity*, vol. 26, Elsevier B.V., 2020, pp. 313–320. DOI: 10.1016/j.prostr.2020.06.040.
- [11] A. Nasirov and I. Fidan, “Prediction of mechanical properties of fused filament fabricated structures via asymptotic homogenization,” *Mechanics of Materials*, vol. 145, Jun. 2020, ISSN: 01676636. DOI: 10.1016/j.mechmat.2020.103372.
- [12] R. cellular plastics — Determination of tensile properties, “Iso 1926,” *ISO*, 2009.
- [13] S. og skumgummi: Bestemmelse av lineære dimensjoner, “Ns-en iso 1923:1981,” *NS-EN ISO*, 1981.

-
- [14] N. S. P. B. av strekkegenskaper Del 1: Generelle prinsipper, “Iso 527,” *Norsk Standard*, 2012.
- [15] E. Kreyszig, *Advanced Engineering Mathematics*, 10th ed. Singapore: John Wiley & Sons, Inc., 2011, ISBN: 978-0-470-64613-7.
- [16] Ultimaker, *Ultimaker tough pla technical data sheet*, Last accessed 02.05.2024, 2024. [Online]. Available: <https://um-support-files.ultimaker.com/materials/2.85mm/tds/TOUGH-PLA/UM220509-Tough-PLA-TDS-RB-v2.10.pdf>.
- [17] A. Meidell, “Homogenization and computational methods for calculating effective properties of some cellular solids and composite structures,” Ph.D. dissertation, NTNU, Trondheim, 2001, ISBN: 82-7984-181-4.
- [18] G. Beeri, “Some mathematical, numerical and engineering aspects of composite structures and perforated solids,” Ph.D. dissertation, Luleå Univeristy of Technology, Luleå, 2009, ISBN: 978-91-86233-76-1.
- [19] A. Öchsner, *Advanced Structured Materials Foundations of Classical Laminate Theory*. Cham: Springer Nature Switzerland AG, 2021, vol. 163, ISBN: 978-3-030-82631-4. [Online]. Available: <http://www.springer.com/series/8611>.
- [20] T. Coburn, *Composite strength (aro4360)*, Accessed: 01.03.2024-25.03.2024. [Online]. Available: <https://www.youtube.com/playlist?list=PLJN7mr1gK7YWjJgwCsjIb8R3TGxLvPipW>.
- [21] A. Nettles, *Basic Mechanics of Laminated Composite Plates*. NASA Reference Publication 1351, 1994, pp. 1–107.
- [22] P. Mallick, *Fiber-Reinforced Composites: Materials, manufacturing, and design*, 2nd ed. Marcel Dekker, Inc, 1993, ISBN: 0824790316.
- [23] S. Farah, D. G. Anderson, and R. Langer, “Physical and mechanical properties of pla, and their functions in widespread applications — a comprehensive review,” *Advanced Drug Delivery Reviews*, vol. 107, pp. 367–392, Dec. 2016, ISSN: 0169409X. DOI: 10.1016/j.addr.2016.06.012.

Appendix A

Matlab Code for CLT

```
% Script to calculate CLT problems
% Input part for CLT computation
ply = 15/0.1; % Determines the ply's by dividing the height by
    layer thickness
layer_angles = repmat( [0 30 -30 60 -60 0 90], [1 (round(ply/7) +1)
    ]); % Use repmat to give repeating angles such as repmat( [45
    -45], [1 eq: rep = ply/2] )
layer_thickness = 0.1; % Assuming that all layers have the same
    thickness through the whole laminate, for this master thesis
    the layer height is 0.1 mm
laminate_thickness = 15; % The laminate is for unreinforced test
    specimen

longitude_moduli = 1008.621; % These mechanical properties is in 12
    direction and given in MPa or N/mm^2
transverse_moduli = 711.108;
shear_moduli = 268.864;
poisson_ratio12 = 0.36; % Difficult to find poisons ratio from
    manufacture but most is used is 0.36
poisson_ratio21 = transverse_moduli*poisson_ratio12/
    longitude_moduli;

Q = [ longitude_moduli/(1 - poisson_ratio12*poisson_ratio21)
    transverse_moduli*poisson_ratio12/(1 - poisson_ratio12*
    poisson_ratio21) 0;
    transverse_moduli*poisson_ratio12/(1 - poisson_ratio12*
    poisson_ratio21) transverse_moduli/(1 - poisson_ratio12*
    poisson_ratio21) 0;
    0 0 shear_moduli]

% Q is stiffness matrix for orthotropic ply

% Some specification of layers and such
lamina_k = zeros(ply,4);

for i = 1:ply
    lamina_k(i,1:4) = [i layer_thickness*(i-1)-ply*layer_thickness
        /2 layer_thickness*i-ply*layer_thickness/2 layer_angles(i)];
```


APPENDIX A. MATLAB CODE FOR CLT

```

        % 1st lamina k, 2nd z_k-1 coordinate in mm, 3rd z_k
        coordinate in mm, 4th angle alpha_k
end

lamina_k

% Calculating QBar or Cbar matrix that transform C_k
engineeringstrain_tru strain_factorisation = [1 0 0; 0 1 0; 0 0 2];
% matrix used to calc. true strain to engineering strain
QBar = zeros(3,3*ply);
for i = 1:ply
    angle_alpha = layer_angles(i)*pi/180;
    % Let first define cos and sine to something simple
    c = cos(angle_alpha);
    s = sin(angle_alpha);
    angle_transform = [ c^2 s^2 2*s*c ; s^2 c^2 -2*s*c ; -s*c s*c c
        ^2-s^2 ]; % transform stress/strain in xy to 12 direction of
        lamina
    inv_angle_transform = [c^2 s^2 -2*s*c ; s^2 c^2 2*s*c ; s*c -s*
        c c^2-s^2]; % transform stress/strain from 12 to xy
        direction

    QBar(1:3,(3*i-2):3*i) = inv_angle_transform * Q *
        engineeringstrain_tru strain_factorisation * angle_transform
        / engineeringstrain_tru strain_factorisation ;
end
QBar

% Creating C* matrix formed of ABBD
A = zeros(3,3);
B = zeros(3,3);
D = zeros(3,3);

for i = 1:3
    for j=1:3
        vectorsummarized_Amatrix = zeros(1,ply);
        for k = 1:ply
            vectorsummarized_Amatrix(1,k) = QBar(i,j+3*k-3) * (
                lamina_k(k,3) - lamina_k(k,2) );
        end
        A(i,j) = sum(vectorsummarized_Amatrix, 'all');
    end
end
end
A % A matrix is units N/mm^2 * mm = N/mm

for i = 1:3
    for j=1:3
        vectorsummarized_Bmatrix = zeros(1,ply);
        for k = 1:ply
            vectorsummarized_Bmatrix(1,k) = QBar(i,j+3*k-3) * (
                lamina_k(k,3)^2 - lamina_k(k,2)^2 );
        end
    end
end

```

```

        end
        B(i,j) = 0.5 * sum(vectorsummarized_Bmatrix,"all");
    end
end
B % B matrix is in units N/mm^2 * mm^2 = N

for i = 1:3
    for j=1:3
        vectorsummarized_Dmatrix = zeros(1,ply);
        for k = 1:ply
            vectorsummarized_Dmatrix(1,k) = QBar(i,j+3*k-3) * (
                lamina_k(k,3)^3 - lamina_k(k,2)^3 );
        end
        D(i,j) = 1/3 * sum(vectorsummarized_Dmatrix,'all');
    end
end
D % D matrix is in units N

% Remember to check units on A B D matrix is correct when used to
% determine
% strains from loads on laminate.
C = [ A B ; B D ] % Generalized elasticity matrix goes from Msi to
% si 18.03.2024 check dimensions and change accordingly in A B and
% D
invC = inv(C)

% Determining engineering constants from laminate

if all( B(:) == 0 ) == 1 || abs(det(B)) <= 10^-20 % If-code to
% determine if the laminate is symmetric or not
    calculation_Ex = A \ [1 ; 0 ; 0];
    tensilemoduli_Ex = 1 / laminate_thickness / calculation_Ex(1,1)
    calculation_Ey = A \ [0 ; 1 ; 0];
    tensilemoduli_Ey = 1 / laminate_thickness / calculation_Ey(2,1)
    calculation_Gxy = A \ [ 0 ; 0 ; 1];
    shearmoduli_Gxy = 1 / laminate_thickness / calculation_Gxy(3,1)
    poissons_ratio_xy = - calculation_Ex(2,1) / calculation_Ex(1,1)
    poissons_ratio_yx = - calculation_Ey(1,1) / calculation_Ey(2,1)
else % For unsymmetric laminates
    tensilemoduli_Ex = 1 / laminate_thickness * det(C) / det( C
        (2:6,2:6) )
    tensilemoduli_Ey = 1 / laminate_thickness * det(C) / det( [ C
        (1,1) C(1,3:6) ; C(3:6,1) C(3:6,3:6) ])
    shearmoduli_Gxy = 1 / laminate_thickness * det(C) / det( [ C
        (1:2,1:2) C(1:2,4:6) ; C(4:6,1:2) C(4:6,4:6) ])
    poissons_ratio_xy = - det([ C(2:6,1) C(2:6,3:6) ]) / det([ C
        (2:6,2:6) ])
    poissons_ratio_yx = - det([ C(1,2:6) ; C(3:6,2:6) ]) / det([ C
        (1,1) C(1,3:6) ; C(3:6,1) C(3:6,3:6) ])
end
end

```

```

% Calculating strains and stresses
generalized_stresses = transpose( input('Give loads in problem [Nx
  Ny Nxy Mx My Mxy]: ') ); % Forces acting on laminate
strain_curvature = invC * generalized_stresses
strain = strain_curvature(1:3);
curvature = strain_curvature(4:6);

% Calculating stresses in each ply in x-y coordinate system
layer_stress_xy_bottom = zeros(3,ply);
layer_stress_xy_middle = zeros(3,ply);
layer_stress_xy_top = zeros(3,ply);

for i = 1:ply
    layer_stress_xy_bottom(1:3,i) = QBar(1:3,(3*i-2):3*i)* (strain
        + lamina_k(i,2) * curvature);
    layer_stress_xy_middle(1:3,i) = QBar(1:3,(3*i-2):3*i)* (strain
        + (lamina_k(i,3) + lamina_k(i,2) )/2 * curvature);
    layer_stress_xy_top(1:3,i) = QBar(1:3,(3*i-2):3*i)* (strain +
        lamina_k(i,3) * curvature);
end

layer_stress_xy_bottom % each colum corresponds to each layer. So
    first column is the first layer and so on.
layer_stress_xy_middle
layer_stress_xy_top

layer_stress_12_bottom = zeros(3,ply);
layer_stress_12_middle = zeros(3,ply);
layer_stress_12_top = zeros(3,ply);

for i = 1:ply
    angle_alpha = layer_angles(i)*pi/180;
    % Let first define cos and sine to something simple
    c = cos(angle_alpha);
    s = sin(angle_alpha);
    angle_transform = [ c^2 s^2 2*s*c ; s^2 c^2 -2*s*c ; -s*c s*c c
        ^2-s^2 ]; % transform stress/strain in xy to 12 direction of
        lamina
    layer_stress_12_bottom(1:3,i) = angle_transform *
        layer_stress_xy_bottom(1:3,i);
    layer_stress_12_middle(1:3,i) = angle_transform *
        layer_stress_xy_middle(1:3,i);
    layer_stress_12_top(1:3,i) = angle_transform *
        layer_stress_xy_top(1:3,i);
end

layer_stress_12_bottom
layer_stress_12_middle
layer_stress_12_top

% Calculating strains in each ply in x-y coordinate system

```

```
layer_strain_xy_bottom = zeros(3,ply);
layer_strain_xy_middle = zeros(3,ply);
layer_strain_xy_top = zeros(3,ply);

for i = 1:ply
    layer_strain_xy_bottom(1:3,i) = strain + lamina_k(i,2) *
        curvature;
    layer_strain_xy_middle(1:3,i) = strain + (lamina_k(i,3) +
        lamina_k(i,2) )/2 * curvature;
    layer_strain_xy_top(1:3,i) = strain + lamina_k(i,3) * curvature
    ;
end
layer_strain_xy_bottom
layer_strain_xy_middle
layer_strain_xy_top
```

Appendix B

Printing Parameters in Ultimaker Cura

Parameter	Default	Thesis settings
Quality		
Layer Height [mm]	0.1	0.1
Initial Layer Height [mm]	0.27	0.1
Line Width [mm]	0.4	0.4
Wall Line Width [mm]	0.4	0.4
Outer Wall Line Width [mm]	0.4	0.4
Inner Wall(s) Line Width [mm]	0.4	0.4
Top/Bottom Line Width [mm]	0.4	0.4
Infill Line Width [mm]	0.4	0.4
Skirt/Brim Line Width [mm]	0.4	0.4
Initial Layer Line Width [%]	100	100
Walls		
Wall Thickness [mm]	0.8	0.4
Wall Line Count [#]	2	1
Wall Transition Length [mm]	0.4	0.4
Wall Distribution Count [#]	1	1
Wall Transitioning Threshold Angle [°]	10	10
Wall Transitioning Filter Margin [mm]	0.1	0.1
Outer Wall Wipe Distance [mm]	0.2	0.2
Outer Wall Inset [mm]	0	0
Optimize Wall Printing Order	-	-
Wall Ordering	Outside To Inside	Outside To Inside
Minimum Wall Line Width [mm]	0.34	0.34

APPENDIX B. PRINTING PARAMETERS IN ULTIMAKER CURA

Parameter	Default	Thesis settings
Minimum Even Wall Line Width [mm]	0.34	0.34
Minimum Odd Wall Line Width [mm]	0.34	0.34
Print Thin Walls	✓	✓
Minimum Feature Size [mm]	0.1	0.1
Minimum Thin Wall Line Width [mm]	0.34	0.34
Walls		
Horizontal Expansion [mm]	-0.01	-0.01
Initial Layer Horizontal Expansion [mm]	-0.09	-0.09
Hole Horizontal Expansion [mm]	0	0
Z Seam Alignment	Sharpest Corner	Sharpest Corner
Seam Corner Preference	None	None
Top/Bottom		
Top Surface Skin Layers [#]	1	-
Top Surface Skin Line Width [mm]	0.4	-
Top Surface Skin Pattern	Lines	-
Monotonic Top Surface Order	✓	-
Top Surface Skin line Directions [°]	-	-
Top/Bottom Thickness [mm]	0.8	0
Top Thickness [mm]	0.8	0
Top Layers [#]	8	0
Bottom Thickness [mm]	0.8	0
Bottom Layers [#]	8	0
Initial Bottom Layers [#]	8	0
Top/Bottom Pattern	Lines	-
Bottom Pattern Initial Layer	Lines	-
Monotonic Top/Bottom Order	-	-
Top/Bottom Line Directions [°]	-	-
Small Top/Bottom Width [mm]	0.8	-
Small Top/Bottom On Surface	-	-
No Skin in Z Gaps	-	-
Extra Skin Wall Count [#]	1	-
Enable Ironing	-	-

Parameter	Default	Thesis settings
Skin Overlap Percentage [%]	20	-
Skin Overlap [mm]	0.08	-
Skin Removal Width [mm]	0.8	-
Top/Bottom		
Top Skin Removal Width [mm]	0.8	-
Bottom Removal Width [mm]	0.8	-
Skin Expand Distance [mm]	0.8	-
Top Skin Expand Distance [mm]	0.8	-
Bottom Skin Expand Distance [mm]	0.8	-
Maximum Skin Angle For Expansion [°]	90	-
Minimum Skin Width For Expansion [mm]	0	-
Infill		
Infill Density [%]	20	Dependent on specimen
Infill Line Distance [mm]	Dependent on Infill density	Dependent on Infill Density
Infill Pattern	Grid	Dependent on specimen
Connect Infill Lines	-	-
Infill Line Directions [°]	-	Dependent on specimen
Infill X Offset [mm]	0	0
Infill Y Offset [mm]	0	0
Randomize Infill Start	-	-
Infill Line Multiplier [#]	1	1
Extra Infill Wall Count [#]	0	0
Infill Overlap Percentage [%]	10	10
Infill Overlap [mm]	0.04	0.04
Infill Wipe Distance [mm]	0.1	0.1
Infill Layer Thickness [mm]	0.1	0.1
Gradual Infill Steps [#]	0	0
Infill Before Walls	✓	✓
Minimum Infill Area [mm ²]	0	0
Skin Edge Support Thickness [mm]	0.4	0

APPENDIX B. PRINTING PARAMETERS IN ULTIMAKER CURA

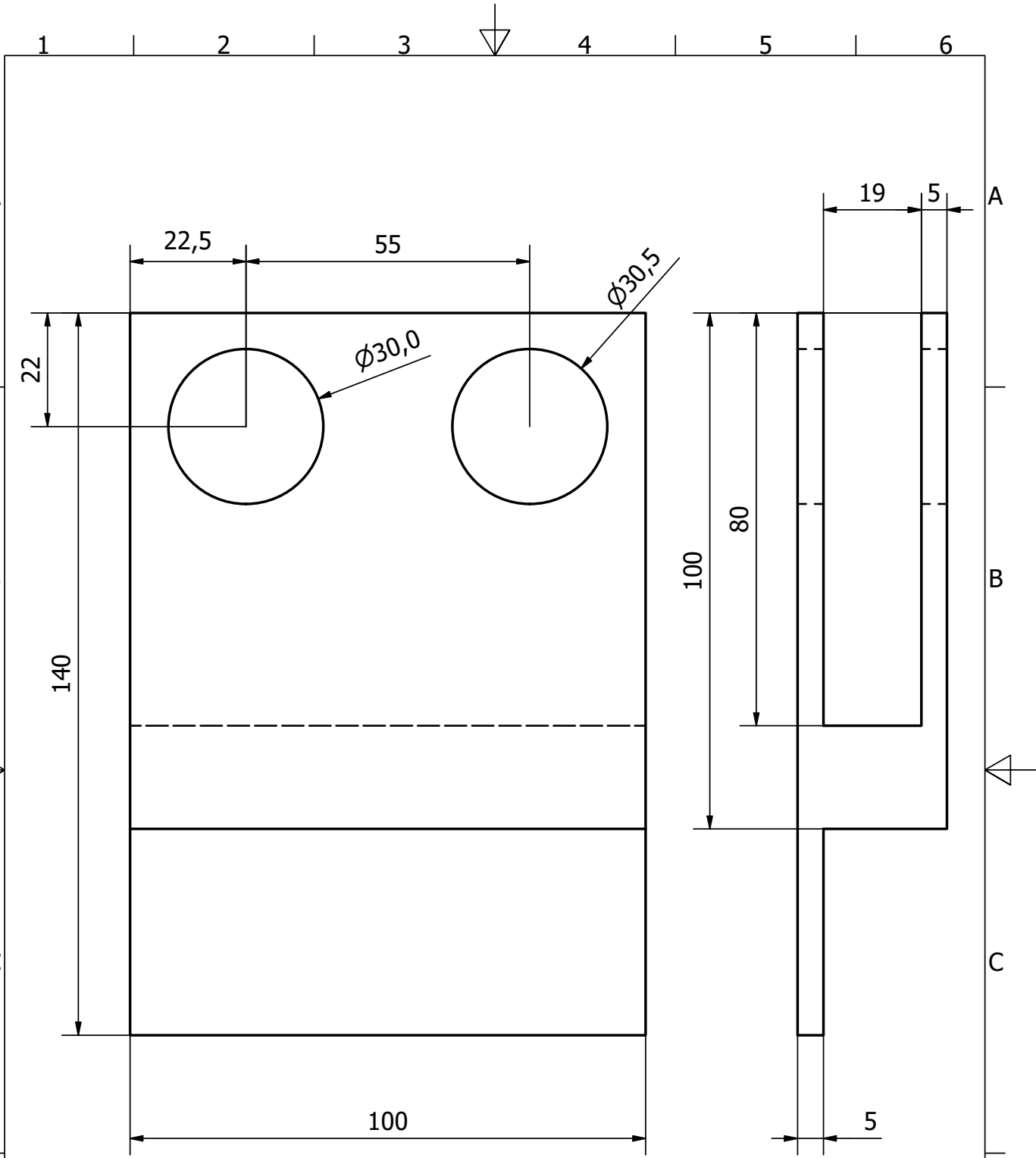
Parameter	Default	Thesis settings
Skin Edge Support Layers [#]	4	4
Material		
Scaling Factor Shrinkage Compensation [%]	100	100
Horizontal Scaling Factor Shrinkage Compensation [%]	100	100
Vertical Scaling Factor Shrinkage Compensation [%]	100	100
Wall Flow [%]	100	100
Outer Wall Flow [%]	100	100
Inner Wall(s) Flow [%]	100	100
Top Surface Outer Wall Flow [%]	100	100
Top Surface Inner Wall(s) Flow [%]	100	100
Top/Bottom Flow [%]	95	-
Top Surface Skin Flow [%]	100	-
Initial Flow [%]	100	100
Skirt/Brim Flow [%]	100	-
Prime Tower Flow [%]	100	100
Initial Layer Flow [%]	100	100
Initial Layer Inner Wall Flow [%]	95	95
Initial Layer Outer Wall Flow [%]	110	110
Initial Layer Bottom Flow [%]	95	-
Gradual flow enabled	-	-
Speed		
Print Speed [mm/s]	50	50
Infill speed [mm/s]	50	50
Wall Speed [mm/s]	40	40
Outer Wall Speed [mm/s]	30	30
Inner Wall Speed [mm/s]	40	40
Top Surface Outer Wall Speed [mm/s]	30	30
Top Surface Inner Wall Speed [mm/s]	40	40
Top Surface Skin Speed [mm/s]	20	-
Top/Bottom Speed [mm/s]	20	-
Speed		

Parameter	Default	Thesis settings
Travel Speed [mm/s]	120	120
Initial Layer Speed [mm/s]	30	30
Initial Layer Print Speed [mm/s]	30	30
Initial Layer Travel Speed [mm/s]	120	120
Skirt/Brim Speed [mm/s]	30	30
Z Hop Speed [mm/s]	10	10
Number of Slow Layers [#]	2	2
Flow Equalization Ratio [%]	110	110
Enable Acceleration Control	-	-
Enable Jerk Control	-	-
Travel		
Enable Retraction	✓	✓
Retract at Layer Change	-	-
Retraction Extra Prime Amount [mm°]	0	0
Retraction Minimum Travel [mm]	0.8	0.8
Maximum Retraction Count [#]	25	25
Minimum Extrusion Distance Window [mm]	1	1
Combing Mode	Not On Outer Surface	Not On Outer Surface
Max Comb Distance With No Retract [mm]	15	15
Retract Before Outer wall	-	-
Avoid Printed Parts When Traveling	✓	✓
Avoid Supports When Traveling	-	-
Travel Avoid Distance [mm]	0.6562	0.6562
Layer Start X [mm]	0	0
Layer Start Y [mm]	0	0
Z Hop When Retracted	-	-
Cooling		
Enable Print Cooling	✓	✓
Cooling		
Fan Speed [%]	100	100
Regular Fan Speed [%]	100	100
Maximum Fan Speed [%]	100	100

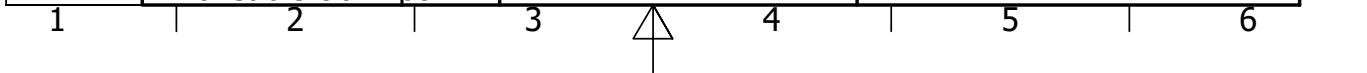
Parameter	Default	Thesis settings
Regular/Maximum Fan Speed Threshold [%]	10	10
Initial Fan Speed [%]	0	0
Regular Fan Speed at Height [mm]	0.27	0.1
Regular Fan Speed at layer [#]	2	2
Minimum Layer Time [s]	5	5
Minimum Speed [mm/s]	10	10
Lift Head	-	-
Small Layer Printing Temperature [°C]	190	190
Build Plate Adhesion		
Build Plate Adhesion Type	Brim	Brim
Skirt/Brim Minimum Length [mm]	250	250
Brim Width [mm]	8	8
Brim Line Count [#]	20	20
Brim Distance [mm]	0	0
Brim Only on Outside	✓	✓
Brim Inside Avoid Margin [mm]	2.5	2.5
Smart Brim	✓	✓

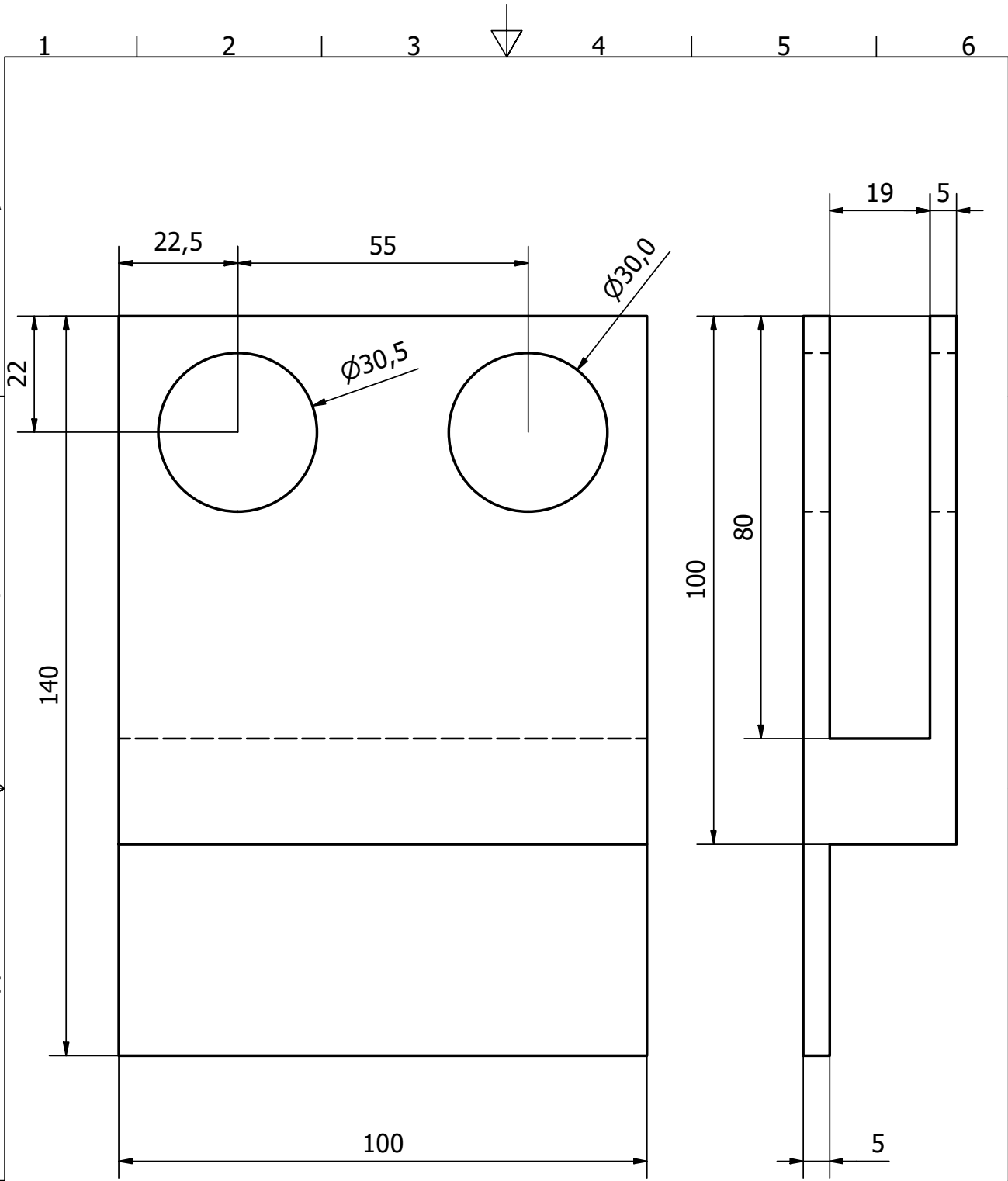
Appendix C

Technical Drawings of Fixture

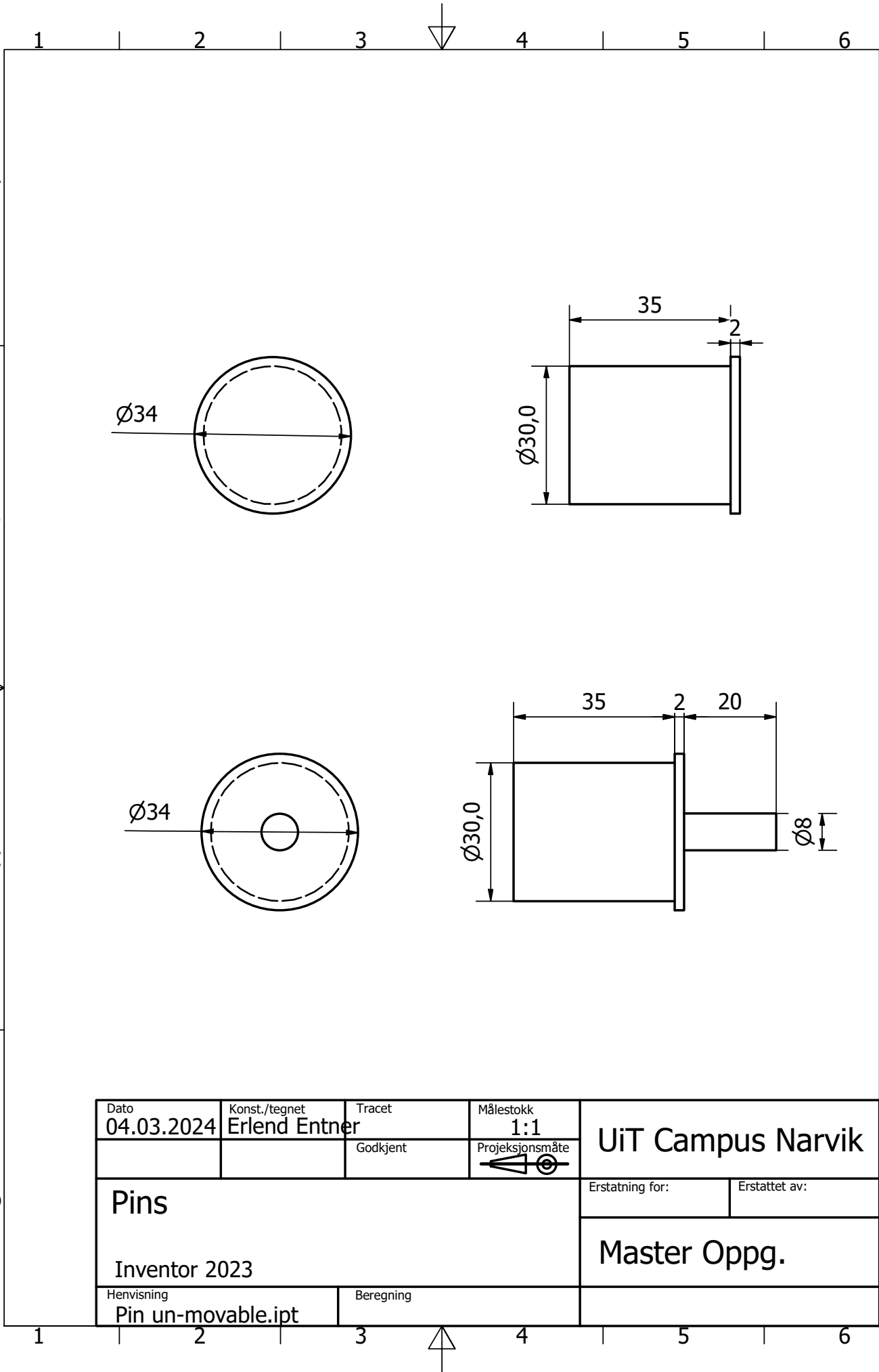


Dato 04.03.2024	Konst./tegnet Erlend Entner	Tracet	Målestokk 1:1	UiT Campus Narvik	
		Godkjent	Projeksjonsmåte 		
Lower Fixture				Erstatning for:	Erstattet av:
Inventor 2023				Master Oppg.	
Henvisning Moveable claw.ipt		Beregning			

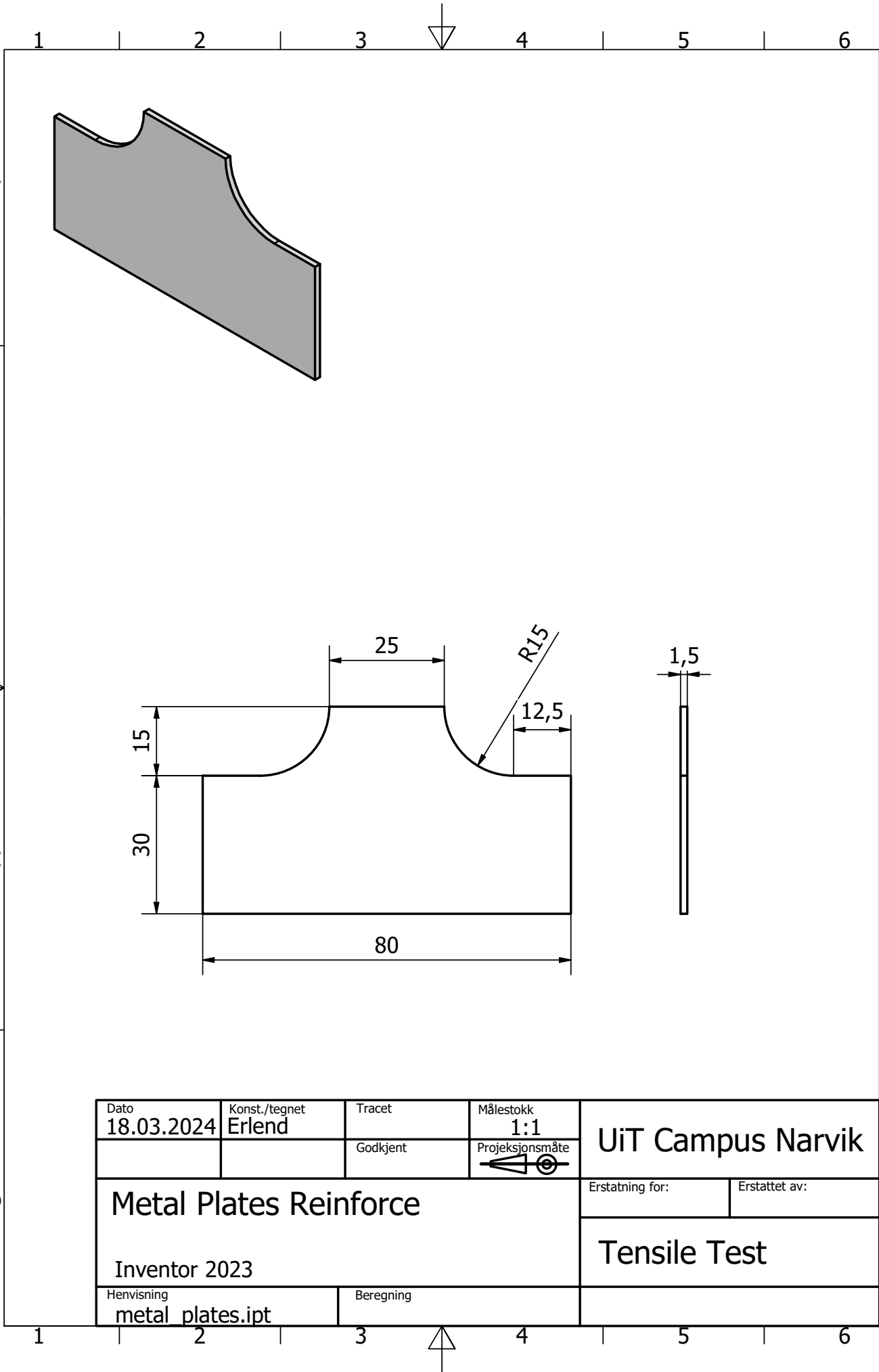




Dato 04.03.2024	Konst./tegnet Erlend Entner	Tracet	Målestokk 1:1	UiT Campus Narvik	
		Godkjent	Projeksjonsmåte 		
Upper Fixture				Erstatning for:	Erstattet av:
Inventor 2023				Master Oppg.	
Henvisning Moveable claw.ipt		Beregning			



Dato 04.03.2024	Konst./tegnet Erlend Entner	Tracet	Målestokk 1:1	UiT Campus Narvik	
		Godkjent	Projeksjonsmåte 		
Pins				Erstatning for:	Erstattet av:
Inventor 2023				Master Oppg.	
Henvising Pin un-movable.ipt		Beregning			



Dato 18.03.2024	Konst./tegnet Erlend	Tracet	Målestokk 1:1	UiT Campus Narvik	
		Godkjent	Projeksjonsmåte 		
Metal Plates Reinforce				Erstatning for:	Erstattet av:
				Tensile Test	
Henvising metal_plates.ipt		Beregning			

Appendix D

Matlab Code for Evaluation of Tensile Test

Example of code for evaluation from tensile testing. This code is specifically for line pattern with raster angle 0° and 100% infill.

```
% Calculation of Tensile moduli from tensile test

width_1 = ( 25.19 + 25.29 + 25.28 ) / 3 ;
width_2 = ( 25.18 + 25.3 + 25.3 ) / 3 ;
width_3 = ( 25.19 + 25.31 + 25.2 ) / 3 ;
width_4 = ( 25.18 + 25.31 + 25.39 ) / 3 ;
width_5 = ( 25.19 + 25.325 + 25.235 ) / 3 ;

Line0Number1_width = ( width_1 + width_2 + width_3 + width_4 +
    width_5 ) / 5 % in mm

thickness_1 = ( 15.23 + 15.19 + 15.22 ) / 3 ;
thickness_2 = ( 15.225 + 15.19 + 15.245 ) / 3 ;
thickness_3 = ( 15.195 + 15.19 + 15.21 ) / 3 ;
thickness_4 = ( 15.215 + 15.21 + 15.235 ) / 3 ;
thickness_5 = ( 15.22 + 15.205 + 15.233 ) / 3 ;

Line0Number1_thickness = ( thickness_1 + thickness_2 + thickness_3 +
    thickness_4 + thickness_5 ) / 5 % in mm

gauge_length = 50 ; % in mm
Line0Number1_area = Line0Number1_width * Line0Number1_thickness ;

%importing data
opts = delimitedTextImportOptions("NumVariables", 2);

% Specify range and delimiter
opts.DataLines = [9, Inf];
opts.Delimiter = "\t";

% Specify column names and types
opts.VariableNames = ["AxialDisplacementMm", "AxialForceKN"];
opts.VariableTypes = ["double", "double"];
```

```

% Specify file level properties
opts.ExtraColumnsRule = "ignore";
opts.EmptyLineRule = "read";

% Specify variable properties
opts = setvaropts(opts, ["AxialDisplacementMm", "AxialForceKN"], "
    TrimNonNumeric", true);
opts = setvaropts(opts, ["AxialDisplacementMm", "AxialForceKN"], "
    DecimalSeparator", ",");
opts = setvaropts(opts, ["AxialDisplacementMm", "AxialForceKN"], "
    ThousandsSeparator", ".");

% Import the data
Line0Number1 = readtable("Tensile_test\Line0\Line0Number1.txt",
    opts)
clear opts

Line0Number1_strain = Line0Number1.AxialDisplacementMm /
    gauge_length
Line0Number1_stress = 1000 * Line0Number1.AxialForceKN /
    Line0Number1_area

Line0Number1_figure1 = figure('NumberTitle','off','Name','Figure','
    Color',[1 1 1]);

% Create axes
axes1 = axes('Parent',Line0Number1_figure1);
hold(axes1,'on');

% Create plot
plot(Line0Number1_strain,Line0Number1_stress);

% Create ylabel
ylabel('Stress $[MPa]$', 'Interpreter','latex');

% Create xlabel
xlabel('Strain $[mm/mm]$', 'Interpreter','latex');

% Create title
title('Stress-Strain Curve', 'Interpreter','latex');

box(axes1,'on');
hold(axes1,'off');
% Set the remaining axes properties
set(axes1,'XGrid','on','YGrid','on');
% Set the remaining axes properties
set(axes1,'XGrid','on','XTick',...
    [0 0.01 0.02 0.03 0.04 0.05 0.06 0.07 0.08 0.09 0.1], '
    XTickLabel',...
    {'0','0.01','0.02','0.03','0.04','0.05','0.06','0.07','0.08','
    0.09','0.1'},...

```

```

        'YGrid','on','YTick',[0 5 10 15 20 25 30 35 40 45 50], '
        YTickLabel',...
        {'0','5','10','15','20','25','30','35','40','45','50'});
xlim(axes1,[0 0.1]);
ylim(axes1,[0 50]);

%exportgraphics(Line0Number1_figure1,'Figures/Line0Number1_stress-
    strain.pdf','ContentType','vector')

% Calculation of tensile modulus
summarizedA11 = zeros(1,size(Line0Number1_strain,1));
summarizedA12 = zeros(1,size(Line0Number1_strain,1));
summarizedA22 = 1;
summarizedB1 = zeros(1,size(Line0Number1_strain,1));
summarizedB2 = zeros(1,size(Line0Number1_strain,1));
for i = 1 : size(Line0Number1_strain,1)
    if 0.0005 <= Line0Number1_strain(i) && Line0Number1_strain(i)
        <= 0.0025
        summarizedA11(i) = Line0Number1_strain(i)^2;
        summarizedA12(i) = Line0Number1_strain(i);
        summarizedA22 = summarizedA22 + 1;
        summarizedB1(i) = Line0Number1_strain(i) *
            Line0Number1_stress(i);
        summarizedB2(i) = Line0Number1_stress(i);
    end
end

A = [ sum(summarizedA11,"all") sum(summarizedA12,"all") ; sum(
    summarizedA12,"all") sum(summarizedA22,"all") ]
B = [ sum(summarizedB1,"all") ; sum(summarizedB2,"all") ]

X = A\B;

Line0Number1_tensile_moduli = X(1,1)

Line0Number1_strain_x = linspace(0,0.015,3000);
Line0Number1_stress_x = X(1,1)*Line0Number1_strain_x + X(2,1);

figure2 = figure('NumberTitle','off','Name','Figure','Color',[1 1
    1]);

% Create axes
axes2 = axes('Parent',figure2);
hold(axes2,'on');

% Create plot
plot(Line0Number1_strain,Line0Number1_stress,Line0Number1_strain_x,
    Line0Number1_stress_x);

% Create ylabel

```

```
ylabel('Stress $[MPa]$', 'Interpreter', 'latex');

% Create xlabel
xlabel('Strain $[mm/mm]$', 'Interpreter', 'latex');

% Create title
title('Stress-Strain Curve', 'Interpreter', 'latex');

box(axes2, 'on');
hold(axes2, 'off');
% Set the remaining axes properties
set(axes2, 'XGrid', 'on', 'YGrid', 'on');

% Calc stress and elongation
[Breakstress_LONumber1, LONumber1_pos] = max(Line0Number1_stress) %
    given in MPa.
break_elongation_LONumber1 = 100* Line0Number1_strain(LONumber1_pos
    ) % given in %
```

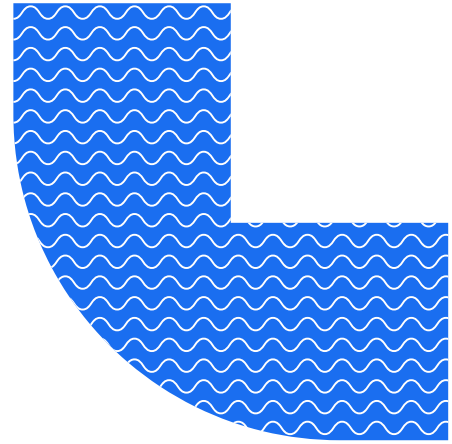
Appendix E

Technical Data Sheet: Tough PLA from Ultimaker

Ultimaker

Ultimaker Tough PLA

Technical data sheet



General overview

Chemical composition	See Tough PLA safety data sheet, section 3
Description	Ultimaker Tough PLA is a technical PLA filament with toughness comparable to Ultimaker ABS. Ideal for reliably printing technical models at large sizes, our Tough PLA offers the same safe and easy use as regular PLA
Key features	<p>With an impact strength similar as and higher stiffness compared to Ultimaker ABS, Tough PLA is less brittle than regular PLA and gives a more matte surface finish quality. Heat resistance is similar to standard PLA filaments, so printed parts should not be exposed to temperature above 58 °C.</p> <p>More reliable than ABS for larger prints, with no delamination or warping. Ultimaker Tough PLA is compatible with Ultimaker support materials (PVA and Breakaway), giving full geometric freedom when designing parts</p>
Applications	Functional prototyping, tooling, manufacturing aids
Non-suitable for	Food contact and in vivo applications. Long term outdoor usage or applications where the printed part is exposed to temperatures higher than 58 °C.

Filament specifications

	Method (standard)	Value
Diameter	-	2.85 ± 0.05 mm
Max roundness deviation	-	0.05 mm
Net filament weight	-	750 g
Filament length	-	~96 m

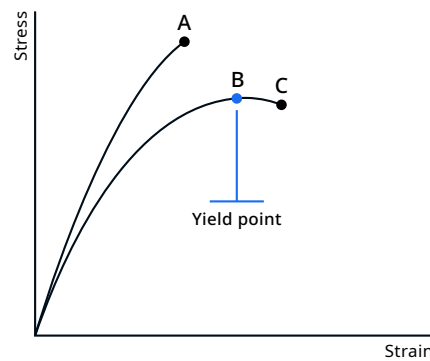
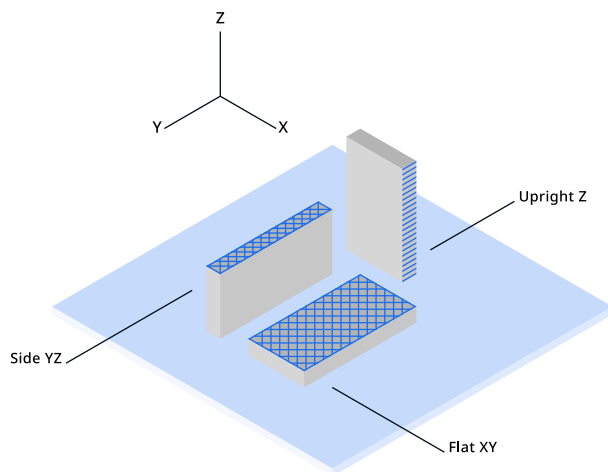
Color information

Color	Color code
Black	RAL 9017
White	RAL 9003
Green	RAL 6038
Red	RAL 3018
Gray	RAL 7000
Yellow	RAL 1018
Blue	RAL 5019

Mechanical properties

All samples were 3D printed. See 'Notes' section for details.

	Test method	Typical value		
		XY (Flat)	YZ (Side)	Z (Up)
Tensile (Young's) modulus	ASTM D3039 (1 mm / min)	2797 ± 151 MPa	2797 ± 99 MPa	2696 ± 180 MPa
Tensile stress at yield	ASTM D3039 (5 mm / min)	45.3 ± 2.0 MPa	47.5 ± 0.5 MPa	33.4 ± 0.5 MPa
Tensile stress at break	ASTM D3039 (5 mm / min)	27.5 ± 7.8 MPa	31.3 ± 4.4 MPa	32.5 ± 0.8 MPa
Elongation at yield	ASTM D3039 (5 mm / min)	3.2 ± 0.0%	3.5 ± 0.0%	2.6 ± 0.1%
Elongation at break	ASTM D3039 (5 mm / min)	9.4 ± 1.9%	8.2 ± 1.8%	3.1 ± 0.7%
Flexural modulus	ISO 178 (1 mm / min)	2882 ± 61 MPa	2503 ± 45 MPa	2358 ± 78 MPa
Flexural strength	ISO 178 (5 mm / min)	91.6 ± 1.3 MPa at 4.1% strain	83.0 ± 1.4 MPa at 4.4% strain	61.3 ± 5.2 MPa at 3.4% strain
Flexural strain at break	ISO 178 (5 mm / min)	No break (>10%)	No break (>10%)	3.4 ± 0.5%
Charpy impact strength (at 23°C)	ISO 179-1 / 1eB (notched)	8.9 ± 0.8 kJ/m ² (Hinge)	-	-
Hardness	ISO 7619-1 (Durometer, Shore D)	80 Shore D	-	-



- A. Tensile stress at break, elongation at break (no yield point)
- B. Tensile stress at yield, elongation at yield
- C. Tensile stress at break, elongation at break

Print orientation

As the FFF process produces parts in a layered structure, mechanical properties of the part vary depending on orientation of the part. In-plane there are differences between walls (following the contours of the part) and infill (layer of 45° lines). These differences can be seen in the data for XY (printed flat on the build plate – mostly infill) and YZ (printed on its side – mostly walls). Additionally, the upright samples (Z direction) give information on the strength of the interlayer adhesion of the material. Typically the interlayer strength (Z) has the lowest strength in FFF. Note: All samples are printed with 100% infill – blue lines in the illustration indicate typical directionality of infill and walls in a printed part.

Tensile properties

Printed parts can yield before they break, where the material is deforming (necking) before it breaks completely. When this is the case, both the yield and break points will be reported. Typical materials that yield before breaking are materials with high toughness like Tough PLA, Nylon and CPE+. If the material simply breaks without yielding, only the break point will be reported. This is the case for brittle materials like PLA and PC Transparent, as well as elastomers (like TPU).



Thermal properties

Samples marked with an asterisk (*) were 3D printed. See 'Notes' section for details.

	Test Method	Typical value
Melt mass-flow rate (MFR)	ISO 1133 (210 °C, 2.16 kg)	6 - 7 g / 10 min
Heat deflection (HDT) at 0.455 MPa*	ISO 75-2 / B	58.3 ± 0.7 °C
Vicat softening temperature*	ISO 306 / A120	63.7 ± 0.3 °C
Glass transition	ISO 11357 (DSC, 10 °C / min)	59 °C
Melting temperature	ISO 11357 (DSC, 10 °C / min)	152 °C

Other properties

Specific gravity	ISO 1183	1.22 g / cm ³
------------------	----------	--------------------------

Notes

*3D Printing: all samples were printed using a new spool of material loaded in an Ultimaker S5 Pro bundle with engineering intent profiles using 0.15 mm layer height with AA0.4 printcore and 100% infill, using Ultimaker Cura 4.9. Samples were printed 'one-at-a-time'. Printed samples were conditioned in room temperature for at least 24h before measuring.

Specimen dimensions (L x W x H):

- Tensile test: 215 x 20 x 4 mm
- Flexural/Vicat/HDT: 80 x 10 x 4 mm
- Charpy: 80 x 10 x 4 mm with printed Notch (Type 1eB)

Disclaimer

Any technical information or assistance provided herein is given and accepted at your risk, and neither Ultimaker nor its affiliates make any warranty relating to it or because of it. Neither Ultimaker nor its affiliates shall be responsible for the use of this information, or of any product, method, or apparatus mentioned, and you must make your own determination of its suitability and completeness for your own use, for the protection of the environment, and for the health and safety of your employees and purchasers of your products. No warranty is made of the merchantability or fitness of any product; and nothing herein waives any of Ultimaker's conditions of sale. Specifications are subject to change without notice.

Version	v2.00
Date	May 9, 2022

